This is a preprint, the final version is subject to change, of the American Mineralogist (MSA)
Cite as Authors (Year) Title. American Mineralogist, in press.
DOI: https://doi.org/10.2138/am-2019-6818

Revision 1

Geochemical Characteristics of Lawsonite Blueschists in Tectonic Mélange from the Tavşanlı Zone, Turkey: Potential Constraints on the Origin of Mediterranean Potassium-rich Magmatism

Yu Wang [1,2,*], Dejan Prelević [3,4] and Stephen F. Foley [2]

[1]State Key Laboratory of Isotope Geochemistry, Guangzhou Institute of Geochemistry, Chinese Academy of Sciences, Guangzhou 510640, China

[2]ARC Centre of Excellence for Core to Crust Fluid Systems/GEMOC; Department of Earth and Planetary Sciences, Macquarie University, NSW 2109, Australia

[3]Faculty of Mining and Geology, Belgrade University, Đušina 7, 11000 Belgrade, Serbia

[4]Institute for Geosciences, University of Mainz, Becherweg 21, Mainz 55099, Germany

*Corresponding author

E-mail address: wangyu@gig.ac.cn (Yu Wang).

This is a preprint, the final version is subject to change, of the American Mineralogist (MSA)
Cite as Authors (Year) Title. American Mineralogist, in press.
DOI: https://doi.org/10.2138/am-2019-6818

ABSTRACT

The petrology, mineralogy and geochemistry of lawsonite blueschists from the Tavşanlı zone in NW Turkey – one of the best-preserved blueschist terranes in the world – have been comprehensively investigated. The blueschist samples contain lawsonite + sodic amphibole + phengite + chlorite + titanite + apatite ± aragonite ± quartz ± relict igneous pyroxene ± Mn-rich garnet and opaque phases. Lawsonite is a significant repository for Sr, Pb, Th, U and REE, whereas phengite carries the most LILE, titanite hosts the highest Nb and Ta as well as considerable amounts of HFSE, and apatite strongly controls Sr. Two groups of blueschist have different origins – enriched continent-derived terrigenous origin and MORB-like submarine basalts – assigned on the basis of whole-rock major and trace element compositions and initial Sr-Nd-Pb isotopic results. Lawsonite in blueschist with enriched origin exhibits strong Th/La fractionation, raising the possibility of the involvement of blueschist facies mélange to explain the origin of Mediterranean potassium-rich magmatism, because similarly high Th/La ratios are also observed in the Mediterranean potassium-rich lavas. We propose that subduction-induced tectonic imbrication took place entirely at shallow depths (<80 km), giving rise to newly formed lithosphere where oceanic and continental crustal materials, sediments, strongly depleted peridotite blocks and metamorphic rocks are all imbricated together, and in which many of the compositional characteristics of the lawsonite blueschist are sequestered. Subsequent melting of the fertile and enriched components in this new lithosphere would result in the generation of potassium-rich post-collisional mafic magmas with diagnostic geochemical affinities.

INTRODUCTION

Blueschists and eclogites result from subduction along cold geothermal gradients. They provide a natural laboratory to investigate the passage of chemical components from subducting crust to the overlying mantle wedge during subduction, and to help understand the origin of earthquakes that may be triggered by the dehydration and embrittlement of subducting oceanic crust (Ernst et al., 1988; Okay, 1989; Maekawa et al., 1993; Maruyama et al., 1996; Fryer et al., 1999; Spandler et al., 2003; Kim et al., 2015; Palin and White, 2015; Okazaki and Hirth, 2016). It is widely recognized that without knowledge of subduction zone metamorphism, it is impossible to fully examine the compositional heterogeneity of the mantle because metamorphic processes during subduction will dramatically affect mantle metasomatism and subduction-related dynamics (Maekawa et al., 1993; Tribuzio et al., 1996; Poli and Schmidt, 1997; Yaxley and Green, 1998; Klemme et al., 2002; Tsujimori and Ernst, 2014).

As subduction occurs, metamorphic breakdown and dehydration of hydrous minerals may result in melting in the mantle wedge, liberating a substantial amount of trace elements. Blueschist, and to a lesser extent eclogite, are the principal high-pressure low-temperature (HPLT) metamorphic reservoirs of these hydrous minerals (e.g. lawsonite, epidote, phengite, chlorite and amphibole), documenting many key features of subduction zone metamorphism. Therefore, diverse aspects of their petrological and geochemical characteristics have been extensively studied (e.g. Okay, 1980, 1982; Ernst, 1988; Tribuzio and Giacomini, 2002; Spandler et al., 2003; Volkova et al., 2009; Ukar and Cloos, 2015) including the pressure-temperature stability of blueschists, and blueschist-greenschist or blueschist-eclogite transition

equilibria and thermodynamics (e.g. Schmidt and Poli, 1994; Poli and Schmidt, 1997; Martin et al., 2011).

Despite the usefulness of blueschists to decipher the subduction process, they occur extremely rarely, restricted to subduction of cold oceanic slabs under high pressure and low temperature environment. In addition, they must be exhumed rapidly enough to avoid transformation to other facies assemblages (Okay et al., 1998; Plunder et al., 2015). Numerous works have been carried out on blueschists, mostly along the Mesozoic and Cenozoic orogenic belts of the circum-Pacific and Tethyan regions. Of particular interest are localities in collisional orogenic belts including the Tethyan domains in Eurasia (Mediterranean, Western Alps, east-central China and Himalaya). Many have contributed specifically to the explanation of the petrogenesis, geochemistry, tectonics and geodynamics of Turkish blueschists occurring in Tavşanlı zone (Okay, 1980, 1982, 1986, 1989, 2002; Davis and Whitney, 2006; Topuz et al., 2008, Seaton et al., 2009; Özbey et al., 2013, Plunder, et al., 2013, 2015; Whitney et al., 2014; Martin et al., 2014; Mulcahy et al., 2014; Pagé et al., 2016). However, no systematic work has been done regarding the whole-rock and mineral trace element compositions, and especially isotopic constraints of the Tavşanlı zone blueschists.

Furthermore, the potential of blueschist facies mélange in deciphering the origin of Mediterranean potassium-rich magmatism is rarely acknowledged. Mélanges with matrices consisting of either clastic sedimentary rock or ophiolitic rock have been recognized in orogenic belts worldwide (Raymond, 1984; Cloos and Shreve, 1988; Parkinson, 1996; Collins and Robertson, 1997; Harris et al., 1998; Fotoohi et al., 2005; King et al., 2006; Bulle et al., 2010; Guo et al., 2014; Ukar and Cloos, 2015). They are typically created in the accretionary wedge above a subduction zone where blueschist-facies rocks are underlain by, or imbricated with, several different

lithologies. Along the Alpine-Himalayan orogenic belt (AHOB), especially in the Mediterranean and Turkey, mélanges that include Cretaceous blueschist have been described widely (e.g. Collins and Robertson, 1997; Tankut et al., 1998; Rojay et al., 2004; Tsujimori et al., 2006; Göncüoğl et al., 2006; 2010; Çeti kaplan et al., 2008; Plunder et al., 2013; 2015; Çelik et al., 2016). It has been proposed recently that blueschist facies mélange might help to understand the geodynamics and compositions of post-collisional potassium-rich AHOB magmatism (e.g. Tommasini et al., 2011; Prelević et al., 2013; Wang et al., 2017). A recent study showed that some lawsonite in the Tavşanlı zone blueschists contains critical trace element characteristics – extremely high Th/La ratios – which might be utilized to decipher the origin of AHOB potassium-rich lavas (Wang et al., 2017). In addition, various geochemical proxies imply an important role for sediments in the source of Mediterranean K-rich lavas (Conticelli et al., 1998; 2002; Peccerillo and Martinotti, 2006; Prelević et al., 2008; Tommasini et al., 2013). Subduction in western Turkey at ~95-90 Ma furnished the base of the Anatolide-Tauride block with sediments and oceanic rocks until the Izmir-Ankara-Erzican suture was sealed by Eocene plutonism (Van Hinsbergen, 2010; Mulcahy et al., 2014; Fornash et al., 2016). Therefore, it is essential to scrutinize the tectonically imbricated mélange as it carries critical, yet complex information about oceanic and continental crustal materials, sediments, strongly depleted peridotite blocks and metamorphic rocks including blueschists, which may be potential source materials for Mediterranean and AHOB potassium-rich post-collisional magmas,

This contribution aims to (i) present a comprehensive set of mineralogical, petrological and geochemical results on representative lawsonite blueschist samples from the Tavşanlı zone, Turkey, (ii) constrain the nature of the protoliths of the

115 Tavşanlı zone blueschist, and (iii) propose a feasible solution to account for the
116 characteristic Th/La conundrum of Mediterranean K-rich magmas.
117

118 ## GEOLOGICAL SETTING

119 The geological background of Western Anatolia and the Tavşanlı zone is
120 detailed in several publications (e.g. Şengö and Yılmaz, 1981; Okay and Tüysüz
121 1999; Pourteau et al., 2010, 2013; Plunder et al., 2013, 2015). Only essential
122 information is outlined here; the reader is referred to Okay and Whitney (2010) and
123 Plunder et al. (2013; 2015) for further details on local geology and tectonic evolution.
124 The Tavşanlı Zone lies south of the Alpine Izmir-Ankara-Erzican suture that
125 marks the closure of the Neotethyan Ocean, dividing Western Anatolia into two major
126 blocks, the Pontides and the Anatolides-Taurides (Şengö and Yılmaz, 1981; Okay
127 and Whitney, 2010). The crust of western Anatolia originated by accretion of
128 numerous continental slivers and island arcs beginning in the Early Mesozoic, and is
129 subdivided into three regions, the Tavşanlı Zone (with length of ~250 km and width
130 of 50-60 km) in the north, the Menderes Massif to the southwest, and the Afyon Zone
131 to the northeast of the Menderes Massif (e.g. Okay and Tüysüz, 1999; Altunkaynak
132 and Genç, 2008; Plunder et al., 2013; Fig. 1a). These comprise the most important
133 metamorphic zones in Gondwana-derived continental domains. The Tavşanlı Zone is
134 commonly recognized as a belt of blueschists tectonically overlain by an oceanic
135 accretionary complex and large peridotite slabs later intruded by the undeformed
136 Early to Middle Eocene granodiorites (Okay and Whitney, 2010). The Tavşanlı Zone
137 blueschists mark the subducted north-facing passive continental margin of the
138 Anatolide-Tauride Block and illustrate an analogous tectonic evolution to those from
139 Oman (e.g., Goffe et al., 1988; Searle et al., 1994).

There are three major units in the Tavşanlı Zone: the lower Orhaneli blueschist sequence (where samples in this study were collected), a Cretaceous accretionary mélange derived from the Tethyan Ocean in the middle, and an upper obducted ophiolitic thrust sheet. The Orhaneli sequence constitutes a coherent stratigraphic series consisting mainly of three major formations of metasedimentary rocks; the Kocasu Formation (metaclastic rocks) at the base, the İnönü Formation (marble) in the middle and the upper Devlez Formation (mostly metabasite) where the samples in this study were collected (Okay and Whitney, 2010; Plunder et al., 2015; 2016; Fig. 1b). The Devlez Formation comprises metabasites, metacherts and phyllites with metabasites constituting >80% of the Formation with a structural thickness of ~1 km to the northeast of Tavşanlı.

Our samples were collected between the villages of Göynücek and Dodurga (coordinates see Table 1) where excellent outcrops of the blueschists of the Devlez Formation are exposed (Fig. 1c). Here, the blueschist outcrops consisted of a sequence of intercalated metabasite, metachert, metashale and metagabbro blocks of different size from 100 to 10 meters in diameter, immersed in a mélange matrix (Fig. 2a). The selected samples were collected from two locations that represented larger blocks of blueschists (Fig. 1b, 2b, c). These metabasites are characterized by a typical paragenesis of sodic amphibole, lawsonite, chlorite, titanite and phengite, which are commonly recognized as the classical "blue" blueschists (Okay, 1980a, Okay and Whitney, 2010). They have been completely recrystallized from possibly submarine lavas, pyroclastic rocks and tuffs with the growth of a penetrative metamorphic fabric and new minerals. A strong foliation and mineral lineation in metabasites and metacherts are defined by the parallel alignment of sodic amphibole grains. The age of the blueschist metamorphism, based on Rb/Sr phengite dating, is Campanian (~80

Ma, Sherlock and Okay, 1999), whereas in a recent in situ $^{40}Ar/^{39}Ar$ phengite dating study (Fornash et al., 2016) ages of 90-93 Ma and 82 ± 2 Ma were interpreted as the ages of peak and retrograde metamorphism, respectively.

RESULTS

The six selected mafic blueschist samples are schistose and finely crystalline. Sodic amphibole, lawsonite and chlorite are the most common phases in all six samples, making up 60-80% of the rock. Except for samples 10tav04 and 05, there is no evidence of extensive metasomatism as only low-grade incipiently high pressure metamorphosed rocks have been reported to show considerable metasomatism effects in the Tavşanlı zone (Okay, 1982). Backscattered SEM images of all samples are shown in Fig. 3, and their parageneses are listed in Table 1.

Sample description

10tav04. Sample 10tav04 is a lawsonite blueschist composed of lawsonite, sodic amphibole, pyroxene, phengite, chlorite, titanite, apatite, aragonite and accessory opaque pyrite and hematite. Euhedral lawsonite is prismatic and rhombic/rectangular, with up to 500 μm grains often filled with tiny sodic amphibole, augite and titanite inclusions along with interstitial anhedral aragonite (Fig. 3a). Aragonite is recognized as the primary $CaCO_3$ polymorph by the lack of the perfect rhombohedral cleavage of calcite or dolomite and higher refractive indices. It is a characteristic mineral of HPLT metamorphism and its occurrence in Tavşanlı zone blueschist has been reported in many previous publications where calcite pseudomorphs after aragonite were also identified (e.g. Okay, 1980a; Okay, 1982; Davis & Whitney 2006; Çeti kaplan et al., 2008; Seaton et al., 2009; Whitney et al., 2014). Small (~20 μm)

and relatively fine-grained igneous augite is found only in sample 10tav04, occurring as either single rectangular crystals or as aggregates of small prismatic grains (Fig. 3a); some previous work found it to be partially or completely replaced by sodic pyroxene (Okay, 1980a, b; 1982; Okay and Whitney, 2010). It is normally overgrown by sodic amphibole at the periphery and along cleavages resulting in bleached, patchy crystals (Okay, 1978; 1980a; Plunder et al., 2015). Sodic amphibole and phengite are intergrown with each other as acicular or elongated columnar crystals, and together with chlorite, they make up most of the groundmass. Titanite grain size varies from 5-100 μm, typically with sphenoidal shapes and intergrown almost everywhere, whereas apatite presents tiny subhedral rounded grains of ~5-15 μm.

10tav05. Sample 10tav05 exclusively exhibits large aragonite pools around lawsonite and quartz with a preferred alignment of phengite, sodic amphibole and, to a lesser extent, chlorite, which clearly differentiates it texturally from other samples (Fig. 3b). Quartz and apatite occur as porphyroblasts in an aragonite matrix together with much smaller euhedral rectangular lawsonite (10-100 μm). Chlorite and phengite are often entwined and aligned parallel to foliation with prismatic lawsonite, enclosing intergrowths of elongated sodic amphibole. Almost all lawsonite crystals in the matrix are idiomorphic and contain no inclusions other than tiny interstitial aragonite patches, implying that carbonation might have taken place entirely prior to lawsonite growth during formation of the foliation. Titanite grain size varies greatly (5-50 μm) and always occurs in crevices as late fillings between different minerals. Apatite is generally included in the aragonite matrix with larger grain size of up to 100 μm. Galena appears only in sample 10tav05 as the accessory sulfide mineral instead of pyrite.

10tav07. Sample 10tav07 has the simplest texture and best preserved idiomorphic mineral assemblage. Lawsonite shows ubiquitous euhedral rhombic or square grains 50-800 μm in size, and it only rarely comprises interstitial titanite, quartz and sodic amphibole inclusions (Fig. 3d). Quartz forms a coarse-grained matrix together with sodic amphibole. Euhedral/subhedral garnets appear only in this sample and are enriched in manganese with occasional titanite or sodic amphibole inclusions of variable size (10-250 μm). Sodic amphibole mostly occurs as single tabular and acicular crystals or lath-like aggregates intergrown with phengite and chlorite. Phengite is also found between quartz and lawsonite grains or enclosing lawsonite. Large titanites (average size ~100 μm) occur throughout the sample, whereas apatite may occur as inclusions in titanite and generally appears as anhedral fine-grained crystals. No sign of carbonation or other later stage alteration is observed in this sample, implying well-preserved initial metamorphism.

10tav06, 10tav08 and 10tav09. These three samples share similar parageneses and textures (Fig. 3c, e and f), with a mineral assemblage of lawsonite, sodic amphibole, quartz, aragonite, phengite, chlorite, titanite, apatite and opaque accessory minerals (pyrite and hematite). Euhedral prismatic lawsonites occur in all three samples as porphyroblasts with variable grain size (50-1000 μm), and usually with interstitial quartz, aragonite, sodic amphibole and titanite crystals as inclusions, exhibiting a patchy surface with sodic amphibole, phengite and chlorite. Aragonite and quartz occur mostly as tiny inclusions embedded in lawsonite grains, whereas sodic amphibole, chlorite and phengite appear almost everywhere intergrown together as acicular or columnar shape with subhedral titanite and apatite crystals inserted in crevices. Calcic amphibole (actinolite) replaces some of the sodic amphibole (glaucophane) at the rim in sample 10tav08, indicating a small degree of retrograde

metamorphism, and occasional oscillatory zoning of lawsonite can be seen only in this sample.

Whole rock geochemistry

The major and trace element compositions of the six samples are listed in Table 2.

Major elements. Samples 10tav06, 08 and 09 have similar major element compositions, implying analogous protoliths. Specifically, they show mafic compositions with consistent SiO_2 contents of 44.8-46.5 wt%, FeO_T 11.1-11.2 wt%, CaO 10-12.2 wt%, Na_2O 2.3-2.8 wt% and almost identical TiO_2, MnO, K_2O contents of 1.4, 0.16 and 0.1 wt%, respectively. Sample 10tav06 has slightly lower Al_2O_3 (14 wt%) and higher MgO (7 wt%) than the other two (15.3-15.5 and 4.7-5.6 wt%), whereas 10tav09 exhibits the lowest Mg number of 42.8. All show similar LOI of approximately 7.5, higher than the typical value of unaltered lawsonite blueschist containing phengite, indicating slight late alteration.

Samples 10tav04 and 05 are mafic with SiO_2 around 45 wt%, whereas sample 10tav07 has higher SiO_2 (57.5 wt%), reflecting its high quartz content. Sample 10tav04 is the most K-, Na-, Ti- and Fe-rich rock with 2.9, 3.8, 1.5 and 13.3 wt%, respectively, and contains the lowest CaO (5.3 wt%). The high K content results from large and abundant phengite grains, indicating a continental sedimentary origin for the blueschist protolith, whereas the Ca depletion is consistent with the lowest lawsonite content in these rocks. Sample 10tav05 has the highest volatile contents (10% LOI) due to its carbonate alteration, whereas sample 10tav07 has the lowest LOI value of 3.9%, marking its well-preserved unaltered nature.

For all six samples, MgO varies little (4.7-7.1 wt%), slightly lower than MORB and higher than GLOSS (Fig. 4), and they present rather low Mg numbers of 42.8-54.9. Samples 10tav06, 08 and 09 show compositions compatible with MORB for major elements, whereas samples 10tav04, 05 and 07 are not compatible with MORB for the majority of major elements (Fig. 4). Contents of Al_2O_3, CaO and K_2O, particularly K_2O indicate GLOSS-like affinities, i.e. continent-derived terrigenous sediment (Fig. 4b, d and f). The enrichment of K and depletion of Ca in Franciscan blueschists was also attributed to the presence of terrigenous sediment in the source (Sorensen et al., 1997; Ukar, 2012; Ukar and Cloos, 2015).

Trace elements. Samples 10tav06, 08 and 09 show similar N-MORB-like trace element affinities (Fig. 5), exhibiting only slight Th and U enrichments and similar Nb, Ta and REE concentrations to N-MORB (Fig. 5). Although slightly enriched in Cs, Rb and Ba relative to N-MORB, these three samples still exhibit significantly lower large-ion lithophile element (LILE) concentrations than GLOSS. In contrast, samples 10tav04, 05 and 07 are substantially enriched in LILE, such as Cs, Rb and Ba 10-1000x N-MORB, except for insignificant/negative Sr anomalies (Fig. 5). Moreover, they have more enriched LILE, Th, U, Nb, Ta and higher light rare earth elements (LREE) similar to GLOSS, particularly for sample 10tav07 (Fig. 5), which clearly distinguishes them from samples 10tav06, 08 and 09. Sample 10tav04 has a notably elevated Ba/Th ratio (825). All six samples are enriched in Pb and Li relative to N-MORB (Fig. 5), and all exhibit variable contents of Ni, Cr and V (Ni = 70-199 ppm, Cr = 145-512 ppm; V = 205-372 ppm).

Mineral chemistry

Major and trace element compositions of all minerals are listed in Table 3, 4, S1-S7. For lawsonite and titanite, iron was assumed to be Fe^{3+}, whereas Fe^{2+} was used for phengite, garnet and chlorite. Fe^{2+} and Fe^{3+} abundances in amphibole were calculated by charge balance (Supplementary file S2; Schumacher, 1997).

Lawsonite. The major element compositions of lawsonite are consistent in all six samples and denote an almost ideal structural formula of $CaAl_2Si_2O_7(OH)_2(H_2O)$. They have ~1.1-1.7 wt% Fe^{3+} and almost negligible Cr and Ti except for sample 10tav08 (0.13 wt% Cr_2O_3, Table 3) where oscillatory zoning is observed, in good agreement with previous studies (e.g. Sherlock and Okay, 1999). Lawsonites in all samples show negative correlation between Si and Al + Ca (atomic) (Fig. S1).

Despite the restricted major element compositional variation, lawsonites exhibit extremely complex and heterogeneous trace element compositions. Numerous studies have affirmed that lawsonite is a significant repository for Sr, Pb, Th, U and REE (e.g. Tribuzio et al., 1996; Ueno, 1999; Spandler et al., 2003; Vitale Brovarone et al., 2014; Martin et al., 2014), because the structure of lawsonite allows divalent elements (e.g. Sr and Pb) to enter the Ca site and trivalent REE to be charge balanced by M^{2+} on the octahedral site. Samples 10tav04 and 10tav07 show the highest REE concentrations with nearly flat REE patterns. Sample 10tav05 exhibits relatively enriched LREE contents (Fig. 6). LILE (Cs, Rb and Ba) are slightly depleted in all lawsonites, whereas HFSE are similar to or slightly higher than chondrite. Th and U are remarkably enriched in sample 10tav07 with over 2 orders of magnitude higher than in other samples.

Another noteworthy feature in lawsonite is its compositional heterogeneity (e.g. Ueno, 1999; Vitale Brovarone et al., 2014; Martin et al., 2014; Dubacq and Plunder, 2018) reflected in large standard deviations in Fig. 6. Using X-ray and Confocal

MicroRaman 3D spectroscopic mapping results (Fig. S2), we can exclude the possibility that this is due to the presence of inclusions and/or impurities, because only tiny quartz, sodic amphibole and titanite grains are identified, none of which has significant abundances of Th, U and REE that could falsify the lawsonite compositions. In addition, we also exclude zoning as the cause of the compositional heterogeneity because except for sample 10tav08, no marked zoning is observed for the lawsonites.

Amphibole. Amphiboles are mostly sodic (6.5-10.4 wt% Na_2O) except in sample 10tav08, which also shows calcic compositions (Supplementary file S2; Fig. S3). Chemically, sodic amphiboles vary from glaucophane to Fe-rich glaucophane/magnesio-riebeckite. All glaucophanes show consistent compositions with ~57 wt% SiO_2, 10 wt% MgO, 10 wt% Al_2O_3 and 12 wt% FeO_T, whereas magnesio-riebeckites have similar SiO_2 and MgO contents but lower Al_2O_3 (~4.5 wt%) and higher FeO_T (~18 wt%). Actinolite in sample 10tav08 has the highest MgO and CaO and the lowest Na_2O content (1.6 wt%). Winchite in sample 10tav05 is higher in sodium and iron.

All amphiboles exhibit consistently flat REE patterns above unity except for glaucophane in 10tav07, which has REE below C1 chondrite (Fig. 7a). Samples 10tav04, 06 and 08 are enriched in Cs, Rb and Ba, possibly because of the presence of retrograde amphiboles (sample 10tav08) or slight contamination by phengite during analysis (Fig. 7a). Winchite in sample 10tav05 exhibits the most Th, U, Nb, Ta and LREE enrichment, whereas glaucophanes in samples 10tav07 and 09 show the most depleted Rb, Ba, Nb and Ta. In Fig. S4, clear distinctions between amphibole types can be seen; calcic amphiboles carry the most Cs, Rb and Ba while glaucophanes and riebeckites host the least, and winchite carries the most Sr.

337 **Phengite.** Mica formulae were calculated using 22 oxygen atoms, and all exhibit
338 high Si contents of up to 7.3 a.p.f.u. (atoms per formula unit) and extremely low Na
339 content of ~0.01 a.p.f.u. indicating no paragonite component (Table S1). Potassium is
340 approximately 10.5 wt% K_2O in all samples, whereas MgO content varies from 5.1 to
341 7.1 wt%. Phengites host considerable LILE (except for Sr) with 2-3 orders of
342 magnitude higher than C1 chondrite (Fig. 7c). Limited by the fine and elongated
343 crystal size, we could only measure phengites in two samples, but these should be
344 representative for all samples since the results are in good agreement with each other
345 and with previous studies (Xiao et al., 2014; Martin et al., 2014). In sample 10tav07,
346 some selected trace element compositions (especially HFSEs such as Th, U, Nb, Ta
347 and HREE) are conspicuously higher than in 10tav04, which exhibits a flat pattern
348 slightly above unity; we interpret this as possible slight lawsonite (Th, U and HREE)
349 or titanite (Nb, Ta) contamination. However, Cs, Rb and Ba will remain unaffected by
350 any titanite contamination, so that the differences between samples 10tav04 and 07 in
351 Fig. S5 are attributable to phengite itself. Sample 10tav07 has higher Ba, Sr and Rb
352 than that of sample 10tav04, whereas Cs is more enriched in sample 10tav04.
353 **Chlorite.** In sample 10tav07, chlorites show the highest Si and Mg contents
354 (6.56 and 6.85 a.p.f.u.), and lowest Al and Fe, suggesting diabantite composition,
355 whereas the other samples present typical chlorite formula of
356 $(Mg,Fe)_3(Si,Al)_4O_{10}(OH)_2 \cdot (Mg,Fe)_3(OH)_6$ with only slight compositional differences
357 (~28 wt% SiO_2, 17 wt% Al_2O_3 and 21 wt% MgO). Chlorites yield the lowest trace
358 element concentrations of all minerals except in sample 10tav04, which shows
359 moderate Cs, Rb and Ba enrichments and slightly higher REE concentrations (Fig. 7e).
360 **Titanite and apatite.** There is little major element variation in titanite and
361 apatite, both close to the standard structural formulae of $CaTi(SiO_4)(O,OH,F)$ and

362 $Ca_5(PO_4)(OH,F,Cl)$. In contrast, there are strong distinctions in the trace element
363 compositions of titanite grains. Titanites in all samples (particularly 10tav05 and 07)
364 contain the highest Nb and Ta of all minerals (up to 723 and 41 ppm, respectively)
365 and relatively high Th, U and REE (Fig. 7b). In sample 10tav05, REE appears to have
366 a slightly downward sloping pattern (HREE-depleted) whereas the rest of samples
367 give uniformly upward arrays (LREE-depleted), most marked in sample 10tav06 with
368 considerably lower concentrations. Spandler et al (2003) attributed these chemical
369 differences to the different timing of titanite growth with respect to other trace
370 element-rich minerals, and to variations in whole-rock trace element contents. The
371 upward sloping REE patterns in our samples probably formed from an LREE-
372 depleted matrix after lawsonite crystallization and in the presence of zircon (indicated
373 by the relatively low Zr and Hf contents), whereas the downward sloping REE pattern
374 of 10tav05 can be interpreted as crystallizing prior to lawsonite because LREE would
375 have been taken up in lawsonite otherwise. Apatite is widely acknowledged as an
376 important host of Sr, Pb and REE (e.g. Haggerty et al., 1994; Martin et al., 2014): in
377 this study it yields moderately enriched REE with slight preference of HREE over
378 LREE in most samples, and all apatites exhibit strong Sr affinity (Fig. 7d).

379 **Other minerals.** Garnet (~1 mode%) is found only in sample 10tav07
380 characterized by decreasing spessartine from core to rim (41% to 25%). This
381 distinctive occurrence of a minute amount of Mn-rich garnet is probably due to
382 multiple factors, including the breakdown of hydrous minerals (e.g. chlorite,
383 amphibole, lawsonite and phengite), the composition of parental rocks and the PT
384 conditions of metamorphic reactions (Xia and Zhou, 2017). Piemontite and Mn-rich
385 garnet are also reported from quartz-rich schists elsewhere in the Tavşanlı zone (Okay,
386 1980; David and Whitney, 2006). In agreement with previous findings (e.g. Hauri et

al., 1994; Van Westrenen et al., 2001), garnet shows extremely strong preference for HREE over LREE with up to ~3 orders of magnitude higher than C1 chondrite (Fig. 7f). Moreover, garnet hosts considerable Th and U, which is uncommon because they would usually not be expected to enter garnet, particularly in the presence of lawsonite (Spandler et al., 2003; Martin et al., 2014). We suggest this might be due to either the effect of the manganese-rich composition on the garnet structure, or possibly minor contamination from other minerals such as titanite or lawsonite. Aragonite is the only carbonate phase, and carries significant amounts of Ba and Sr (Fig. 7f). Galena is only seen in sample 10tav05 whereas hematite and pyrite are found in all samples. Hematite unexpectedly hosts significant amounts of Ba, Th, U and REE with strong LREE affinity over HREE of ~3 orders of magnitude higher than C1 chondrite (Fig. 7f).

Isotope constraints

This study provides the first Sr-Nd-Pb isotopic constraints of the Tavşanlı zone blueschists (Table 5 and 6). Whole rock Sr, Nd and Pb isotopic results together with incompatible trace element concentrations indicate considerable differences in the extent of trace element enrichment among the samples, which lead over time to a wide variety of isotopic signatures in blueschists (Fig. 8 and 9).

Samples 10tav06, 08 and 09 have low concentrations of K, Th, U and REE, plotting in a restricted area on the Sr-Nd isotopic diagram (Fig. 8), with unradiogenic $^{87}Sr/^{86}Sr$ (0.7052-0.7057) and radiogenic $^{143}Nd/^{144}Nd$ (~0.5129) similar to MORB. Samples 10tav06 and 08 also have the most unradiogenic $^{206}Pb/^{204}Pb$ (18.33-18.42), $^{207}Pb/^{204}Pb$ (15.57-15.60) and $^{208}Pb/^{204}Pb$ (38.37-38.47) compositions (Fig. 9), plotting broadly within the depleted MORB mantle (DMM) field, consistent with a

MORB-like oceanic crust protolith. Samples 10tav04, 05 and 07, which are more enriched in K, Th, U and LREE, have variably radiogenic $^{87}Sr/^{86}Sr$ and mostly unradiogenic $^{143}Nd/^{144}Nd$. Sample 10tav04 has similar radiogenic $^{143}Nd/^{144}Nd$ (~0.5129) to samples 10tav06, 08 and 09 but much more radiogenic $^{87}Sr/^{86}Sr$ (up to 0.7070) compositions (Fig. 8), whereas its Pb isotopes are slightly higher than 10tav06 and 08 (Fig. 9), implying an enriched protolith and addition of slab derived Sr-rich fluid. Sample 10tav07 has the most unradiogenic $^{87}Sr/^{86}Sr$ (~0.7053) and $^{143}Nd/^{144}Nd$ (0.5125) as well as the most radiogenic $^{206}Pb/^{204}Pb$ (19.35), $^{207}Pb/^{204}Pb$ (15.66) and $^{208}Pb/^{204}Pb$ (39.74) compositions, implying the presence of some enriched, probably continental crust-like, component. Samples 10tav04 and 07 show more radiogenic $^{206}Pb/^{204}Pb$, $^{207}Pb/^{204}Pb$ and $^{208}Pb/^{204}Pb$ isotopic compositions relative to 10tav06 and 08, although they mostly plot close to the Northern Hemisphere Reference Line (NHRL; Hart, 1984; Fig. 9).

DISCUSSION

Blueschists with two different protolith lithologies

Possible protolith lithologies of blueschists. Constraining blueschist protoliths can reveal several key pieces of information concerning the tectonic evolution and related volcano-sedimentary processes at subduction zones (Ernst, 1988; Stern, 2005; Palin and White, 2015). Protolith lithologies of mafic blueschists in oceanic subduction zones are widely acknowledged to be derived from the upper part of the oceanic crust consisting of a thin veneer of sediments, segments of igneous rocks, and depleted peridotite (Karson, 2002; Klemd, 2013). Specifically, the protoliths of mafic blueschist could be normal or enriched mid-ocean ridge basalt (N-/E-MORB; e.g. Honegger et al., 1989; Becker et al., 2000; Song et al., 2009; Zheng et al., 2010; Ukar

et al., 2015), ocean island basalt (OIB; e.g. Volkova and Budanov, 1999; Tang and Zhang, 2013; Ge et al., 2016), and sometimes both MORB and OIB (e.g. Patočka and Pin, 2005; Maulana et al., 2013). In addition, some blueschists could be derived from an ophiolitic complex (e.g. Volkova et al., 2009; Zhang et al., 2009), or volcanoclastic rocks (e.g. Miller et al., 2009). Clear enriched affinities have also been identified in protoliths of mafic blueschists: some have been attributed to the involvement of sediments in the source (e.g. Bernard-Griffiths et al., 1986; Ukar, 2012), whereas Zhu et al. (2015) proposed that they originated from a continental rift environment. Furthermore, dehydration at high pressures may induce metasomatism that could exert a strong effect on blueschist compositions, and these metasomatizing fluids would dramatically reshape the trace element compositions by fluid-rock interaction (e.g. Beinlich et al., 2010; Klemd, 2013; Vitale Brovarone et al., 2014; Kleine et al., 2014).

Only few petrological and geochemical studies of the Tavşanlı zone blueschists have focused on the protoliths. The general consensus is that they are derived from volcano-sedimentary sequences, whereas the mafic blueschists in this study were often interpreted as former basaltic rocks (e.g. Okay, 1980; 1982; Çetinkaplan et al., 2008; Okay and Whitney, 2010). Davis and Whitney (2006) proposed that these blueschists have an NMORB-like protolith that experienced seafloor metamorphism or fluid infiltration during subduction but prior to HP-LT metamorphism; Özbey et al. (2013) argued that they originated from both OIB and MORB sources, possibly affected by crustal contamination and variable amounts of fractional crystallization. However, more diagnostic geochemical proxies, especially isotopic compositions, are required to further constrain the protoliths of mafic blueschists in the Tavşanlı zone.

Two groups of blueschists in this study. Based on the whole-rock major and trace element geochemistry, mineral parageneses and isotopic affinities, we divide our samples into two groups, namely MORB-like blueschist and enriched terrigenous blueschist. The first group includes samples 10tav06, 08 and 09, and is characterized by low concentrations of LILE (K, Cs, Rb and Ba), HFSE (Th, U, Nb, Ta and REE, coupled with variably unradiogenic $^{87}Sr/^{86}Sr$ and radiogenic $^{143}Nd/^{144}Nd$ compositions similar to MORB (Fig. 5, 8). The second group includes samples 10tav04, 05 and 07 and differs from the first group in having LILE (up to 2.9% K_2O), HFSE (e.g. Th up to 7.8 ppm) and REE contents considerably higher than MORB, together with more radiogenic $^{87}Sr/^{86}Sr$ and unradiogenic $^{143}Nd/^{144}Nd$ isotopic compositions (particularly 10tav07, Fig. 5, 8), consistent with an enriched continental sedimentary source.

Since the contents of fluid-mobile elements such as K, Na, Rb, Ba, Cs, Rb, La and Ce are subject to later stage processes, whilst elements such as HFSE (high field strength element), REEs (except for La and Ce), Ni, V and Cr should survive these relatively unchanged, the latter are often utilized to identify magmatic affinity (Rollinson, 1993). Here we use Ti, Zr and Nb to interpret the original tectonic settings of the magmatism as these elements should be little modified in blueschist metamorphism (Pearce and Cann, 1973; Pearce, 1975; Winchester and Floyd, 1976; Wood, 1980; Ukar and Cloos, 2015). All blueschists but one plot in the tholeiitic field, although 10tav04 falls very close to the border between alkaline and tholeiitic in Fig. 10a. Their tholeiitic nature is more pronounced in the P_2O_5 vs Zr (Fig. 10b) and V vs Ti plots (Fig. S5). In the Th/Yb vs Ta/Yb diagram, samples 10tav06, 08 and 09 are clearly MORB-like, whereas 10tav05 and 07 plot towards the enriched end, which we attribute to continental crustal material (Fig. 10c). Th is much more sensitive to continental crust involvement than Ta, whereas Yb usually remains relatively stable

in diverse enrichment processes (Pearce, 1983). Sample 10tav04, however, plots together with MORB-like blueschists and does not show a pronounced continental crust affinity (Fig. 10c). A similar situation is seen in Ce/Nb vs Th/Nb where samples 10tav05 and 07 plot well outside the N-MORB field and samples 10tav04, 06, 08 and 09 all fall near the N-MORB area (Fig. 10d), implying two different mantle sources for the oceanic basalts. Samples 10tav04, 06, 08 and 09 are of regular MORB origin whereas samples 10tav05 and especially 07, are clearly affected by a continental crust component, probably terrigenous sediments similar to GLOSS (Saunders et al., 1988; Plank and Langmuir, 1998).

Although sample 10tav04 is interpreted as of enriched terrigenous origin, it may have been reshaped by another component. Turner et al. (1996) found the Ba/Th ratio is indicative of fluids derived by dehydration of subducted oceanic crust. Sample 10tav04 has substantially elevated Ba/Th ratio (825), which, together with its radiogenic $^{87}Sr/^{86}Sr$ values (up to 0.7070), suggests the addition of a Sr-rich fluid (Fig. 11), which has later modified its trace element budget. Its extreme Ba/Th ratio also identifies sample 10tav04 as the only one that has undergone strong fluid metasomatism. Although the Ba/Th ratio of sample 10tav05 is not particularly high (29), its higher carbonate content along with comparable radiogenic $^{87}Sr/^{86}Sr$ to sample 10tav04 suggest it might have also undergone fluid metasomatism, and that its protolith might have been more carbonate-rich, possibly as carbonates atop subducted oceanic crust or decapitated seamounts.

Therefore, the protoliths of the MORB-like group are rather uniform, whereas the protoliths of the enriched blueschists are evidently affected by a terrigenous component to differing extent (Fig. 8, 9, 10) and may have undergone strong Sr-rich fluid metasomatism (sample 10tav04). The protoliths of the enriched group are also

511 oceanic basaltic rocks, but as their geochemical signature is characterized by the
512 presence of continent-derived terrigenous sedimentary component, they were possibly
513 volcanoclastics.

514 ***Fractional crystallization and crustal contamination.*** The primary tholeiitic
515 magmas of the blueschist protoliths may have experienced considerable fractional
516 crystallization or crustal contamination as indicated by their low Mg-numbers and
517 variable contents of Ni, Cr and V. REE ratios that are relatively insensitive to
518 fractional crystallization can help to constrain the melting conditions and the source
519 of the magmas (Thirlwall et al., 1994; Miller et al., 1999; Zhu et al., 2015). In Fig. 12,
520 all the blueschists plot along or parallel to the trajectory for non-modal fractional
521 melts of a spinel peridotite source rather than that of garnet peridotite (Fig. 12),
522 suggesting that the primary magmas of blueschist samples were produced by differing
523 degrees of partial melting of spinel-facies peridotites, especially the MORB-like
524 group (Miller et al., 1999; Zhu et al., 2015). As summarized by Hofmann et al. (1986),
525 Nb/U and Ce/Pb ratios fall consistently in the ranges 47 ± 10 and 25 ± 5 in mantle-
526 derived oceanic basalts, and deviations may indicate crustal contamination or
527 assimilation. Our samples yield variably low Nb/U (8.7-55) and Ce/Pb (1.1-29) values,
528 implying possible minor crustal contamination except for sample 10tav07, which
529 gives Nb/U of 21 and Ce/Pb of 29. Sample 10tav09 exhibits the lowest Nb/U (8.7)
530 and Ce/Pb (1.1) values, indicating the strongest crustal influence. This is more clearly
531 seen in Fig. S6 as both high Ba/Rb and low Nb/La are reliable trace element indices
532 of crustal contamination (e.g. Kieffer et al., 2004).
533

534 **Whole-rock trace element budget for blueschist**

To better understand how trace elements are distributed among the mineral inventory of blueschist, we calculated the trace element budgets using average trace element compositions, the modal abundances of the minerals, and the corresponding whole-rock compositions. The modal abundances for minerals were first obtained by point counting in thin sections, then cross checked by least squares mass balance (Table 1). The calculated elemental distributions are illustrated in Fig. 13. It is quite difficult to accurately determine the budgets of all the trace elements (such as Zr and Hf) in blueschists because of their fine grain size, complex mineralogy, and important yet rare occurrence of accessory minerals (e.g. Spandler et al., 2003). We attribute the imprecise elemental budgets particularly to the lack of data for minor phases rich in key trace elements, such as zircon, phengite and hematite, but also possibly due to zoning and contamination giving rise to heterogeneous trace element compositions. Nonetheless, the budgets for most elements in the major blueschist phases are well constrained, especially for samples 10tav04 and 07 because of their simpler mineralogy.

Zr and Hf are predominantly accommodated in zircon (e.g. Rubatto, 2002; Belousova et al., 2002), which is believed to account for the poor Zr and Hf matches in several samples (Fig. 13). Lawsonite hosts ~50% of REE, nearly all Sr and ~40% of Th in sample 10tav07, with hematite and Mn-garnet being the significant carriers of LREE and HREE, respectively (Fig. 13). In a similar budget estimation for mafic lawsonite blueschist, Spandler et al (2003) also found lawsonite to be the main host for ~90% of Sr, ~30% of LREE and substantial proportions of Th. Generally, titanite accommodates the majority of Nb, Ta and Ti, whereas phengite governs the LILE, and sodic amphibole controls Li and Mn, which is in good agreement with previous

559 studies (Fig. 13; Spandler et al., 2003; Martin et al., 2014). Th, U, Sr and REE are
560 controlled jointly by lawsonite, titanite, apatite and hematite.

561 Using the available mineral data, we can reconstruct and compensate the element
562 budgets for the less well-constrained samples. For some phases we only managed to
563 obtain trace element results for one sample (e.g. hematite in 10tav07 and aragonite in
564 10tav05). In 10tav05, LILE are very poorly constrained because of the lack of
565 phengite data, and in 10tav06, 08 and 09, hematite should account for the
566 discrepancies in Th, U and LREE. Minor and accessory phases such as apatite, titanite,
567 hematite and zircon are significant in controlling trace element distributions and can
568 thus affect the trace element behavior dramatically.

569

570 **Significance of lawsonite geochemistry**

571 Lawsonite is recognized as one of the most significant hydrous minerals in mafic
572 rocks for transporting water and key trace elements (e.g. Sr, Th, U and REE) to great
573 depths during subduction (Baur, 1978; Schmidt, 1995; Tribuzio et al., 1996; Spandler
574 et al., 2003; Tsujimori et al., 2006; Usui et al., 2007; Martin et al., 2014; Vitale
575 Brovarone et al., 2014). Our results agree well with previous findings, and indicate
576 that lawsonite in blueschists of different origins exhibits strong variations in trace
577 element behavior (e.g. Martin et al., 2014).

578 Generally, lawsonite in the enriched terrigenous blueschists shows higher LREE
579 and Sr than MORB-like blueschists (Fig. 14a, b). Allanite, usually accounts for La,
580 Ce, Pr and Nd in blueschists (Hermann, 2002; Gieré and Sorensen, 2004), but is
581 absent from the blueschists in this study. LREE contents in our lawsonites are thus not
582 compromised by allanite and yield enriched compositions, especially in enriched
583 blueschist samples (10tav04, 05 and 07), where Th and U are strikingly enriched as

584 well (Fig. 5). Pb and Sr are commonly hosted by high-pressure phases such as apatite
585 and aragonite, which should host high Pb/Ce and Sr contents instead of lawsonite
586 (Spandler et al., 2003, Martin et al., 2014). However, lawsonite in 10tav05 exhibits
587 higher Pb/Ce ratio and Sr content than apatite, probably due to the rock's higher
588 degree of alteration and large abundance of aragonite (Fig. 14a, b). The negative
589 correlation between Pb/Ce ratio and Ce content in all samples except 10tav05 (Fig.
590 14a) indicates that lawsonite fails to fractionate Pb from Ce regardless of its origin.
591 A more distinctive feature is illustrated in Fig. 14c: lawsonites in blueschists of
592 continent-derived terrigenous origin exhibit much higher La concentrations and
593 La/Dy ratios than those in MORB-like blueschists. La/Dy ratio correlates positively
594 with La content in all lawsonites, suggesting that lawsonite not only hosts substantial
595 amount of LREE, but is capable of fractionating LREE (La) from MREE (Dy). Martin
596 et al. (2014) found that lawsonites in metasomatic rocks have elevated La/Dy, La, and
597 Ce contents along with lower Pb/Ce, which is also seen in our sample 10tav04 that is
598 believed to have undergone fluid metasomatism. As for HREE, lawsonites in enriched
599 samples yield much higher Dy/Lu ratios than those of MORB origin, which results in
600 a negative REE slope (Fig. 6), whereas titanite and apatite have more enriched Lu
601 concentrations and lower Dy/Lu.
602 Despite the common major element characteristics of the lawsonites, they show
603 extremely heterogeneous trace element concentrations (Fig. 14). Martin et al. (2014)
604 attributed this to the flexible crystal structure capable of incorporating variable sizes
605 of trace elements. Our study demonstrates that lawsonite is prone to chemical
606 variations that reflect its protolith. Different protoliths give rise to chemically variable
607 lawsonite despite similar parageneses. Trace elements in lawsonites in MORB-like
608 blueschists differ considerably from those with enriched origin, with the latter being

more enriched in Sr, Th, U and LREE, and showing more pronounced LREE/HREE fractionation, indicating the significance of continent-derived terrigenous sediments in shaping the trace element distribution in lawsonite blueschists.

Potential constraints on the origin and geochemistry of potassium-rich magmatism

Key geochemical signature of Mediterranean potassium-rich magmas. Along with the high K_2O content, strongly enriched incompatible elements, elevated $^{87}Sr/^{86}Sr$, $^{207}Pb/^{204}Pb$, $^{187}Os/^{188}Os$, and low $^{143}Nd/^{144}Nd$ and $^{176}Hf/^{177}Hf$ ratios, the extremely high Th/La ratio has recently been recognized to uniquely fingerprint magmas of the Alpine-Himalayan Orogenic Belt (AHOB; Tommasini et al., 2011; Prelević et al., 2013; Wang et al., 2017). For most mantle-derived magmas, Th/La ratios are no larger than 0.5 (Fig. 15), because it is difficult to fractionate Th from La by either dehydration or melting processes that carry slab material to the arc source (Plank, 2005). Tommasini et al. (2011) proposed that the strikingly high Th/La signature of Tethyan Realm lamproites could be explained by lawsonite and zoisite/epidote veins and segregations in chaotic mélange domains accreted to the Eurasian plate during collisional events. This argument is echoed by Prelević et al. (2013), who reported the same extreme Th/La ratios in Mediterranean and Tibetan post-collisional (but not lamproitic) mafic lavas, and they also attributed it to the possible presence of a blueschist facies end member including lawsonite and zoisite veins.

Unravelling the high Th/La enigma. We here demonstrate that lawsonites with differing origins in the Tavşanlı zone blueschists have distinct Th/La fractionation characteristics (Fig. 15): lawsonites with enriched continent-derived terrigenous

634 origin show similar Th/La vs Sm/La to AHOB lavas, whereas those with MORB-like
635 origin are similar to OIB, MORB and arc magmas. In other words, not all lawsonite
636 blueschists can account for the unique Th/La ratios observed in AHOB magmas, but
637 only those with terrigenous input. Melting of mélange that contains lawsonite
638 blueschist with enriched terrigenous origin is thus the most appealing explanation of
639 the trace element characteristics of the Mediterranean and AHOB potassium-rich
640 magmatism in a realistic geodynamic setting.

641 Pb isotope geochemistry supports an important role of lawsonite blueschist in the
642 elevated Th/La ratios. Th/La ratios of both the blueschist whole-rocks and lawsonites
643 yield strongly heterogeneous values where the most elevated Th/La ratios correspond
644 to the continent-derived terrigenous geochemical component (Fig. 16). The most
645 radiogenic $^{206}Pb/^{204}Pb$, $^{207}Pb/^{204}Pb$ and $^{208}Pb/^{204}Pb$ occur in the enriched blueschists
646 (Fig. 9), with 10tav07 showing similar isotopic compositions to GLOSS (Fig. 16).
647 The Pb isotope compositions of Tethyan lamproites and AHOB lavas plot above the
648 mantle array (MORBs and OIBs in Fig. 16), indicating an end-member with
649 considerable time-integrated enrichment of thorogenic Pb isotopes, and their
650 decoupling from uranogenic isotopes (Tommasini et al., 2011). This end-member also
651 has high Th/La. The most enriched blueschist sample (10tav07) does not plot close to
652 this hypothetical end-member, and the less enriched blueschist samples plot toward
653 the mantle array and MORB compositions along a hyperbolic mixing line (Fig. 16),
654 but it should be stressed that we only have the age of metamorphism to constrain the
655 initial Pb isotope compositions of the blueschists (the protolith of the blueschist must
656 be older than its metamorphic age of ~80 Ma). So hypothetically, if the blueschist
657 protoliths, especially those with enriched crust-like origin, have a much older
658 formation age (Tommasini et al., 2011), they could account for the Pb isotope

659 evolution of Tethyan lamproites and AHOB lavas. These enriched blueschists have
660 similar Pb isotopic affinities to GLOSS, whose present day Pb isotopic compositions
661 can be used to successfully explain the Pb isotope evolution of Tethyan lamproites
662 (Fig. 9 in Tommasini et al., 2011). Thus, only the blueschists with enriched origin
663 from the mé ange have the potential to provide the geochemical ingredient
664 responsible for the continental crust-like composition and elevated Th/La ratios in the
665 AHOB lavas.

666 ***Melting of a newly formed lithosphere.*** The Alpine-Himalayan orogenic belt
667 resulted from a long-lasting convergence between Eurasia and Gondwana, beginning
668 in the Permian. This convergence involved accretion of thin continental slivers that
669 mostly originated by rifting from northern Gondwanaland, and numerous oceanic
670 island arcs, which eventually formed an orogenic system consisting of multiple belts.
671 The net effect of this accretion was a complex interfingering of geologically and
672 geochemically contrasting compositions, resulting in a very heterogeneous
673 lithospheric mantle under the Mediterranean region. Generally, the mantle might be
674 heavily metasomatised by melts derived from subducted continent-derived
675 terrigenous sediments (e.g. Prelević et al., 2013), and melting of this metasomatised
676 source accounts for the widespread orogenic fingerprint identified in potassium-rich
677 post-collisional magmas (e.g. Prelević et al., 2008; 2013; Lustrino et al., 2011).

678 At least some part of this mantle is newly formed during accretion of microplates
679 or other small continental blocks, composed of a mixture of strongly depleted forearc
680 peridotites, oceanic crust, oceanic and continental sediments (Prelević et al., 2008;
681 Gonzalez et al., 2015; Wang et al., 2017). However, the significance of new
682 lithosphere of this type, in which blueschist, mélange and other blocks are all

683 imbricated together, is often underestimated or overlooked when investigating the
684 origin of potassium-rich orogenic magmatism.

685 Here, we tentatively propose that the unique high Th/La signature seen in AHOB
686 potassium-rich magmas could be derived from lawsonite blueschist with continent-
687 derived terrigenous origin. This Th/La signature could be imparted to the lavas by
688 melting of newly formed lithosphere that contains mélanges including blueschists
689 imbricated together with other types of rocks at shallow levels (< 80 km). Unlike
690 Andean-style subduction where a succession of additional reactions would modify
691 and dilute the Th/La signature, shallow tectonic imbrication preserves many of the
692 geochemical characteristics and stores them in the new lithosphere. However, the high
693 Th/La signature is not conveyed by a single-stage process from lawsonite blueschist
694 to ensuing magmas as proposed previously (Wang et al., 2017), but probably results
695 from a series of metamorphic and magmatic processes that steadily increase the Th/La
696 ratio.

697 Mediterranean potassium-rich magmatism may be triggered by two major factors,
698 namely the roll-back of the underthrust lithospheric slab which causes post-collisional
699 extension, collapse of the orogenic belts and large-scale elevation of several orogenic
700 massifs, combined with the initiation and progression of a slab tear (e.g. Prelević et al.,
701 2015 and references therein). Before the continental lithosphere blocks collided, intra-
702 oceanic subduction induced by closure of small ocean basins gave rise to many
703 geological events in the Mediterranean region during the Mesozoic. This closure of
704 small ocean basins may result in obduction of ophiolites onto a passive margin or
705 accretionary uplift and collision of continental blocks, resulting in thickened
706 continental crust. Mé ange that includes blueschists on the interface between the
707 subducting oceanic slab and the overlying mantle are likely to imbricate with oceanic

crust chunks at ~60–80 km (e.g. Fig. 8 in Gonzalez et al., 2015; Fig. 11 in Wang et al., 2017). Heat from the convecting mantle after slab break-off or lithospheric delamination and slab roll-back would preferentially melt previously enriched domains (mélanges) stored at shallow depths within the lithospheric mantle. The preferential melting of fertile, enriched components results in the generation of potassium-rich mafic magmas with diagnostic geochemical characteristics.

IMPLICATIONS

This study provides a new, comprehensive geochemical dataset of whole-rock major and trace element compositions and the first radiogenic isotopic measurements on eastern Mediterranean lawsonite blueschists. This allows us to recognize two groups of blueschist with differing protoliths of MORB-like and continent-derived terrigenous origin. As the most important hydrous mineral in hosting Th, U, Sr and LREE in blueschist, lawsonite has great potential to explain the enigmatic geochemistry of Mediterranean potassium-rich magmatism because it is the only mineral that can carry the unusually high Th/La signature, which is unique to AHOB potassium-rich magmas (Fig. 15). However, only those lawsonite blueschists with continental input can explain this Th/La feature.

Given the significance of lawsonite blueschist in transporting such a unique signature, mélange should be considered when discussing the geodynamics of magma origin, as this is an environment where subducted sediments, oceanic crust, blueschist and mantle peridotite are tectonically imbricated together.

Trace element data of lawsonite blueschist in the AHOB is rather scarce, hindering acceptance of the hypothesis that blueschist-bearing mélange is important. However, the extremely high Th/La feature has not been observed in any minerals

733 other than lawsonite and all accessory minerals can be discounted. Lawsonite has also
734 been reported to carry a high Th/La signature (up to 4.88) from nearby Sivrihisar in
735 Turkey and Alpine Corsica in France (Vitale Brovarone et al., 2014; Martin et al.,
736 2014). It is thus reasonable to link lawsonite blueschist to the genesis of AHOB
737 potassium-rich magmatism, and to consider the melting of newly-formed lithosphere
738 that contains blueschist-bearing mélanges in other areas.

ACKNOWLEDGEMENTS

We are very grateful to Steve Galer, Heinz Feldmann, Reimund Jotter and Peter Wieland for their help with isotope measurements. Regina Mertz, Will Powell, David Adams and Norman Pearson are thanked for their instruction during laser and microprobe analyses. Simone Tommasini and Alexis Plunder gave insightful comments on an early version of this manuscript. We appreciate Estibalitz Ukar and an anonymous reviewer for their constructive reviews and the editorial support of Gregory Dumond. This work was supported by the Strategic Priority Research Program (B) of Chinese Academy of Sciences (Grant No. XDB18000000), National Natural Science Foundation of China (Grant No. 41773055) and the ARC Centre of Excellence for Core to Crust Fluid Systems/GEMOC. This is contribution XXX from the ARC Centre of Excellence for Core to Crust Fluid Systems and XXXX in the GEMOC Key Centre. The Macquarie University HDR Fund supported experimental and analytical work. Fieldwork in Turkey was funded by the Deutsche Forschungsgemeinschaft. Details of analytical techniques, seven supplementary figures and all the data for this paper are available in supporting information S1 and S2.

REFERENCES CITED

Agard, P., Yamato, P., Jolivet, L., Burov, E., 2009. Exhumation of oceanic blueschists and eclogites in subduction zones: timing and mechanisms. Earth-Science Reviews, 92(1-2): 53-79.

Altunkaynak, S., Genç, S. ., 2008. Petrogenesis and time-progressive evolution of the Cenozoic continental volcanism in the Biga Peninsula, NW Anatolia (Turkey). Lithos, 102(1-2): 316-340.

Baur, W.H., 1978. Crystal structure refinement of lawsonite. American Mineralogist, 63(3-4): 311-315.

Becker, H., Jochum, K.P., Carlson, R.W., 2000. Trace element fractionation during dehydration of eclogites from high-pressure terranes and the implications for element fluxes in subduction zones. Chemical Geology, 163(1): 65-99.

Beinlich, A., Klemd, R., John, T., Gao, J., 2010. Trace-element mobilization during Ca-metasomatism along a major fluid conduit: Eclogitization of blueschist as a consequence of fluid–rock interaction. Geochimica et Cosmochimica Acta, 74(6): 1892-1922.

Belousova, E., Griffin, W.L., O'Reilly, S.Y., Fisher, N.L., 2002. Igneous zircon: trace element composition as an indicator of source rock type. Contributions to Mineralogy and Petrology, 143(5): 602-622.

Bernard-Griffiths, J., Carpenter, M.S.N., Peucat, J.J., Jahn, B.M., 1986. Geochemical and isotopic characteristics of blueschist facies rocks from the Île de Groix, Armorican Massif (northwest France). Lithos, 19(3): 235-253.

Bulle, F., Bröcker, M., Gärtner, C., Keasling, A., 2010. Geochemistry and geochronology of HP mélanges from Tinos and Andros, cycladic blueschist belt, Greece. Lithos, 117(1-4): 61-81.

781 Çeli , Ö.F. et al., 2016. Jurassic metabasic rocks in the Kızılırmak accretionary
782 complex (Kargı region, Central Pontides, Northern Turkey). Tectonophysics,
783 672: 34-49.
784 Çetinkaplan, M., Candan, O., Oberhänsli, R., Bousquet, R., 2008. Pressure-
785 temperature evolution of lawsonite eclogite in Sivrihisar; Tavşanlı Zone-
786 Turkey. Lithos, 104(1-4): 12-32.
787 Cloos, M., Shreve, R.L., 1988. Subduction-channel model of prism accretion,
788 melange formation, sediment subduction, and subduction erosion at
789 convergent plate margins: 1. Background and description. Pure and Applied
790 Geophysics, 128(3-4): 455-500.
791 Conticelli, S., 1998. The effect of crustal contamination on ultrapotassic magmas with
792 lamproitic affinity: mineralogical, geochemical and isotope data from the
793 Torre Alfina lavas and xenoliths, Central Italy. Chemical Geology, 149(1): 51-
794 81.
795 Conticelli, S., D'Antonio, M., Pinarelli, L., Civetta, L., 2002. Source contamination
796 and mantle heterogeneity in the genesis of Italian potassic and ultrapotassic
797 volcanic rocks: Sr–Nd–Pb isotope data from Roman Province and Southern
798 Tuscany. Mineralogy and Petrology, 74(2-4): 189-222.
799 Collins, A.S., Robertson, A.H.F., 1997. Lycian melange, southwestern Turkey: an
800 emplaced Late Cretaceous accretionary complex. Geology, 25(3): 255-258.
801 Davis, P.B., Whitney, D.L., 2006. Petrogenesis of lawsonite and epidote eclogite and
802 blueschist, Sivrihisar Massif, Turkey. Journal of Metamorphic Geology, 24(9):
803 823-849.
804 Dubacq, B., Plunder, A., 2018. Controls on Trace Element Distribution in Oxides and
805 Silicates. Journal of Petrology, 59(2): 233-256.

806 Ernst, W.G., 1988. Tectonic history of subduction zones inferred from retrograde
807 blueschist P-T paths. Geology, 16(12): 1081-1084.
808 Fornash, K.F., Cosca, M.A., Whitney, D.L., 2016. Tracking the timing of subduction
809 and exhumation using $^{40}Ar/^{39}Ar$ phengite ages in blueschist- and eclogite-
810 facies rocks (Sivrihisar, Turkey). Contributions to Mineralogy and Petrology,
811 171(7), 67.
812 Fryer, P., Wheat, C.G., Mottl, M.J., 1999. Mariana blueschist mud volcanism:
813 Implications for conditions within the subduction zone. Geology, 27(2): 103-
814 106.
815 Gonzalez, C.M., Gorczyk, W., Gerya, T.V., 2015. Decarbonation of subducting slabs:
816 Insight from petrological-thermomechanical modeling. Gondwana Research,
817 36: 314-332.
818 Galer, S.J.G., 1999. Optimal double and triple spiking for high precision lead isotopic
819 measurement. Chemical Geology, 157(3): 255-274.
820 Ge, M.-h. et al., 2016. Geochemistry and geochronology of the blueschist in the
821 Heilongjiang Complex and its implications in the late Paleozoic tectonics of
822 eastern NE China. Lithos, 261: 232-249.
823 Gieré, R., Sorensen, S.S., 2004. Allanite and Other REE-Rich Epidote-Group
824 Minerals. Reviews in Mineralogy and Geochemistry, 56(1): 431-493.
825 Goffe B., Michard A., Kienast J.R. and Le Mer O., 1988. A case of obduction-related
826 high-pressure, low-temperature metamor- phism in upper crustal nappes,
827 Arabian continental margin, Oman: P-T paths and kinematic interpretation.
828 Tectonophysics, 151: 363-386.
829 Göncüoglu M.C., Yalınız, M.K., Tekin, U.K., 2006. Geochemistry, tectono-
830 Magmatic discrimination and radiolarian ages of basic extrusives within the

831 Izmir-Ankara Suture Belt (NW Turkey): Time constraints for the Neotethyan
832 evolution. Ofioliti, 31(1): 25-38.
833 Göncüoglu, M.C., Sayit, K., Tekin, U.K., 2010. Oceanization of the northern
834 Neotethys: Geochemical evidence from ophiolitic melange basalts within the
835 İzmir–Ankara suture belt, NW Turkey. Lithos, 116(1): 175-187.
836 Gonzalez, C.M., Gorczyk, W., Gerya, T.V., 2015. Decarbonation of subducting slabs:
837 Insight from petrological–thermomechanical modeling. Gondwana Research,
838 36: 314-332.
839 Guo, Z. et al., 2014. The role of subduction channel mélanges and convergent
840 subduction systems in the petrogenesis of post-collisional K-rich mafic
841 magmatism in NW Tibet. Lithos, 198-199(0): 184-201.
842 Haggerty, S.E., Fung, A.T., Burt, D.M., 1994. Apatite, phosphorus and titanium in
843 eclogitic garnet from the upper mantle. Geophysical Research Letters, 21(16):
844 1699-1702.
845 Hart, S.R., 1984. A large-scale isotope anomaly in the Southern Hemisphere mantle.
846 Nature, 309(5971): 753.
847 Harris, R.A., Sawyer, R.K., Audley-Charles, M.G., 1998. Collisional melange
848 development: Geologic associations of active melange-forming processes with
849 exhumed melange facies in the western Banda orogen, Indonesia. Tectonics,
850 17(3): 458-479.
851 Hauri, E.H., Wagner, T.P., Grove, T.L., 1994. Experimental and natural partitioning
852 of Th, U, Pb and other trace elements between garnet, clinopyroxene and
853 basaltic melts. Chemical Geology, 117(1-4): 149-166.
854 Hermann, J., 2002. Allanite: thorium and light rare earth element carrier in subducted
855 crust. Chemical Geology, 192(3-4): 289-306.

856 Hofmann, A.W., Jochum, K.P., Seufert, M., White, W.M., 1986. Nb and Pb in
857 oceanic basalts: new constraints on mantle evolution. Earth and Planetary
858 Science Letters, 79(1): 33-45.
859 Honegger, K., Le Fort, P., Mascle, G., Zimmermann, J.L., 1989. The blueschists
860 along the Indus Suture Zone in Ladakh, NW Himalaya. Journal of
861 Metamorphic Geology, 7(1): 57-72.
862 Jochum, K.P. et al., 2011. Determination of Reference Values for NIST SRM 610-
863 617 Glasses Following ISO Guidelines. Geostandards and Geoanalytical
864 Research, 35(4): 397-429.
865 Karson, J.A., 2002. Geologic structure of the uppermost oceanic crust created at fast-
866 to intermediate-rate spreading centers. Annual Review of Earth and Planetary
867 Sciences, 30(1): 347-384.
868 Kieffer, B., N. Arndt, H. Lapierre, F. Bastien, D. Bosch, A. Pecher, G. Yirgu, D.
869 Ayalew, D. Weis, and D. A. Jerram (2004), Flood and Shield Basalts from
870 Ethiopia: Magmas from the African Superswell, Journal of Petrology, 45(4),
871 793-834(742).
872 King, R.L., Bebout, G.E., Moriguti, T., Nakamura, E., 2006. Elemental mixing
873 systematics and Sr–Nd isotope geochemistry of mélnge formation: Obstacles
874 to identification of fluid sources to arc volcanics. Earth and Planetary Science
875 Letters, 246(3): 288-304.
876 Kim, D., I. Katayama, S. Wallis, K. Michibayashi, A. Miyake, Y. Seto, and S. Azuma
877 (2015), Deformation microstructures of glaucophane and lawsonite in
878 experimentally deformed blueschists: Implications for intermediate-depth
879 intraplate earthquakes, Journal of Geophysical Research: Solid Earth, 120(2),
880 1229-1242.

881 Kleine, B.I., Skelton, A.D.L., Huet, B., Pitcairn, I.K., 2014. Preservation of
882 Blueschist-facies Minerals along a Shear Zone b Coupled Metasomatism and
883 Fast-flowing CO_2-bearing Fluids. Journal of Petrology.
884 Klemme, S., Blundy, J.D., Wood, B.J., 2002. Experimental constraints on major and
885 trace element partitioning during partial melting of eclogite. Geochimica et
886 Cosmochimica Acta, 66(17): 3109-3123.
887 Klemd, R., 2013. Metasomatism During High-Pressure Metamorphism: Eclogites and
888 Blueschist-Facies Rocks, Metasomatism and the Chemical Transformation of
889 Rock. Lecture Notes in Earth System Sciences. Springer Berlin Heidelberg,
890 pp. 351-413.
891 Leake, B.E. et al., 1997. Report. Nomenclature of amphiboles: report of the
892 subcommittee on amphiboles of the international mineralogical association
893 commission on new minerals and mineral names. Mineralogical magazine,
894 61(2): 295-321.
895 Lugmair, G.W., Galer, S.J.G., 1992. Age and isotopic relationships among the
896 angrites Lewis Cliff 86010 and Angra dos Reis. Geochimica Et Cosmochimica
897 Acta, 56(4): 1673-1694.
898 Lugmair, G.W., Marti, K., 1978. Lunar initial $^{143}Nd/^{144}Nd$: Differential evolution of
899 the lunar crust and mantle. Earth and Planetary Science Letters, 39(3): 349-
900 357.
901 Lustrino, M., Duggen, S., Rosenberg, C.L., 2011. The Central-Western
902 Mediterranean: anomalous igneous activity in an anomalous collisional
903 tectonic setting. Earth-Science Reviews, 104(1): 1-40.
904 Maekawa, H., Shozul, M., Ishii, T., Fryer, P., Pearce, J.A., 1993. Blueschist
905 Metamorphism in an Active Subduction Zone. Nature, 364(6437): 520-523.

906 Martin, L.A.J. et al., 2014. Lawsonite geochemistry and stability implication for trace
907 element and water cycles in subduction zones. Journal of Metamorphic
908 Geology, 32(5): 455-478.
909 Martin, L.A.J., Wood, B.J., Turner, S., Rushmer, T., 2011. Experimental
910 Measurements of Trace Element Partitioning Between Lawsonite, Zoisite and
911 Fluid and their Implication for the Composition of Arc Magmas. Journal of
912 Petrology, 52(6): 1049-1075.
913 Maruyama, S., Liou, J.G., Terabayashi, M., 1996. Blueschists and Eclogites of the
914 World and Their Exhumation. International Geology Review, 38(6): 485-594.
915 Maulana, A., Christy, A.G., Ellis, D.J., Imai, A., Watanabe, K., 2013. Geochemistry
916 of eclogite- and blueschist-facies rocks from the Bantimala Complex, South
917 Sulawesi, Indonesia: Protolith origin and tectonic setting. Island Arc, 22(4):
918 427-452.
919 Miller, C., R. Schuster, U. Klötzli, W. Frank, and F. Purtscheller (1999), Post-
920 collisional potassic and ultrapotassic magmatism in SW Tibet: geochemical
921 and Sr–Nd–Pb–O isotopic constraints for mantle source characteristics and
922 petrogenesis, Journal of Petrology, 40(9), 1399-1424.
923 Miller, D.P., Marschall, H.R., Schumacher, J.C., 2009. Metasomatic formation and
924 petrology of blueschist-facies hybrid rocks from Syros (Greece): Implications
925 for reactions at the slab–mantle interface. Lithos, 107(1-2): 53-67.
926 Mulcahy, S.R., Vervoort, J.D., Renne, P.R., 2014. Dating subduction zone
927 metamorphism with combined garnet and lawsonite Lu-Hf geochronology.
928 Journal of Metamorphic Geology, 32(5): 515-533.
929 Okay, A.I., 1978. Sodic pyroxenes from metabasites in the eastern Mediterranean.
930 Contributions to Mineralogy and Petrology, 68(1): 7-11.

931 Okay, A.I., 1980a. Mineralogy, petrology, and phase relations of glaucophane-
932 lawsonite zone blueschists from the Tavşanli Region, Northwest Turkey.
933 Contributions to Mineralogy and Petrology, 72(3): 243-255.
934 Okay, A.I., 1980b. Lawsonite zone blueschists and a sodic amphibole producing
935 reaction in the Tavşanli Region, Northwest Turkey. Contributions to
936 Mineralogy and Petrology, 75(3): 179-186.
937 Okay, A.I., 1982. Incipient blueschist metamorphism and metasomatism in the
938 Tavşanli region, Northwest Turkey. Contributions to Mineralogy and
939 Petrology, 79(4): 361-367.
940 Okay, A.I., 1986. High-pressure/low-temperature metamorphic rocks of Turkey.
941 Geological Society of America Memoirs, 164: 333-347.
942 Okay, A.I., 1989. Alpine-Himalayan Blueschists. Annual Review of Earth and
943 Planetary Sciences, 17(1): 55-87.
944 Okay, A.I., 2002. Jadeite-chloritoid-glaucophane-lawsonite blueschists in north-west
945 Turkey: unusually high P/T ratios in continental crust. Journal of Metamorphic
946 Geology, 20(8): 757-768.
947 Okay, A.I., Harris, N.B.W., Kelley, S.P., 1998. Exhumation of blueschists along a
948 Tethyan suture in northwest Turkey. Tectonophysics, 285(3-4): 275-299.
949 Okay, A.I., Tüysüz, O., 1999. Tethyan sutures of northern Turkey. Geological
950 Society, London, Special Publications, 156(1): 475-515.
951 Okay, A.I., Whitney, D.L., 2010. Blueschists, Eclogites, Ophiolites and Suture Zones
952 in Northwest Turkey: A Review and a Field Excursion Guide. Ofioliti, 35(2):
953 131-171.
954 Okazaki, K., Hirth, G., 2016. Dehydration of lawsonite could directly trigger
955 earthquakes in subducting oceanic crust. Nature, 530(7588): 81-84.

Özbey, Z., Ustaömer, T., Robertson, A.H.F., 2013. Mesozoic magmatic and sedimentary development of the Tavşanlı Zone (NW Turkey): implications for rifting, passive margin development and ocean crust emplacement. Geological Society, London, Special Publications, 372.

Pagé, L., Hattori, K., de Hoog, J.C.M., Okay, A.I., 2016. Halogen (F, Cl, Br, I) behaviour in subducting slabs: A study of lawsonite blueschists in western Turkey. Earth and Planetary Science Letters, 442: 133-142.

Palin, R.M., White, R.W., 2015. Emergence of blueschists on Earth linked to secular changes in oceanic crust composition. Nature Geoscience, 9: 60-64.

Parkinson, C.D., 1996. The origin and significance of metamorphosed tectonic blocks in mélanges: evidence from Sulawesi, Indonesia. Terra Nova, 8(4): 312-323.

Patočka, F., Pin, C., 2005. Sm-Nd isotope and trace element evidence for heterogeneous igneous protoliths of Variscan mafic blueschists in the East Krkonoše Complex (West Sudetes, NE Bohemian Massif, Czech Republic). Geodinamica Acta, 18(5): 363-374.

Pearce, J.A., 1975. Basalt geochemistry used to investigate past tectonic environments on Cyprus. Tectonophysics, 25(1): 41-67.

Pearce, J.A., 1983. The role of sub-continental lithosphere in magma genesis at destructive plate margins. Continental Basalts & Mantle Xenoliths, 147(6): 2162-2173.

Pearce, J.A., Cann, J.R., 1973. Tectonic Setting of Basic Volcanic Rocks determined using Trace Element Analyses. Earth & Planetary Science Letters, 19(2): 290-300.

Peccerillo, A., Martinotti, G., 2006. The Western Mediterranean lamproitic magmatism: origin and geodynamic significance. Terra Nova, 18(2): 109-117.

981 Peccerillo, A., Frezzotti, M.L., 2015. Magmatism, mantle evolution and geodynamics
982 at the converging plate margins of Italy. Journal of the Geological Society,
983 172(4): 407-427.
984 Plank, T., 2005. Constraints from Thorium/Lanthanum on Sediment Recycling at
985 Subduction Zones and the Evolution of the Continents. Journal of Petrology,
986 46(5): 921-944.
987 Plank, T., Langmuir, C.H., 1998. The chemical composition of subducting sediment
988 and its consequences for the crust and mantle. Chemical Geology, 145(3-4):
989 325-394.
990 Plunder, A., Agard, P., Chopin, C., Okay, A.I., 2013. Geodynamics of the Tavşanlı
991 zone, western Turkey: Insights into subduction/obduction processes.
992 Tectonophysics, 608(0): 884-903.
993 Plunder, A., Agard, P., Chopin, C., Pourteau, A., Okay, A.I., 2015. Accretion,
994 underplating and exhumation along a subduction interface: From subduction
995 initiation to continental subduction (Tavşanlı zone, W. Turkey). Lithos,
996 226(0): 233-254.
997 Poli, S., Schmidt, M.W., 1997. The high-pressure stability of hydrous phases in
998 orogenic belts: an experimental approach on eclogite-forming processes.
999 Tectonophysics, 273(1-2): 169-184.
1000 Pourteau, A., Candan, O., Oberhänsli, R., 2010. High-pressure metasediments in
1001 central Turkey: Constraints on the Neotethyan closure history. Tectonics,
1002 29(5): TC5004.
1003 Pourteau, A. et al., 2013. Neotethys closure history of Anatolia: insights from ^{40}Ar-
1004 ^{39}Ar geochronology and P-T estimation in high-pressure metasedimentary
1005 rocks. Journal of Metamorphic Geology, 31(6): 585-606.

1006 Prelević, D. et al., 2012. Ultrapotassic Mafic Rocks as Geochemical Proxies for Post-
1007 collisional Dynamics of Orogenic Lithospheric Mantle: the Case of
1008 Southwestern Anatolia, Turkey. Journal of Petrology, 53(5): 1019-1055.
1009 Prelević, D., Akal, C., Romer, R.L., Mertz-Kraus, R., Helvacı, C., 2015. Magmatic
1010 Response to Slab Tearing: Constraints from the Afyon Alkaline Volcanic
1011 Complex, Western Turkey. Journal of Petrology. 56(3): 527–562.
1012 Prelević, D., Foley, S.F., 2007. Accretion of arc-oceanic lithospheric mantle in the
1013 Mediterranean: Evidence from extremely high-Mg olivines and Cr-rich spinel
1014 inclusions in lamproites. Earth and Planetary Science Letters, 256(1-2): 120-
1015 135.
1016 Prelević, D., Foley, S.F., Romer, R., Conticelli, S., 2008. Mediterranean Tertiary
1017 lamproites derived from multiple source components in postcollisional
1018 geodynamics. Geochimica et Cosmochimica Acta, 72(8): 2125-2156.
1019 Prelević, D., Jacob, D.E., Foley, S.F., 2013. Recycling plus: A new recipe for the
1020 formation of Alpine-Himalayan orogenic mantle lithosphere. Earth and
1021 Planetary Science Letters, 362: 187-197.
1022 Raymond, L.A., 1984. Classification of melanges. Geological Society of America
1023 Special Papers, 198: 7-20.
1024 Rollinson, H.R., 2014. Using geochemical data: evaluation, presentation,
1025 interpretation. Routledge, London.
1026 Rubatto, D., 2002. Zircon trace element geochemistry: partitioning with garnet and
1027 the link between U–Pb ages and metamorphism. Chemical Geology, 184(1):
1028 123-138.

1029 Saunders, A.D., Norry, M.J., Tarney, J., 1988. Origin of MORB and Chemically-
1030 Depleted Mantle Reservoirs: Trace Element Constraints. Journal of Petrology,
1031 Special Volume(1): 415-445.
1032 Schumacher, J.C., 1997. Appendix 2: the estimation of ferric iron in electron
1033 microprobe analysis of amphiboles. Mineralogical Magazine, 61(405): 312-
1034 321.
1035 Schmidt, M.W., 1995. Lawsonite: Upper pressure stability and formation of higher
1036 density hydrous phases. American Mineralogist, 80(11-12): 1286-1292.
1037 Schmidt, M.W., Poli, S., 1994. The stability of lawsonite and zoisite at high pressures:
1038 Experiments in CASH to 92 kbar and implications for the presence of hydrous
1039 phases in subducted lithosphere. Earth and Planetary Science Letters, 124(1-
1040 4): 105-118.
1041 Seaton, N.C.A., Whitney, D.L., Teyssier, C., Toraman, E., Heizler, M.T., 2009.
1042 Recrystallization of high-pressure marble (Sivrihisar, Turkey).
1043 Tectonophysics, 479: 241-253.
1044 Searle M., Waters D.J., Martin H.N. and Rex D.C., 1994. Structure and
1045 metamorphism of blueschist-eclogite facies rocks from the northeastern Oman
1046 Mountains. Journal of the Geological Society, 151: 555- 576.
1047 Şengör, A.M., Yilmaz, Y., 1981. Tethyan evolution of Turkey: a plate tectonic
1048 approach. Tectonophysics, 75(3): 181-241.
1049 Sherlock, S., Kelley, S., Inger, S., Harris, N., Okay, A., 1999. ^{40}Ar-^{39}Ar and Rb-Sr
1050 geochronology of high-pressure metamorphism and exhumation history of the
1051 Tavsanli Zone, NW Turkey. Contributions to Mineralogy and Petrology,
1052 137(1-2): 46-58.

1053 Shervais, J.W., 1982. Ti-V plots and the petrogenesis of modern and ophiolitic lavas.
1054 Earth and Planetary Science Letters, 59(1): 101-118.
1055 Song, S. et al., 2009. Tectonic evolution of early Paleozoic HP metamorphic rocks in
1056 the North Qilian Mountains, NW China: New perspectives. Journal of Asian
1057 Earth Sciences, 35(3): 334-353.
1058 Sorensen, S.S., Grossman, J.N., Perfit, M.R., 1997. Phengite-hosted LILE Enrichment
1059 in Eclogite and Related Rocks: Implications for Fluid-Mediated Mass Transfer
1060 in Subduction Zones and Arc Magma Genesis. Journal of Petrology, 38(1): 3-
1061 34.
1062 Spandler, C., Hermann, J., Arculus, R., Mavrogenes, J., 2003. Redistribution of trace
1063 elements during prograde metamorphism from lawsonite blueschist to eclogite
1064 facies; implications for deep subduction-zone processes. Contributions to
1065 Mineralogy and Petrology, 146(2): 205-222.
1066 Steiger, R.H., Jäger, E., 1977. Subcommission on geochronology: Convention on the
1067 use of decay constants in geo- and cosmochronology. Earth and Planetary
1068 Science Letters, 36(3): 359-362.
1069 Stern, R.J., 2005. Evidence from ophiolites, blueschists, and ultrahigh-pressure
1070 metamorphic terranes that the modern episode of subduction tectonics began
1071 in Neoproterozoic time. Geology, 33(7): 557-560.
1072 Stracke, A., Bizimis, M., Salters, V.J.M., 2003. Recycling oceanic crust: Quantitative
1073 constraints. Geochemistry, Geophysics, Geosystems, 4(3): 8003.
1074 Sun, S.S., McDonough, W.F., 1989. Chemical and isotopic systematics of oceanic
1075 basalts: implications for mantle composition and processes. Geological
1076 Society, London, Special Publications, 42(1): 313-345.

1077 Tang, X.-C., Zhang, K.-J., 2013. Lawsonite- and glaucophane-bearing blueschists
1078 from NW Qiangtang, northern Tibet, China: mineralogy, geochemistry,
1079 geochronology, and tectonic implications. International Geology Review,
1080 56(2): 150-166.
1081 Tankut, A., Dilek, Y., Önen, P., 1998. Petrology and geochemistry of the Neo-
1082 Tethyan volcanism as revealed in the Ankara melange, Turkey. Journal of
1083 Volcanology and Geothermal Research, 85(1): 265-284.
1084 Thirlwall, M. F., B. G. J. Upton, and C. Jenkins (1994), Interaction between
1085 continental lithosphere and the Iceland plume — Sr-Nd-Pb isotope
1086 geochemistry of Tertiary basalts, NE Greenland, Journal of Petrology, 35(3),
1087 839-879.
1088 Tommasini, S., Avanzinelli, R., Conticelli, S., 2011. The Th/La and Sm/La
1089 conundrum of the Tethyan realm lamproites. Earth and Planetary Science
1090 Letters, 301(3-4): 469-478.
1091 Topuz, G., Okay, A.I., Altherr, R., Satir, M., Schwarz, W.H., 2008. Late Cretaceous
1092 blueschist facies metamorphism in southern Thrace (Turkey) and its
1093 geodynamic implications. Journal of Metamorphic Geology, 26(9): 895-913.
1094 Tribuzio, R., Giacomini, F., 2002. Blueschist facies metamorphism of peralkaline
1095 rhyolites from the Tenda crystalline massif (northern Corsica): evidence for
1096 involvement in the Alpine subduction event? Journal of Metamorphic
1097 Geology, 20(5): 513-526.
1098 Tribuzio, R., Messiga, B., Vannucci, R., Bottazzi, P., 1996. Rare earth element
1099 redistribution during high-pressure-low-temperature metamorphism in
1100 ophiolitic Fe-gabbros (Liguria, northwestern Italy): Implications for light REE
1101 mobility in subduction zones. Geology, 24(8): 711.

Tsujimori, T., Ernst, W.G., 2014. Lawsonite blueschists and lawsonite eclogites as proxies for palaeo-subduction zone processes: a review. Journal of Metamorphic Geology, 32(5): 437-454.

Tsujimori, T., Sisson, V., Liou, J., Harlow, G., Sorensen, S., 2006. Very-low-temperature record of the subduction process: A review of worldwide lawsonite eclogites. Lithos, 92(3-4): 609-624.

Turner, S. et al., 1996. U-series isotopes and destructive plate margin magma genesis in the Lesser Antilles. Earth and Planetary Science Letters, 142(1): 191-207.

Ueno, T., 1999. REE-bearing sector-zoned lawsonite in the Sanbagawa pelitic schists of the eastern Kii Peninsula, central Japan. European Journal of Mineralogy, 11(6): 993-998.

Ukar, E., 2012. Tectonic significance of low-temperature blueschist blocks in the Franciscan mélange at San Simeon, California. Tectonophysics, 568–569(0): 154-169.

Ukar, E., Cloos, M., 2015. Magmatic origin of low-T mafic blueschist and greenstone blocks from the Franciscan mélange, San Simeon, California. Lithos, 230(0): 17-29.

Usui, T., Kobayashi, K., Nakamura, E., Helmstaedt, H., 2007. Trace element fractionation in deep subduction zones inferred from a lawsonite-eclogite xenolith from the Colorado Plateau. Chemical Geology, 239(3-4): 336-351.

Van Hinsbergen, D.J.J., 2010. A key extensional metamorphic complex reviewed and restored: the Menderes Massif of western Turkey. Earth-Science Reviews, 102(1-2): 60-76.

Van Westrenen, W., Blundy, J.D., Wood, B.J., 2001. High field strength element/rare earth element fractionation during partial melting in the presence of garnet:

1127 Implications for identification of mantle heterogeneities. Geochemistry,
1128 Geophysics, Geosystems, 2(7): 223-235.
1129 Vitale Brovarone, A., Alard, O., Beyssac, O., Martin, L., Picatto, M., 2014. Lawsonite
1130 metasomatism and trace element recycling in subduction zones. Journal of
1131 Metamorphic Geology: 489-514.
1132 Volkova, N.I., Budanov, V.I., 1999. Geochemical discrimination of metabasalt rocks
1133 of the Fan–Karategin transitional blueschist/greenschist belt, South Tianshan,
1134 Tajikistan: seamount volcanism and accretionary tectonics. Lithos, 47(3-4):
1135 201-216.
1136 Volkova, N.I., Stupakov, S.I., Babin, G.A., Rudnev, S.N., Mongush, A.A., 2009.
1137 Mobility of trace elements during subduction metamorphism as exemplified
1138 by the blueschists of the Kurtushibinsky Range, Western Sayan. Geochemistry
1139 International, 47(4): 380-392.
1140 Wang, Y., Prelević, D., Buhre, S., Foley, S.F., 2017. Constraints on the sources of
1141 post-collisional K-rich magmatism: The roles of continental clastic sediments
1142 and terrigenous blueschists. Chemical Geology, 455: 192-207.
1143 Wehrmeister, U., Jacob, D. E., Soldati, A. L., Loges, N., Häger, T., Hofmeister, W.,
1144 2011. Amorphous, nanocrystalline and crystalline calcium carbonates in
1145 biological materials. Journal of Raman Spectroscopy, 42(5): 926-935.
1146 Whitney, D.L., Teyssier, C., Seaton, N.C.A., Fornash, K.F., 2014. Petrofabrics of
1147 high-pressure rocks exhumed at the slab-mantle interface from the “point of
1148 no return” in a subduction zone (Sivrihisar, Turkey). Tectonics, 33: 2315-
1149 2341.

1150 Winchester, J.A., Floyd, P.A., 1976. Geochemical magma type discrimination:
1151 application to altered and metamorphosed basic igneous rocks. Earth and
1152 Planetary Science Letters, 28(3): 459-469.
1153 Wood, D.A., 1980. The application of a Th Hf Ta diagram to problems of
1154 tectonomagmatic classification and to establishing the nature of crustal
1155 contamination of basaltic lavas of the British Tertiary Volcanic Province.
1156 Earth & Planetary Science Letters, 50(1): 11-30.
1157 Xia, Q.-X., Zhou, L.-G., 2017. Different origins of garnet in high pressure to ultrahigh
1158 pressure metamorphic rocks. Journal of Asian Earth Sciences, 145: 130-148.
1159 Xiao, Y. et al., 2014. Trace element budgets and (re-)distribution during subduction-
1160 zone ultrahigh pressure metamorphism: Evidence from Western Tianshan,
1161 China. Chemical Geology, 365(0): 54-68.
1162 Yaxley, G.M., Green, D.H., 1998. Reactions between eclogite and peridotite: mantle
1163 refertilisation by subduction of oceanic crust. 78: 243-255.
1164 Zhang, L., Wang, Q., Song, S., 2009. Lawsonite blueschist in Northern Qilian, NW
1165 China: P–T pseudosections and petrologic implications. Journal of Asian
1166 Earth Sciences, 35(3-4): 354-366.
1167 Zheng, B. et al., 2010. Subducted Precambrian oceanic crust: Geochemical and Sr Nd
1168 isotopic evidence from metabasalts of the Aksu blueschist, NW China. Journal
1169 of the Geological Society, 167(6): 1161-1170.
1170 Zhu, C.Y. et al., 2015. Geochronology and geochemistry of the Yilan blueschists in
1171 the Heilongjiang Complex, northeastern China and tectonic implications.
1172 Lithos, 216-217: 241-253.

This is a preprint, the final version is subject to change, of the American Mineralogist (MSA)
Cite as Authors (Year) Title. American Mineralogist, in press.
DOI: https://doi.org/10.2138/am-2019-6818

Sample	Location	Coordinates	Mineral assemblage (mode %)
10tav04	Tavşanlı Zone, Turkey	39°43'49.72"N; 29°49'19.93"E	Amp (26), Chl (24), Phen (18), Law (8), Tnt (6), Arg (6), Cpx (5), Apa (5), *Py, Hem*
10tav05	Tavşanlı Zone, Turkey	39°43'49.72"N; 29°49'19.93"E	Chl (26), Amp (18), Law (15), Arg (12), Qrz (8), Phen (8), Apa (6), Tnt (3), *Ga*
10tav06	Tavşanlı Zone, Turkey	39°45'27.23"N; 29°50'53.70"E	Amp (30), Law (25), Chl (14), Arg (8), Phen (7), Apa (6), Tnt (4), Qrz (4), *Py, Hem*
10tav07	Tavşanlı Zone, Turkey	39°43'49.72"N; 29°49'19.93"E	Amp (30), Law (25), Qrz (15), Phen (10), Chl (8), Arg (8), Apa (6), Tnt (3), Mn-Grt (1), P*y, Hem*
10tav08	Tavşanlı Zone, Turkey	39°45'27.23"N; 29°50'53.70"E	Law (26), Amp (18), Chl (16), Phen (10), Arg (10), Apa (8), Qrz (6), Tnt (3), *Py, Hem*
10tav09	Tavşanlı Zone, Turkey	39°43'49.72"N; 29°49'19.93"E	Amp (28), Law (25), Chl (12), Phen (10), Arg (10), Apa (6), Qrz (4), Tnt (3), *Py, Hem*

Minerals in Italic denote opaque accessory minerals identified in samples. Amp: amphibole; Chl: chlorite; Phen: phengite; Law: lawsonite; Tnt: titanite; Arg: aragonite; Cpx: clinopyroxene; Apa: apatite; Py: pyrite; Hem: hematite; Qrz: quartz; Mn-Grt: Mn-rich garnet; Ga: galena.

Table 1. Mineral assemblages and mineral modal abundances of blueschist samples.

This is a preprint, the final version is subject to change, of the American Mineralogist (MSA)
Cite as Authors (Year) Title. American Mineralogist, in press.
DOI: https://doi.org/10.2138/am-2019-6818

1176

Sample	10tav04	10tav05	10tav06	10tav07	10tav08	10tav09
Number of analyses	5	5	5	5	5	5
SiO_2	47.6	43.8	45.4	57.5	46.5	44.8
TiO_2	1.5	0.9	1.4	1.2	1.4	1.4
Al_2O_3	13.9	14.9	13.9	12.9	15.5	15.3
FeO_T	13.3	9.3	11.2	8.2	11.1	11.2
MnO	0.19	0.21	0.18	0.15	0.15	0.16
MgO	7.1	6.3	7.0	5.6	5.4	4.7
CaO	5.3	11.9	11.2	6.0	10.0	12.2
Na_2O	3.8	2.1	2.7	3.1	2.3	2.8
K_2O	2.9	0.7	0.1	0.9	0.1	0.1
P_2O_5	0.2	0.1	0.1	0.2	0.1	0.1
Cr_2O_3	0.02	0.07	0.04	0.03	0.04	0.05
NiO	0.01	0.02	0.02	0.02	0.01	0.01
LOI	4.0	10.0	7.2	3.9	8.0	7.6
Sum	99.9	100.2	100.4	99.7	100.4	100.3
Li	27	25	22	27	33	37
Sc	45	40	42	27	43	35
Ti	10287	6399	9999	10364	10872	6770
V	372	235	248	205	287	227
Cr	145	512	270	254	309	210
Mn	1360	1620	1346	1233	1303	845
Co	42	51	39	28	49	35
Ga	18	14	15	17	18	13
Rb	75	17	2.6	22	2.1	2.1
Sr	42	343	185	144	84	71
Y	35	24	28	37	34	26
Zr	80	58	75	212	97	65
Nb	5.9	20	5.1	32	4.5	2.8
Cs	3.2	0.68	0.14	0.5	0.11	0.16
Ba	297	56	11	144	5.3	17
La	6.2	15	4.4	36	5.2	6.8

Ce	15	26	11	69	13	11
Pr	2.3	3.0	1.7	8.5	2.1	2.2
Nd	12	13	9.4	35	11	10
Sm	4.0	3.0	3.3	7.8	3.7	3.1
Eu	1.4	1.1	1.1	2.1	1.4	1.1
Gd	5.4	3.7	4.0	7.5	5.0	3.7
Tb	0.95	0.60	0.74	1.1	0.91	0.66
Dy	6.6	4.1	5.0	7.0	6.2	4.4
Ho	1.4	0.91	1.1	1.4	1.4	0.94
Er	3.9	2.7	3.1	3.9	3.9	2.7
Tm	0.53	0.38	0.47	0.55	0.53	0.39
Yb	3.5	2.6	3.3	3.6	3.7	2.6
Lu	0.47	0.38	0.46	0.52	0.53	0.40
Hf	2.3	1.6	2.2	5.1	2.7	1.8
Ta	0.32	1.1	0.31	2.0	0.27	0.15
Pb	1.8	10	2.0	2.4	5.7	10
Th	0.36	1.9	0.36	7.9	0.38	0.24
U	0.27	0.37	0.18	1.6	0.26	0.33
Ba/Th	825	29	31	18	14	71
Ce/Nb	2.5	1.3	2.2	2.2	2.9	3.9
La/Sm	1.6	5.0	1.3	4.6	1.4	2.2
Rb/Sr	1.8	0.05	0.01	0.15	0.03	0.03
Ba/Rb	4.0	3.3	4.2	6.5	2.5	8.1
Nb/La	0.95	1.3	1.2	0.89	0.87	0.41
Th/Yb	0.10	0.73	0.11	2.2	0.10	0.09
La/Yb	1.8	5.8	1.3	10	1.4	2.6
Ta/Yb	0.09	0.42	0.09	0.56	0.07	0.06
Ce/Pb	8.3	2.6	5.5	29	2.3	1.1
Nb/U	22	54	28	20	17	8.5
Th/Nb	0.06	0.10	0.07	0.25	0.08	0.09

1177 **Table 2.** Major (wt%) and trace (ppm) element compositions of blueschists.

1178

Sample	10tav04	10tav05	10tav06	10tav07	10tav08	10tav09
Number of analyses	20	8	15	22	11	14
SiO_2	38.29	37.46	37.84	37.94	37.87	37.90
TiO_2	0.29	0.11	0.08	0.17	0.22	0.10
Al_2O_3	30.02	30.68	30.28	30.16	29.99	31.09
FeO	1.26	1.75	1.77	1.11	1.12	1.39
MnO	0.01	0.02	0.01	0.01	0.01	NA
MgO	0.01	0.01	NA	0.01	0.01	NA
CaO	16.57	17.56	17.28	16.95	16.88	17.58
Na_2O	0.01	NA	NA	NA	NA	0.01
K_2O	0.01	0.01	0.01	NA	NA	0.01
Cr_2O_3	0.04	0.05	0.05	0.09	0.13	0.08
Total	86.51	87.65	87.32	86.43	86.24	88.16
Si	2.05	1.99	2.02	2.04	2.04	2.00
Ti	0.01	<0.01	<0.01	0.01	0.01	<0.01
Al	1.89	1.92	1.90	1.91	1.90	1.93
Fe	0.06	0.08	0.08	0.05	0.05	0.06
Ca	0.95	1.00	0.99	0.98	0.97	0.99
Total	4.96	5.00	4.99	4.98	4.98	5.00

Structural formula based on 5 cations and 8 oxygen

Table 3. Major element (wt%) compositions of lawsonite in blueschists.

Sample	10tav04		10tav05		10tav06		10tav07		10tav08		10tav09	
N	75	1 SD	53	1 SD	54	1 SD	120	1 SD	45	1 SD	65	1 SD
Li	2.0	0.42	6.6	1.1	0.52	0.13	1.4	0.36	1.5	0.22	2.3	0.38
Sc	5.3	0.77	2.1	0.33	3.5	0.44	3.7	0.55	4.6	1.1	3.3	0.53
Ti	2856	463	292	45	2004	328	4743	791	1469	235	2083	373
V	630	84	340	67	471	63	329	56	588	77	423	55
Cr	95	13	165	32	295	58	340	49	502	109	443	61
Mn	113	26	571	49	72	11	70	14	121	31	96	13
Co	2.2	0.46	16	2.2	0.69	0.23	2.3	0.42	2.2	0.34	2.1	0.34
Ga	26	5.9	23	3.8	27	4.4	32	5.1	29	3.0	26	4.6
Rb	0.51	0.26	0.46	0.23	0.12	0.08	0.59	0.18	0.42	0.18	0.21	0.10
Sr	398	75	2215	339	76	5.9	394	67	208	34	116	23
Y	149	28	41	7.2	26	3.8	60	18	32	4.5	40	8.9
Zr	23	6.1	0.25	0.10	24	4.1	40	16	13	2.3	21	4.2
Nb	1.4	0.83	0.22	0.08	0.73	0.14	13	3.4	0.37	0.12	0.64	0.24
Cs	0.04	0.02	0.05	0.02	0.05	0.03	0.12	0.07	0.08	0.04	0.04	0.02
Ba	3.1	0.45	45	3.8	1.3	0.22	3.2	0.55	3.2	0.45	6.4	1.8
La	77	9.7	33	4.1	2.4	0.37	35	9.2	4.7	0.67	5.2	1.5
Ce	196	54	56	7.6	6.4	0.85	87	16	14	0.22	14	1.9
Pr	27	4.8	5.6	0.85	1.1	0.30	14	2.2	2.2	0.36	2.2	0.35
Nd	127	30	22	3.2	5.5	0.69	60	23	13	0.27	12	2.4
Sm	32	8.4	4.9	0.74	2.0	0.41	16	4.5	4.6	0.78	4.2	1.2
Eu	10	3.2	2.0	0.39	0.76	0.19	4.6	0.92	1.7	0.41	1.7	0.35
Gd	36	5.5	5.4	0.71	2.9	0.17	16	3.8	6.1	0.82	5.7	0.78
Tb	5.0	0.91	0.95	0.38	0.55	0.11	2.4	0.83	0.95	0.44	1.1	0.20
Dy	28	5.2	6.4	0.92	3.9	0.32	13	4.6	5.5	1.1	7.1	0.95
Ho	5.7	1.4	1.4	0.09	0.98	0.25	2.5	1.1	1.2	0.30	1.6	0.31
Er	13	2.9	4.1	0.72	2.9	0.34	5.7	2.9	3.1	0.55	4.2	0.56
Tm	1.2	0.43	0.52	0.11	0.41	0.12	0.62	0.12	0.37	0.12	0.56	0.19
Yb	7.1	2.1	3.1	0.28	2.9	0.44	3.4	0.83	2.4	0.72	3.8	0.48
Lu	0.98	0.37	0.40	0.17	0.42	0.07	0.48	0.12	0.38	0.15	0.54	0.28
Hf	0.49	0.25	0.06	0.04	0.71	0.13	1.3	0.44	0.40	0.17	0.61	0.29
Ta	0.08	0.06	0.17	0.08	0.05	0.02	0.65	0.21	0.03	0.02	0.04	0.02
Pb	50	28	719	183	21	3.7	13	3.8	35	7.2	89	25
Th	4.3	1.7	0.83	0.45	0.13	0.07	12	4.1	0.34	0.13	0.15	0.08
U	1.6	0.88	1.3	0.72	0.12	0.06	3.1	1.2	0.56	0.14	0.16	0.11

1182 **Table 4.** Mean trace element compositions of lawsonite (ppm) in blueschist.

This is a preprint, the final version is subject to change, of the American Mineralogist (MSA)
Cite as Authors (Year) Title. American Mineralogist, in press.
DOI: https://doi.org/10.2138/am-2019-6818

Sample	Formation	Age (Ma)	Rb	Sr	$^{87}Rb/^{86}Sr$	$^{87}Sr/^{86}Sr$*	2s	$(^{87}Sr/^{86}Sr)_i$	Sm	Nd	$^{147}Sm/^{144}Nd$	$^{143}Nd/^{144}Nd$*	2s	$(^{143}Nd/^{144}Nd)_i$	$\varepsilon Nd_{(T)}$
10tav04	Devlez	80	76	50	4.29	0.711778	6	0.706902	3.9	12	0.21	0.512967	6	0.512856	6.4
						0.711827†	6	0.706951				0.512982	8	0.512871	6.7
						0.711828†	6	0.706952				0.513003†	8	0.512892	7.1
												0.513010†	8	0.512899	7.3
10tav05	Devlez	80	18	300	0.17	0.707000#	6	0.706808	3.0	13	0.15	0.512803#	6	0.512724	3.8
10tav06	Devlez	80	3	180	0.05	0.705219	6	0.705167	3.3	9.4	0.22	0.512995	8	0.512881	6.9
						0.705217†	6	0.705164				0.513001†	8	0.512887	7.0
						0.705210†	6	0.705157							
10tav07	Devlez	80	22	123	0.50	0.705294	6	0.704720	7.8	35	0.14	0.512545	6	0.512472	-1.1
						0.705254†	6	0.704680				0.512543	6	0.512470	-1.1
10tav08	Devlez	80	2.1	71	0.08	0.705777	6	0.705687	3.7	11	0.21	0.512998	6	0.512889	7.1
						0.705780†	6	0.705690				0.512986†	6	0.512877	6.8
						0.705792†	6	0.705702				0.512969†	6	0.512860	6.5
10tav09	Devlez	80	3	89	0.10	0.705769#	6	0.705661	3.1	10	0.19	0.513000#	6	0.512900	7.3

*Repeat, individual isotope measurements; †Second, duplicate dissolution run by Reimund Jotter, MPIC; #Run by Peter Wieland, Macquarie University.

Table 5. Whole rock Rb, Sr, Nd and Sm concentrations (ppm) and Sr, Nd isotope result of blueschist samples.

This is a preprint, the final version is subject to change, of the American Mineralogist (MSA)
Cite as Authors (Year) Title. American Mineralogist, in press.
DOI: https://doi.org/10.2138/am-2019-6818

1187

Sample	Age (Ma)	Pb	U	Th	$(^{206}Pb/^{204}Pb)_m$	2s	$(^{206}Pb/^{204}Pb)_i$	$(^{207}Pb/^{204}Pb)_m$	2s	$(^{207}Pb/^{204}Pb)_i$	$(^{208}Pb/^{204}Pb)_m$	2s	$(^{208}Pb/^{204}Pb)_i$
10tav04	80	1.8	0.27	0.36	18.692	2	15.633	38.783	3	18.572	15.627	8	38.731
10tav06	80	2.0	0.18	0.36	18.424	1	15.57	38.468	1	18.353	15.567	2	38.421
10tav07	80	2.4	1.6	7.9	19.354	2	15.658	39.743	2	18.809	15.632	5	38.859
10tav08	80	5.7	0.26	0.38	18.336	1	15.599	38.368	1	18.300	15.597	4	38.351

1188 Footnote m and i denote measured and calculated initial composition using given age, respectively. Note that the age used here is metamorphism age, not the age of the protoliths.

1189 **Table 6.** Whole rock Pb, U and Th concentrations (ppm) and Pb isotope result of blueschist samples.

FIGURE CAPTIONS

Fig. 1 (a) Tectonic map of western Anatolia showing the position of the Tavşanlı zone (blue). Modified from Plunder et al. (2015). Topography of this area from Geomapapp 3.3.6 (http://www.geomapapp.org/). **(b)** Simplified schematic cross-section across the Tavşanlı zone showing tectonostratigraphic units and structure (not to scale). Note the three major formations in the Orhaneli Group: Kocasu Formation (metaclastic rocks) at the base, the İnönü Marble in the middle and the upper Devlez Formation (metabasite and metachert) where the samples in this study were collected. Modified from Okay and Whitney. (2010). **(c)** Geological map of the region north-east of Tavşanlı showing the locations of the samples (orange stars). Modified from Okay and Whitney. (2010).

Fig. 2 Field photographs: **(a)** Blueschist outcrops consist of a sequence of intercalated metabasite, metachert, metashale and metagabbro blocks of different sizes in diameter, immersed in the mélange matrix; **(b)** Location where blueschist samples 10tav04, 05, 07 and 09 were collected; **(c)** Location where blueschist samples 10tav06 and 08 were collected.

Fig. 3 Representative back-scattered electron images of Tavşanlı blueschists, **(a)** Sample 10tav04. Euhedral lawsonite filled with tiny sodic amphibole, augite and titanite as inclusions along with interstitial anhedral aragonite; **(b)** Sample 10tav05. The only sample with highly carbonated foliation characterized by the preferred alignment of phengite, sodic amphibole, and to a lesser extent, chlorite; **(c) (e) (f)** Samples 10tav06, 08 and 09, respectively. These three samples share similar paragenesis of euhedral prismatic lawsonites coexisting with sodic amphibole, aragonite, phengite, chlorite, titanite and apatite; **(d)** Sample 10tav07 shows the simplest texture and best-preserved idiomorphic mineral assemblage of all six samples, and is the only sample where Mn-rich garnet occurs. Law: lawsonite; Gln: glaucophane; Mrb: magnesio-riebeckite; Tnt: titanite; Apa: apatite; Phe: phengite; Chl: chlorite; Aug: augite; Arg: aragonite; Grt: garnet; Qtz: quartz.

Fig. 4 MgO variation diagrams of six key major elements (Ti, Al, Fe, Ca, Na and K from **(a)** to **(f)**, respectively) in the Tavşanlı zone blueschists. Also shown are MORB compositions (orange shaded fields, GEOROC database, http://georoc.mpch-mainz.gwdg.de/georoc) and GLOSS (grey stars, Plank and Langmuir, 1998). Blue shaded "MORB origin" fields include samples 10tav06, 08 and 09, whereas yellow shaded "enriched origin" fields include samples 10tav04, 05 and 07.

Fig. 5 Whole rock trace element compositions of blueschist samples from the Tavşanlı zone along with Global Subducted Sediments (GLOSS, Plank and Langmuir, 1998), normalised to N-MORB (Sun and McDonough, 1989).

Fig. 6 Trace element compositions of lawsonite in the Tavşanlı zone blueschists, normalised to C1 chondrite (Sun and McDonough, 1989). Error bars indicate propagated uncertainties as single standard deviations.

Fig. 7 Trace element compositions of minerals in the Tavşanlı zone blueschists, normalised to C1 chondrite (Sun and McDonough, 1989). **(a)-(f)**, sodic amphibole, titanite, phengite, apatite, chlorite and other minerals (aragonite, galena, Mn-garnet and hematite).

Fig. 8 $^{87}Sr/^{86}Sr$ and $^{143}Nd/^{144}Nd$ isotopic variation (initial values) of lawsonite blueschists. Sr and Nd isotopic data for MORB and OIB from the GEOROC database (http://georoc.mpch-mainz.gwdg.de/georoc), terrigenous sediment field from Rollinson (1993).

Fig. 9 Pb isotopic variation of the Tavşanlı zone blueschists (modified from Prelević et al., 2015). **(a)** $^{206}Pb/^{204}Pb$ vs $^{207}Pb/^{204}Pb$ and **(b)** $^{206}Pb/^{204}Pb$ vs $^{208}Pb/^{204}Pb$. NHRL, Northern Hemisphere Reference Line from Hart (1984).

Fig. 10 Discrimination diagrams: **(a)** TiO_2 vs Zr/P_2O_5. Most blueschist samples are of tholeiitic affinity, except for sample 10tav04 which falls close to the line between alkaline and tholeiitic (after Winchester and Floyd, 1976); **(b)** P_2O_5 vs Zr (ppm) (after Winchester and Floyd, 1976). All blueschists plot within the tholeiitic field; **(c)** Th/Yb vs Ta/Yb discrimination diagram after Pearce (1983); **(d)** Ce/Nb vs Th/Nb discrimination diagram following Saunders et al (1988). DMM: Depleted MORB Mantle; RSC: Residual Slab Component; SDC: Slab-Derived Component; GLOSS: Global Subducted Sediments.

Fig. 11 $^{87}Sr/^{86}Sr_{initial}$ vs Ba/Th diagram showing three-component mixing (MORB, sediment and fluid derived by dehydration of the subducted oceanic crust) to explain the geochemistry of blueschist samples from the Tavşanlı zone (after Turner et al., 1996). Note that sample 10tav04 exhibits distinctly higher Ba/Th ratio (827) than the rest of samples, suggesting an addition of Sr-rich slab-derived fluid in the source.

Fig. 12 La/Yb vs Yb (ppm) discrimination diagram of blueschist samples from the Tavşanlı zone (partial melting curves calculated from batch melting; adapted from Miller et al., 1999; Zhu et al., 2015). La and Yb contents of Primitive mantle from Sun and McDonough (1989). All six blueschist samples plot along or parallel to the trajectory for non-modal fractional melts of a spinel peridotitic source, suggesting that the parental magmas of blueschist samples were produced from the differing degrees of partial melting of spinel-facies peridotites.

Fig. 13 Trace element budget for the Tavşanlı zone blueschist samples. See text for details.

Fig. 14 (a) Pb/Ce vs Ce (ppm); **(b)** Sm/Nd vs Sr (ppm); **(c)** La/Dy vs La (ppm) and **(d)** Dy/Lu vs Lu (ppm) diagrams for Tavşanlı zone lawsonites. For comparison, titanite (filled diamonds) and apatite (empty diamonds) in blueschist samples from this study are also shown.

Fig. 15 Th/La vs Sm/La comparison of lawsonite in blueschist sample 10tav07 (enriched terrigenous origin) and in the blueschists of MORB origin with Alpine-Himalayan Orogenic Belt lavas (Wang et al., 2017), OIB (GEOROC database, http://georoc.mpch-mainz.gwdg.de/georoc), MORB (GEOROC database, http://georoc.mpch-mainz.gwdg.de/georoc), and arc magmas related to slab-derived mantle metasomatism (data from Tommasini et al., 2011 and references therein). Note the distinction between "enriched" and MORB-like lawsonites is as striking as that between AHOB and other lavas.

Fig. 16 ($^{208}Pb/^{206}Pb$)i vs ($^{206}Pb/^{204}Pb$)i variation of lawsonite blueschists in the Tavşanlı zone mé ange, AHOB lavas, Tethyan Realm lamproites, and anorogenic intracratonic lamproites along with MORBs and OIBs, adapted from Tommasini et al (2011). Also shown are GLOSS and Serbian flysch. MORB and OIB data from Stracke et al (2003) and GEOROC database, data for Tethyan Realm lamproites and anorogenic intracratonic lamproites from Tommasini et al (2011), AHOB data from Supplementary data source file, Serbian flysch data from Prelević et al (2007) and GLOSS data from Plank and Langmuir (1998).

Figure 1

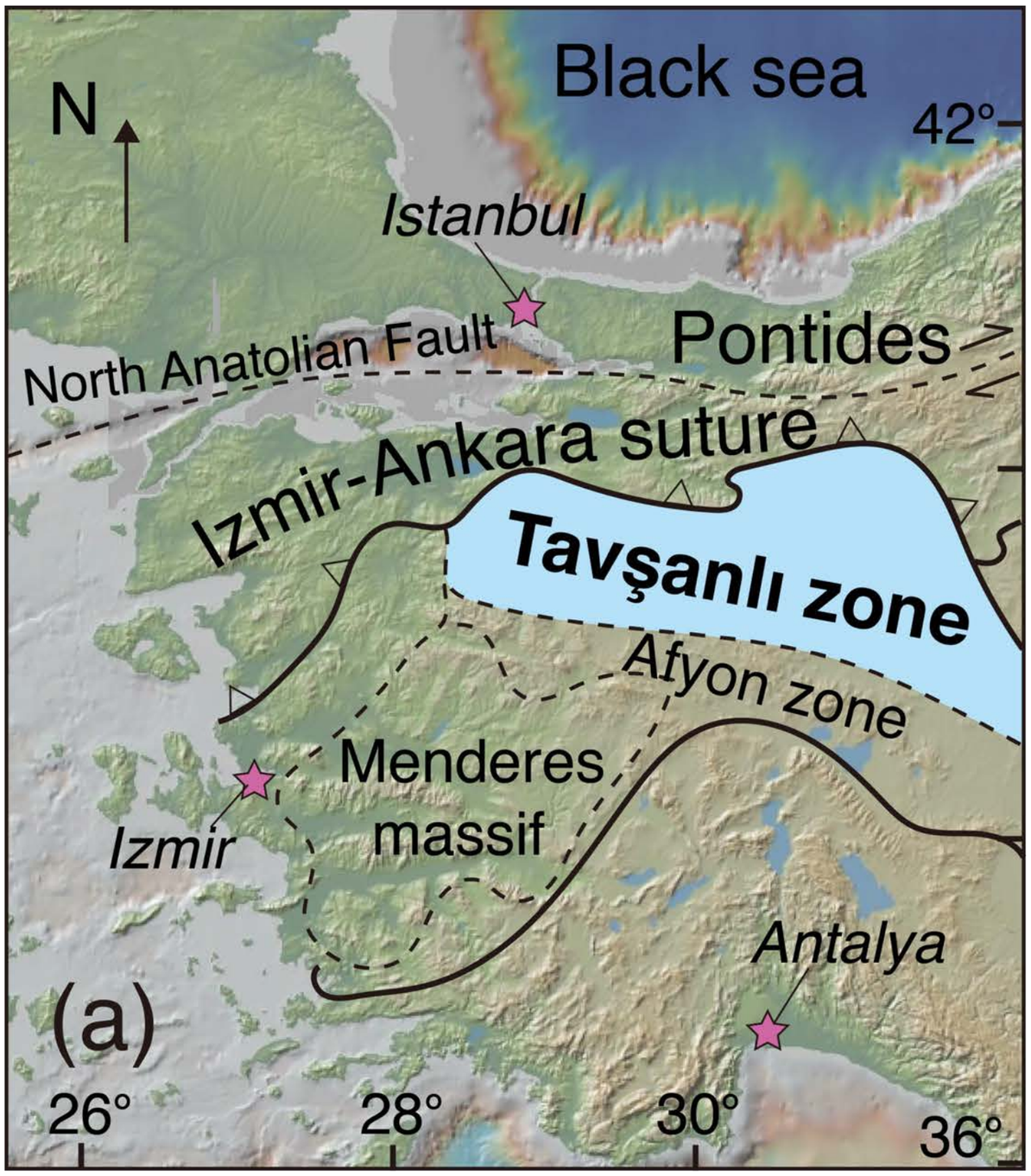
N
Black sea
42°
Istanbul
North Anatolian Fault
Pontides
Izmir-Ankara suture
Tavşanlı zone
Afyon zone
Menderes
massif
Izmir
Antalya
(a)
26°
28°
30°
36°

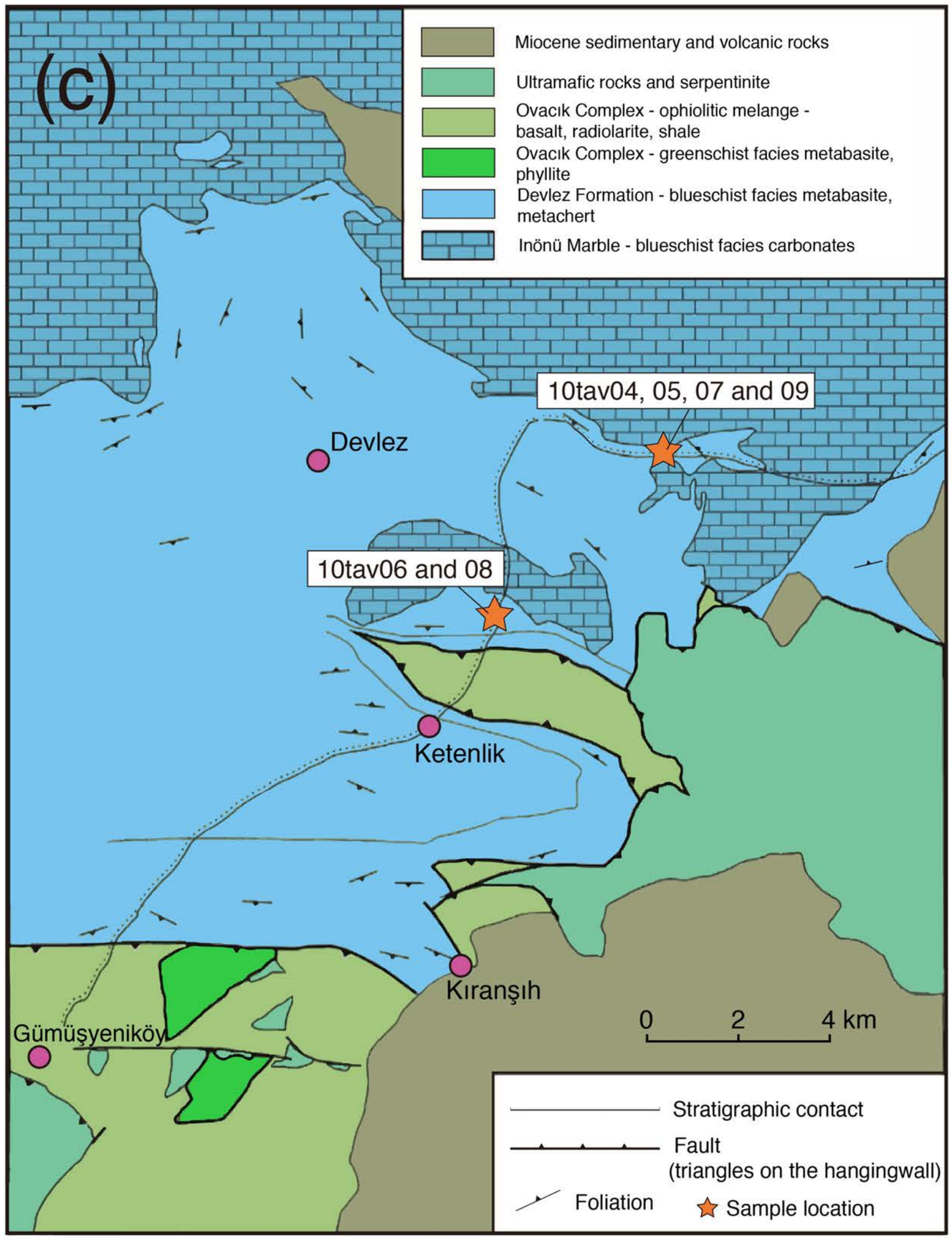
(c)
Miocene sedimentary and volcanic rocks
Ultramafic rocks and serpentinite
Ovacık Complex - ophiolitic melange - basalt, radiolarite, shale
Ovacık Complex - greenschist facies metabasite, phyllite
Devlez Formation - blueschist facies metabasite, metachert
Inönü Marble - blueschist facies carbonates
10tav04, 05, 07 and 09
Devlez
10tav06 and 08
Ketenlik
Kıranşıh
Gümüşyeniköy
0 2 4 km
Stratigraphic contact
Fault
(triangles on the hangingwall)
Foliation
Sample location

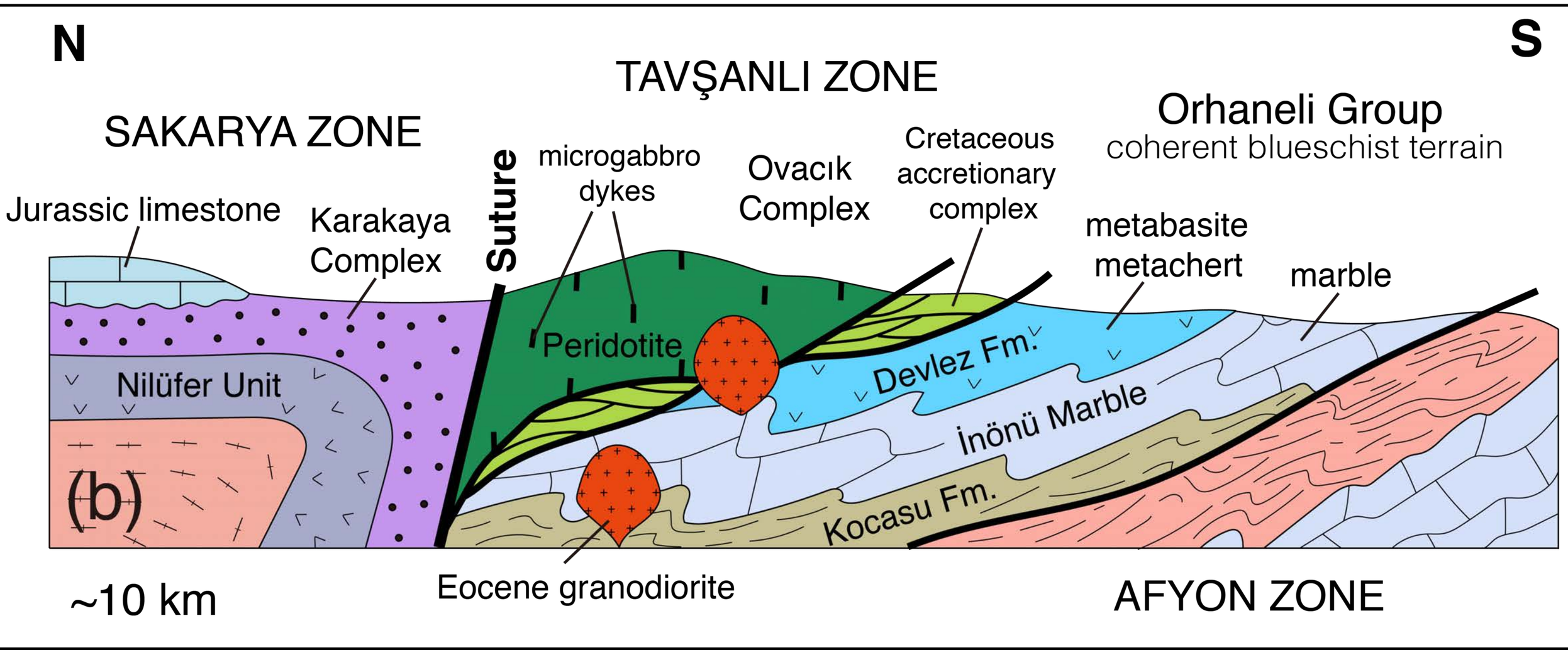
N
S
TAVŞANLI ZONE
SAKARYA ZONE
Orhaneli Group
coherent blueschist terrain
Jurassic limestone
Karakaya Complex
Suture
microgabbro dykes
Ovacık Complex
Cretaceous accretionary complex
metabasite metachert
marble
Peridotite
Devlez Fm.
Nilüfer Unit
İnönü Marble
Kocasu Fm.
(b)
~10 km
Eocene granodiorite
AFYON ZONE

Figure 2

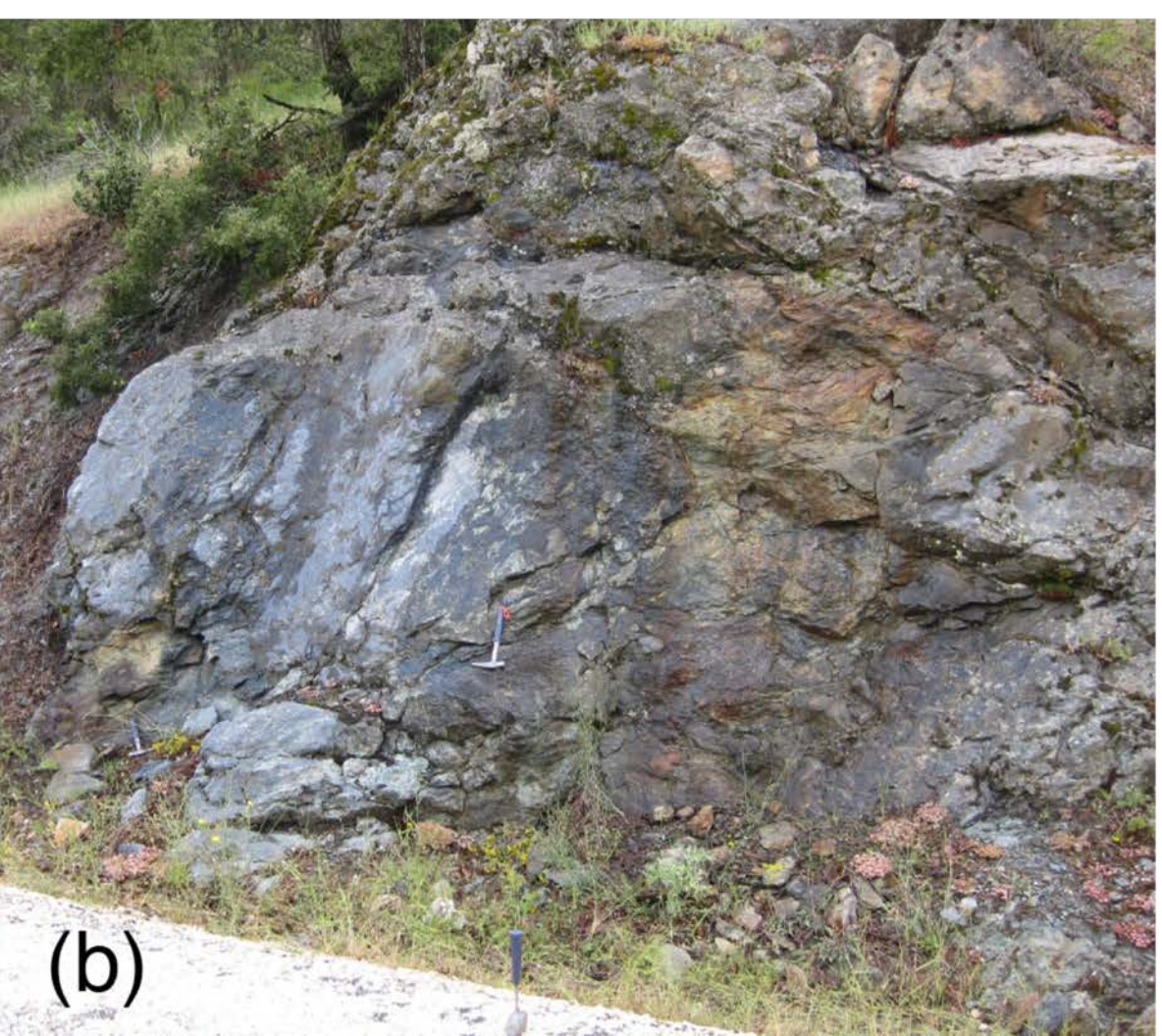

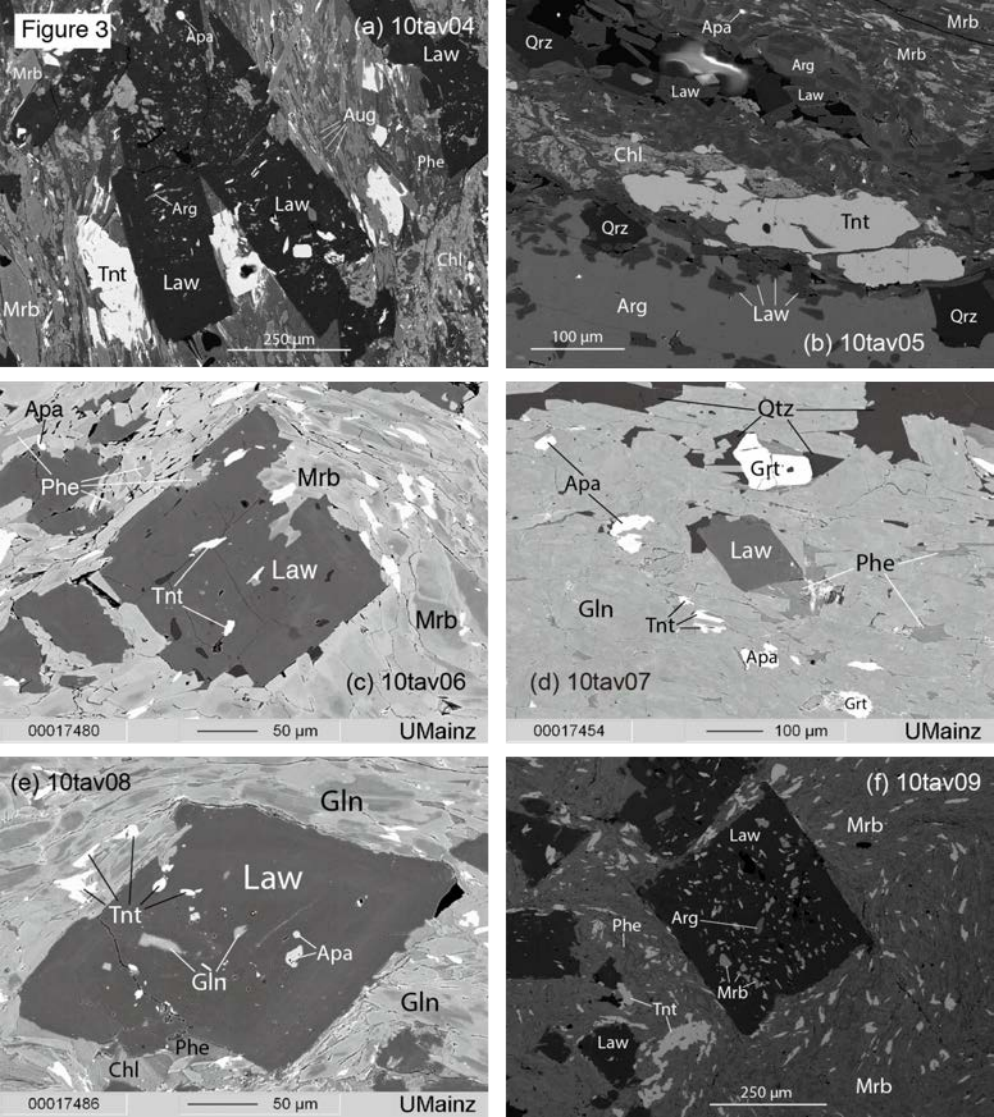
Figure 3
(a) 10tav04
Apa
Law
Mrb
Aug
Phe
Arg
Law
Tnt
Law
Chl
Mrb
250 µm
Apa
Mrb
Qrz
Arg
Mrb
Law
Law
Chl
Qrz
Tnt
Arg
Law
Qrz
100 µm
(b) 10tav05
Apa
Mrb
Phe
Mrb
Law
Tnt
Mrb
(c) 10tav06
00017480
50 µm
UMainz
Qtz
Grt
Apa
Law
Phe
Gln
Tnt
Apa
(d) 10tav07
Grt
00017454
100 µm
UMainz
(e) 10tav08
Gln
Law
Tnt
Apa
Gln
Gln
Phe
Chl
00017486
50 µm
UMainz
(f) 10tav09
Law
Mrb
Phe
Arg
Mrb
Tnt
Law
250 µm
Mrb

Figure 4

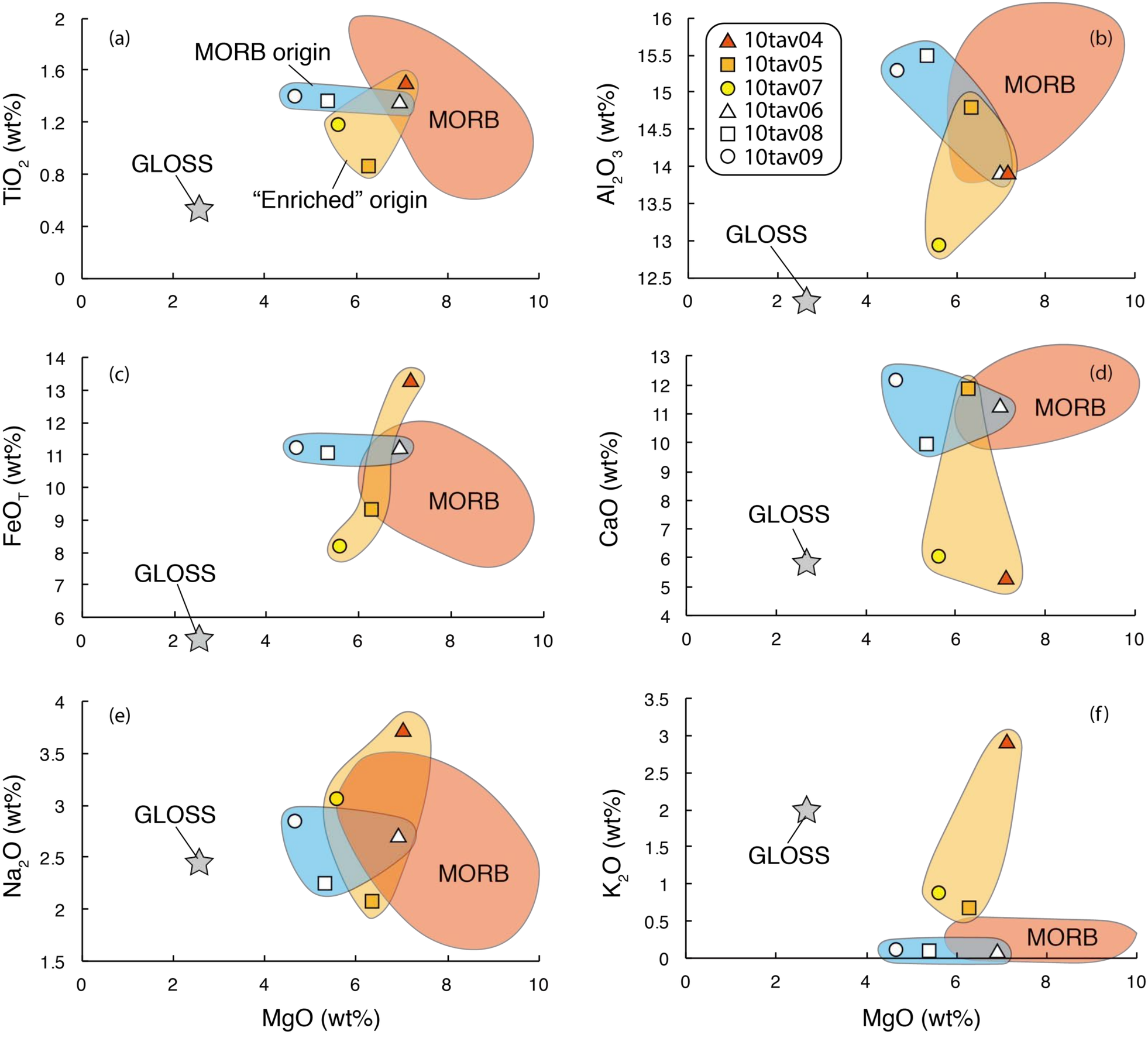
(a)
MORB origin
MORB
GLOSS
"Enriched" origin
TiO2 (wt%)
(b)
10tav04
10tav05
10tav07
10tav06
10tav08
10tav09
MORB
GLOSS
Al2O3 (wt%)
(c)
MORB
GLOSS
FeOT (wt%)
(d)
MORB
GLOSS
CaO (wt%)
(e)
GLOSS
MORB
Na2O (wt%)
MgO (wt%)
(f)
GLOSS
MORB
K2O (wt%)
MgO (wt%)

Figure 5

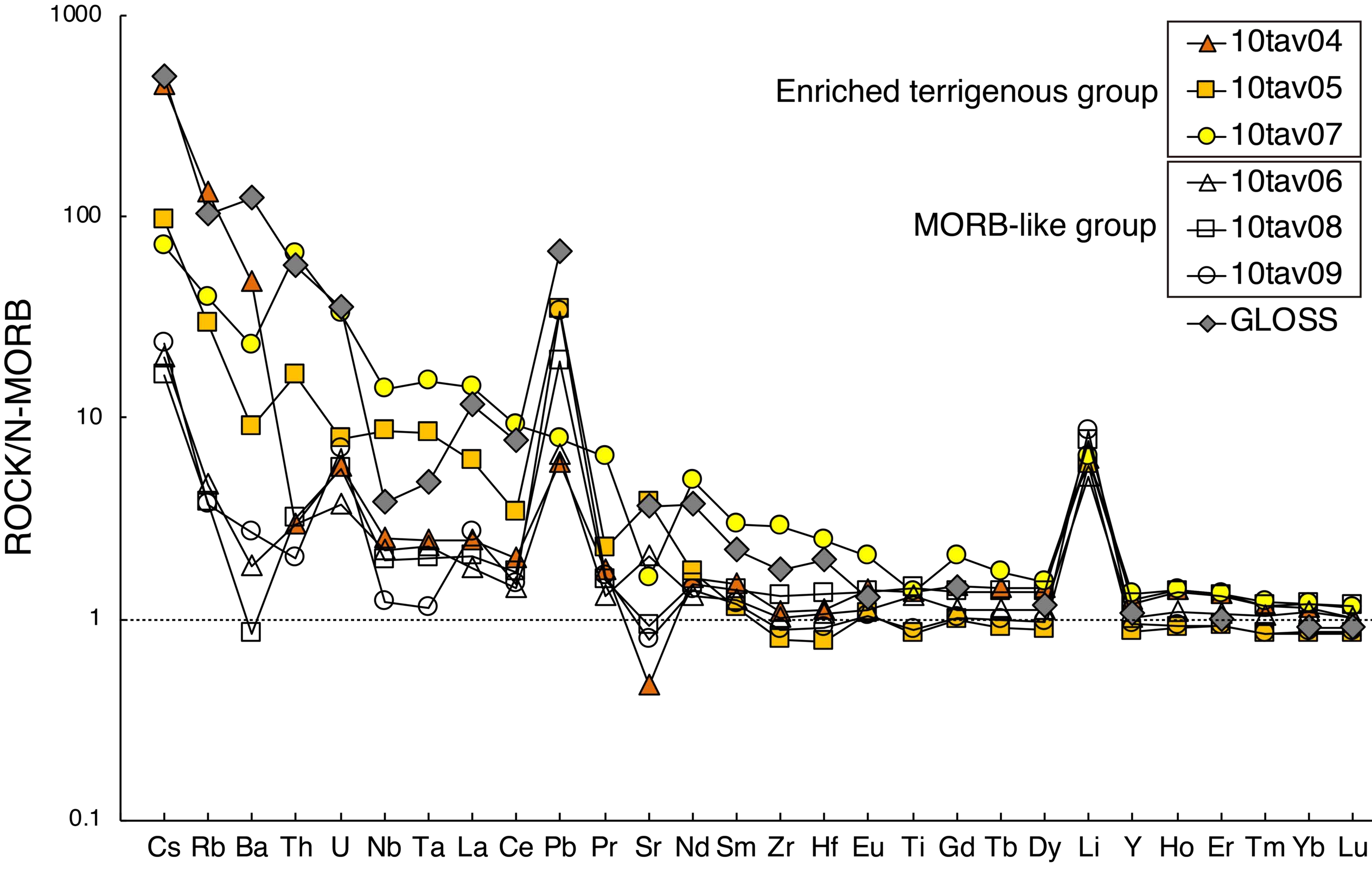
1000
100
10
1
0.1
ROCK/N-MORB
Cs Rb Ba Th U Nb Ta La Ce Pb Pr Sr Nd Sm Zr Hf Eu Ti Gd Tb Dy Li Y Ho Er Tm Yb Lu
Enriched terrigenous group
10tav04
10tav05
10tav07
MORB-like group
10tav06
10tav08
10tav09
GLOSS

Figure 6

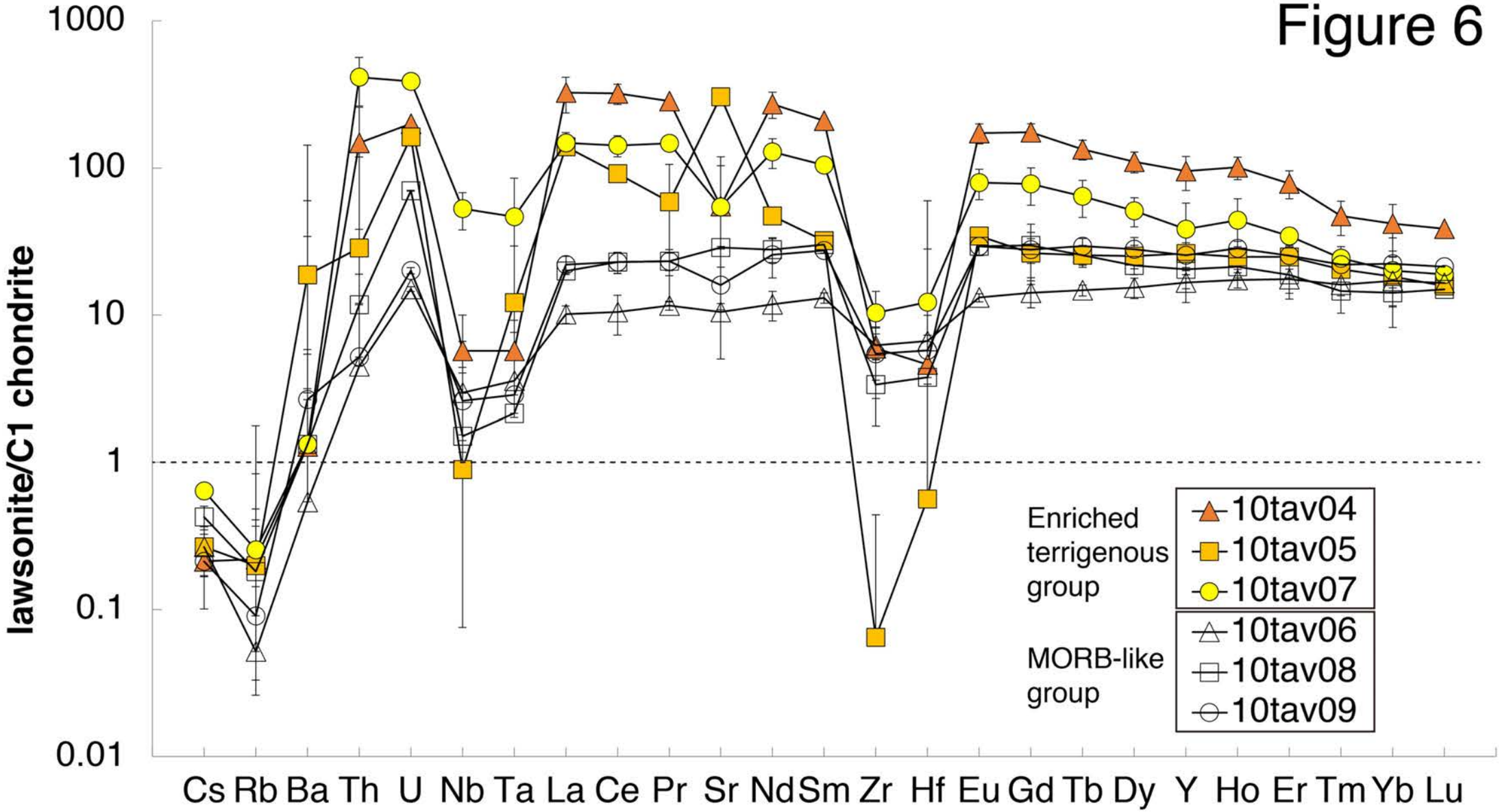
1000
100
10
1
0.1
0.01
lawsonite/C1 chondrite
Cs Rb Ba Th U Nb Ta La Ce Pr Sr Nd Sm Zr Hf Eu Gd Tb Dy Y Ho Er Tm Yb Lu
Enriched terrigenous group
10tav04
10tav05
10tav07
MORB-like group
10tav06
10tav08
10tav09

Figure 7

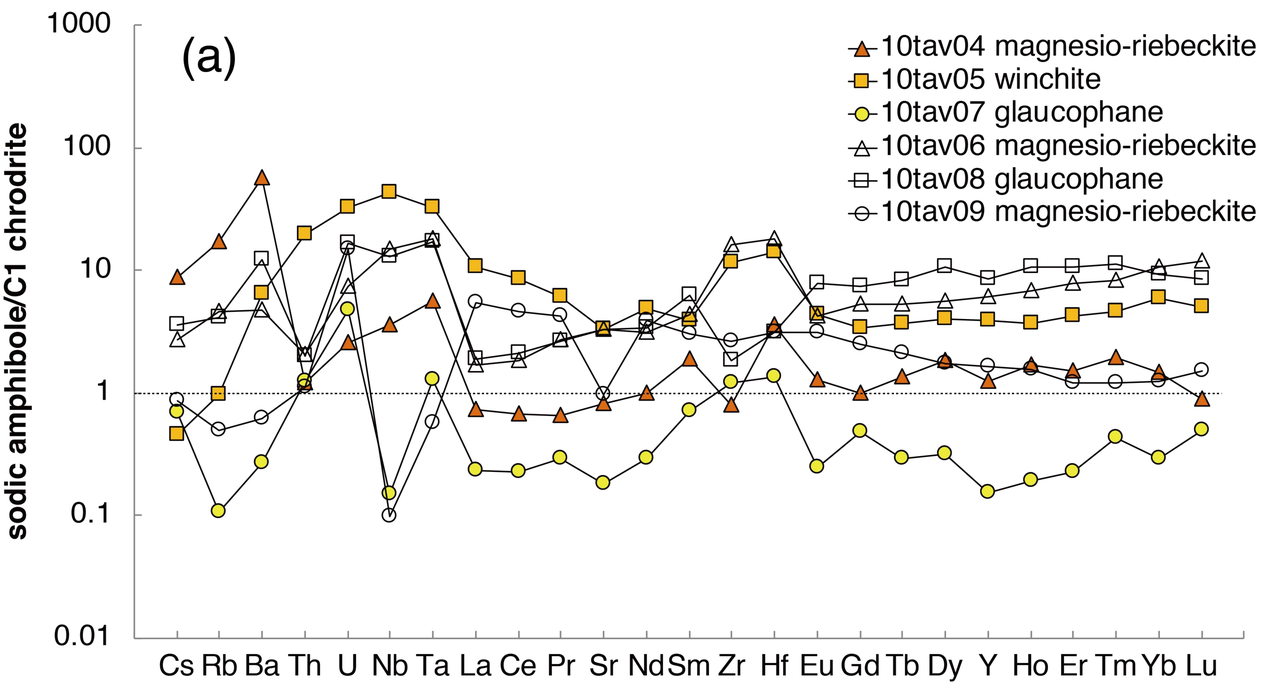
(a)
sodic amphibole/C1 chrodrite
10tav04 magnesio-riebeckite
10tav05 winchite
10tav07 glaucophane
10tav06 magnesio-riebeckite
10tav08 glaucophane
10tav09 magnesio-riebeckite
1000
100
10
1
0.1
0.01
Cs Rb Ba Th U Nb Ta La Ce Pr Sr Nd Sm Zr Hf Eu Gd Tb Dy Y Ho Er Tm Yb Lu

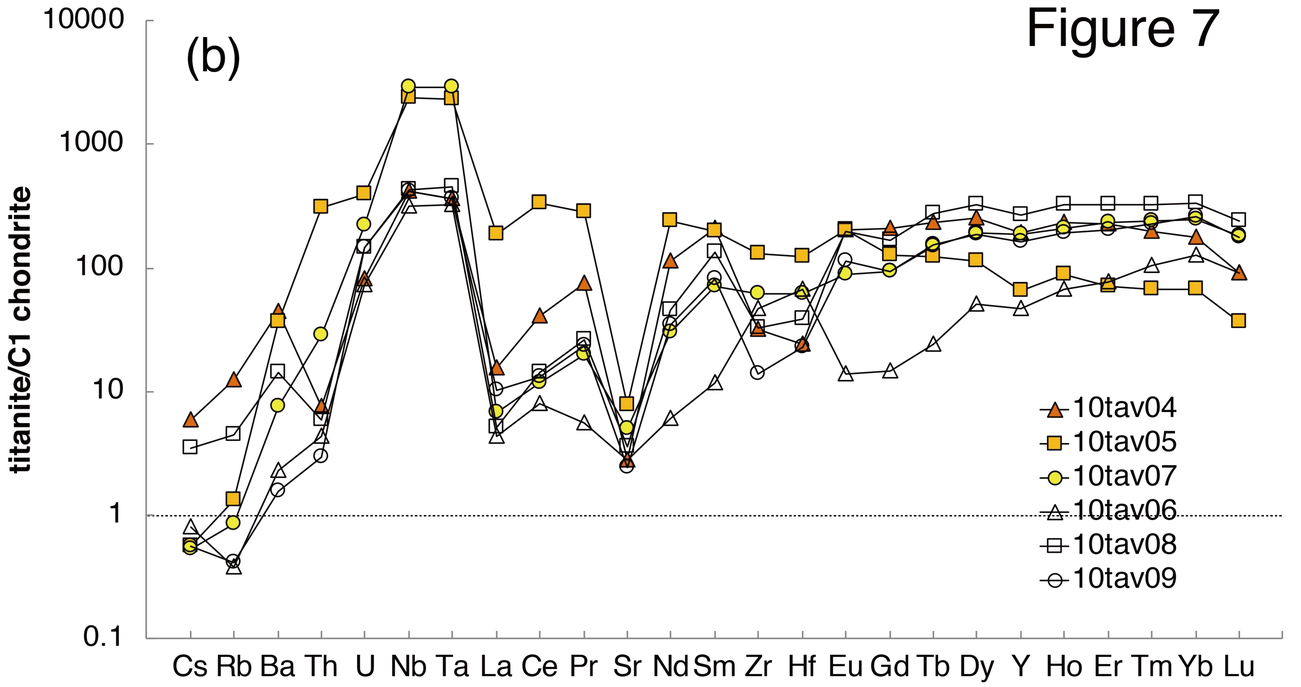
(b)
titanite/C1 chondrite
10tav04
10tav05
10tav07
10tav06
10tav08
10tav09
10000
1000
100
10
1
0.1
Cs Rb Ba Th U Nb Ta La Ce Pr Sr Nd Sm Zr Hf Eu Gd Tb Dy Y Ho Er Tm Yb Lu

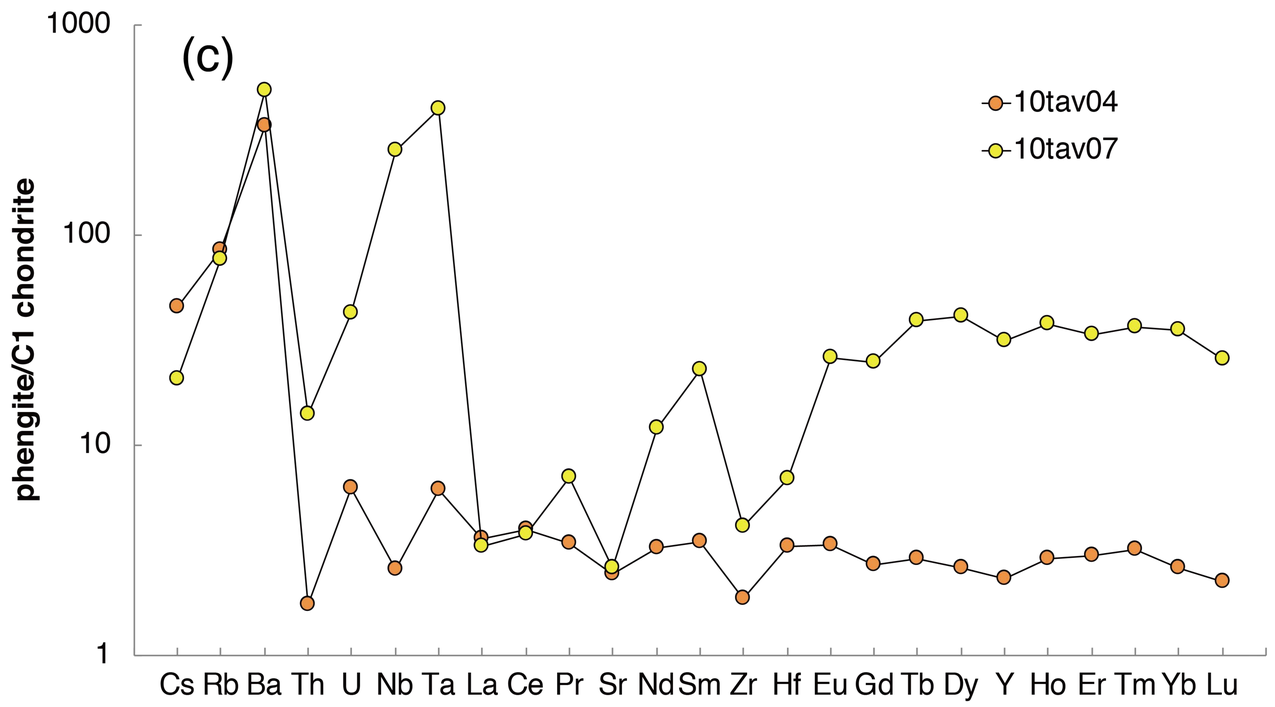
(c)
phengite/C1 chondrite
10tav04
10tav07
1000
100
10
1
Cs Rb Ba Th U Nb Ta La Ce Pr Sr Nd Sm Zr Hf Eu Gd Tb Dy Y Ho Er Tm Yb Lu

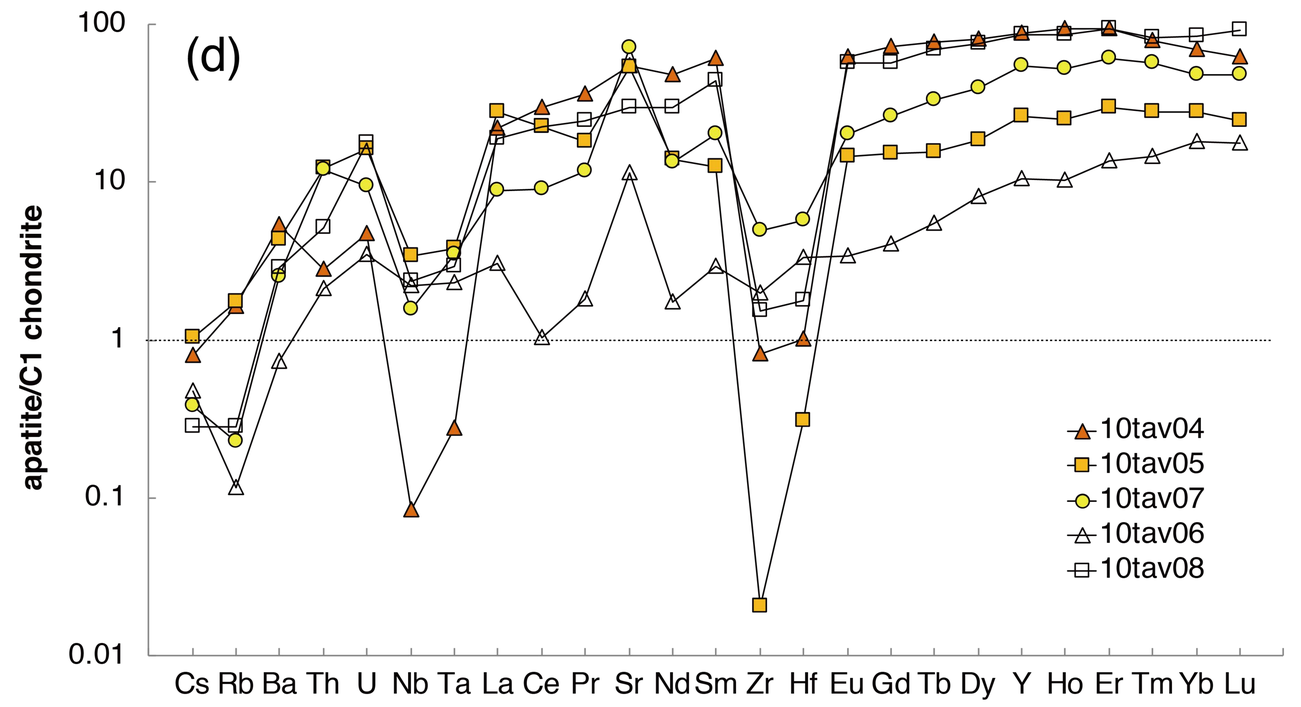
(d)
apatite/C1 chondrite
10tav04
10tav05
10tav07
10tav06
10tav08
100
10
1
0.1
0.01
Cs Rb Ba Th U Nb Ta La Ce Pr Sr Nd Sm Zr Hf Eu Gd Tb Dy Y Ho Er Tm Yb Lu

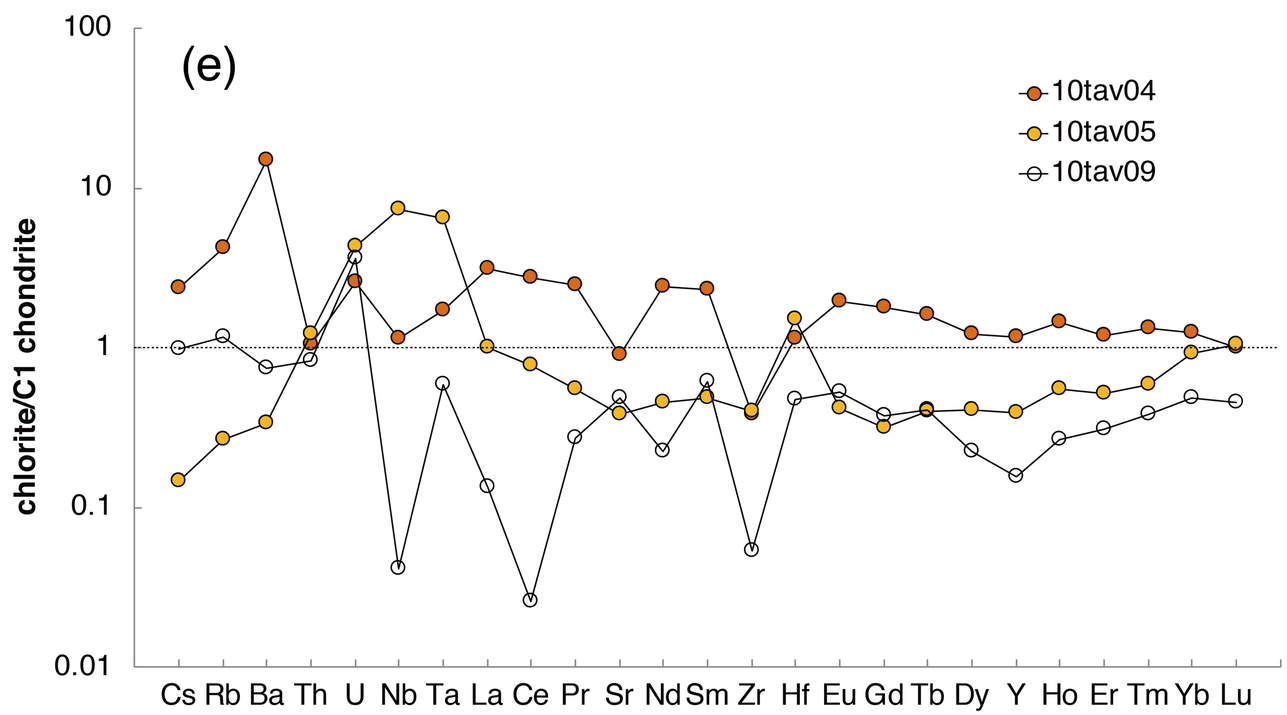
(e)
chlorite/C1 chondrite
10tav04
10tav05
10tav09
100
10
1
0.1
0.01
Cs Rb Ba Th U Nb Ta La Ce Pr Sr Nd Sm Zr Hf Eu Gd Tb Dy Y Ho Er Tm Yb Lu

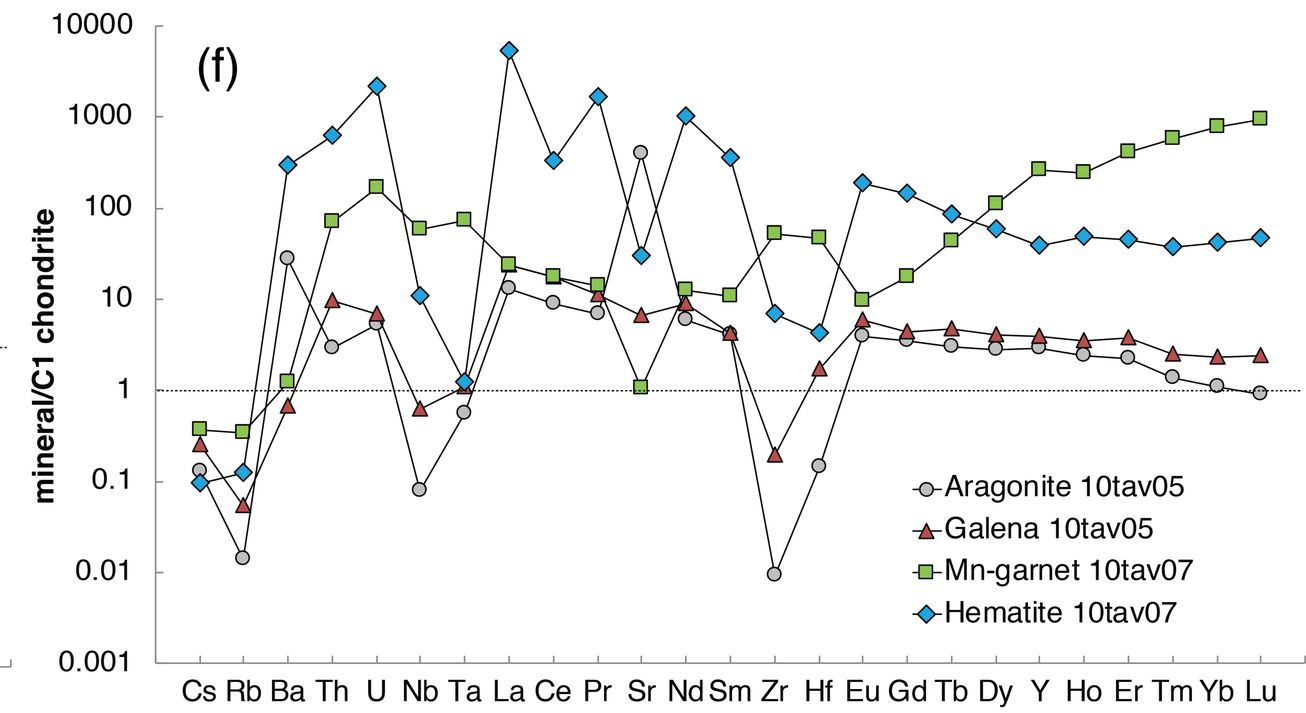
(f)
mineral/C1 chondrite
Aragonite 10tav05
Galena 10tav05
Mn-garnet 10tav07
Hematite 10tav07
10000
1000
100
10
1
0.1
0.01
0.001
Cs Rb Ba Th U Nb Ta La Ce Pr Sr Nd Sm Zr Hf Eu Gd Tb Dy Y Ho Er Tm Yb Lu

Figure 8

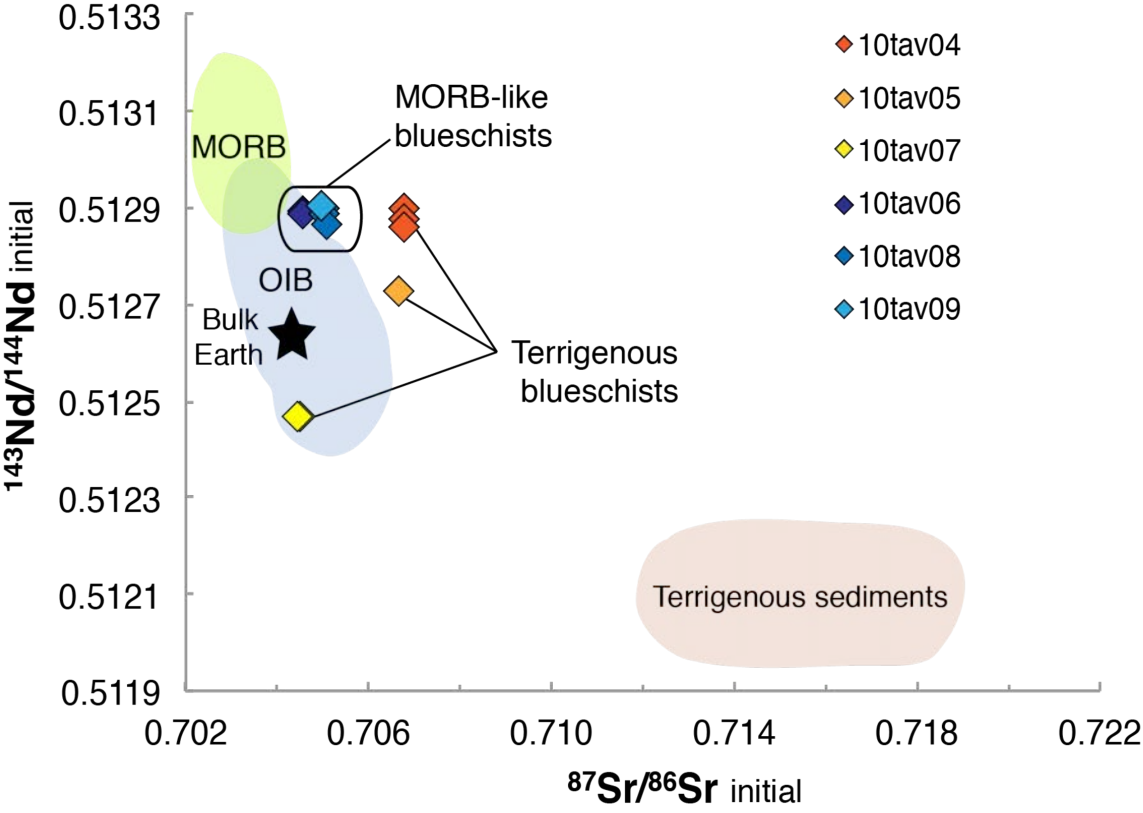
0.5133
0.5131
0.5129
0.5127
0.5125
0.5123
0.5121
0.5119
143Nd/144Nd initial
0.702
0.706
0.710
0.714
0.718
0.722
87Sr/86Sr initial
MORB
MORB-like blueschists
OIB
Bulk Earth
Terrigenous blueschists
Terrigenous sediments
10tav04
10tav05
10tav07
10tav06
10tav08
10tav09

Figure 9

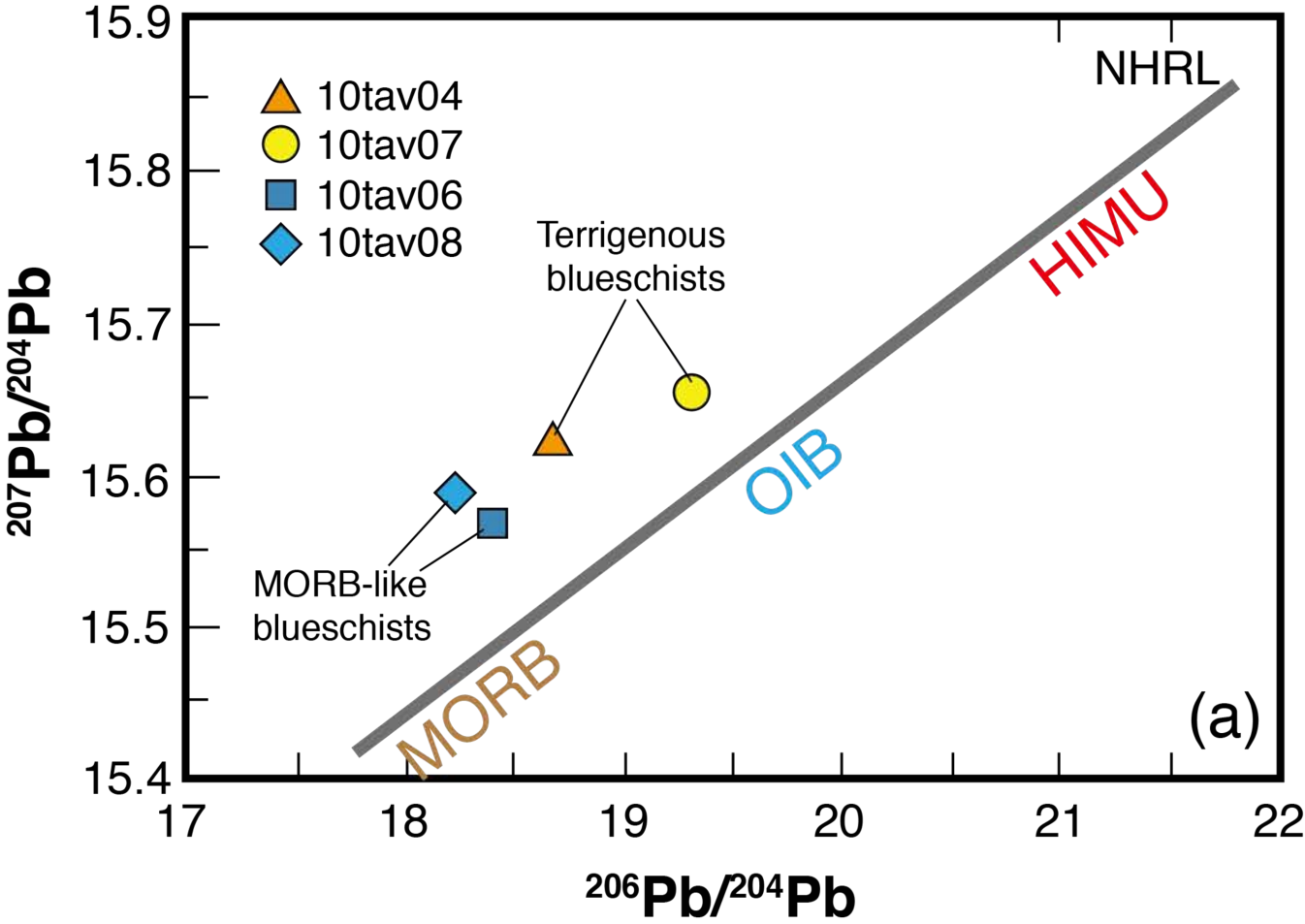
15.9
15.8
15.7
15.6
15.5
15.4
17
18
19
20
21
22
$^{207}Pb/^{204}Pb$
$^{206}Pb/^{204}Pb$
10tav04
10tav07
10tav06
10tav08
NHRL
HIMU
OIB
MORB
Terrigenous blueschists
MORB-like blueschists
(a)

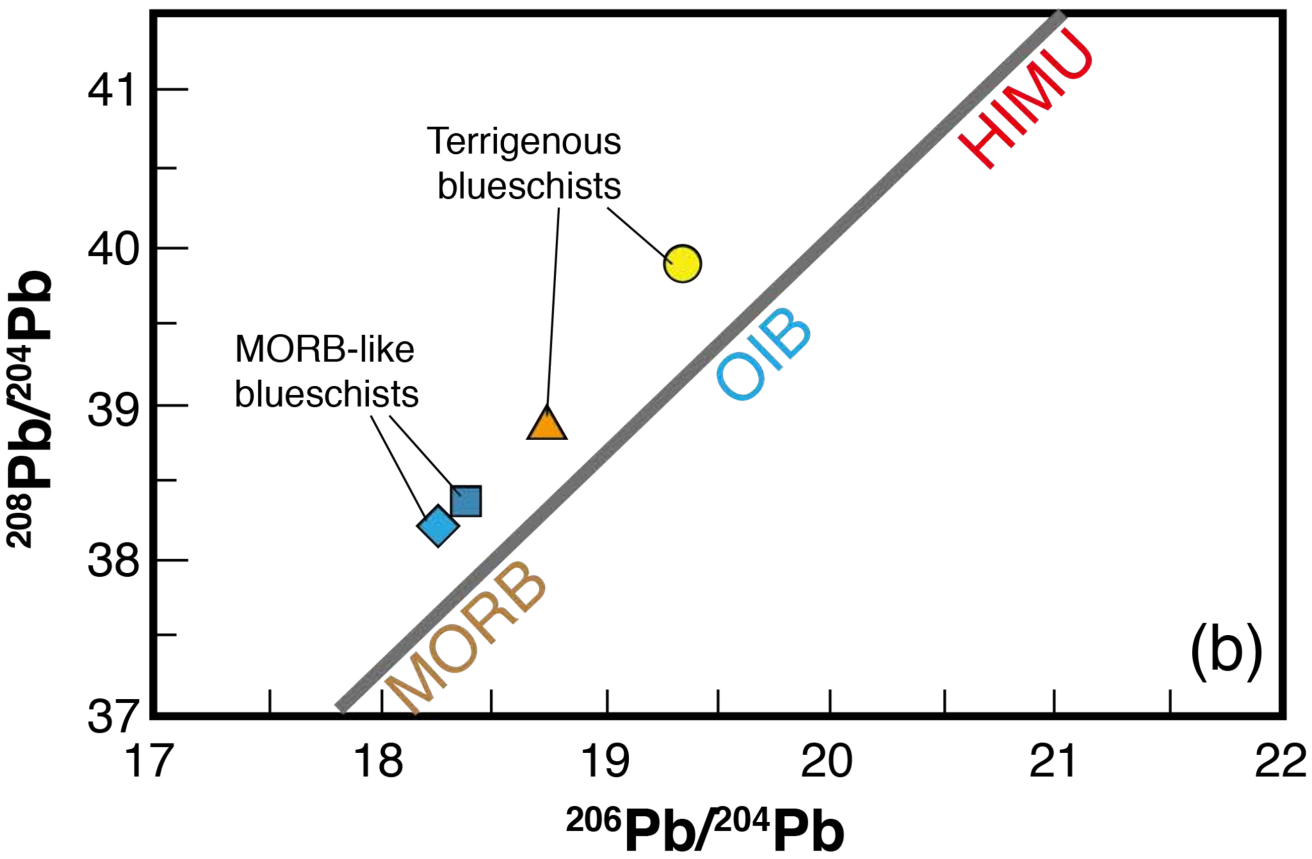
41
40
39
38
37
17
18
19
20
21
22
$^{208}Pb/^{204}Pb$
$^{206}Pb/^{204}Pb$
HIMU
OIB
MORB
Terrigenous blueschists
MORB-like blueschists
(b)

Figure 10

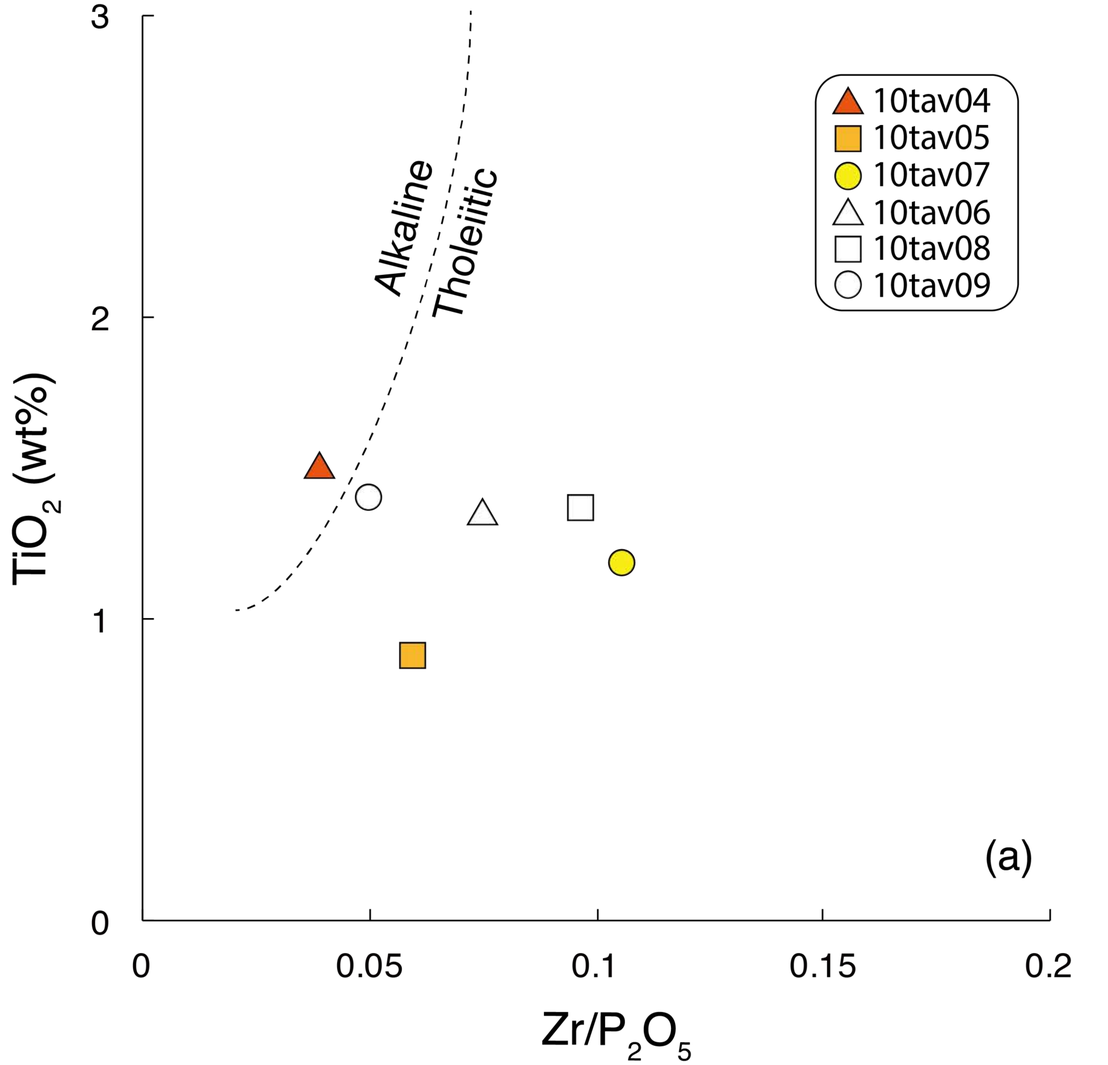
3
2
1
0
TiO_2 (wt%)
Alkaline
Tholeiitic
0
0.05
0.1
0.15
0.2
Zr/P_2O_5
10tav04
10tav05
10tav07
10tav06
10tav08
10tav09
(a)

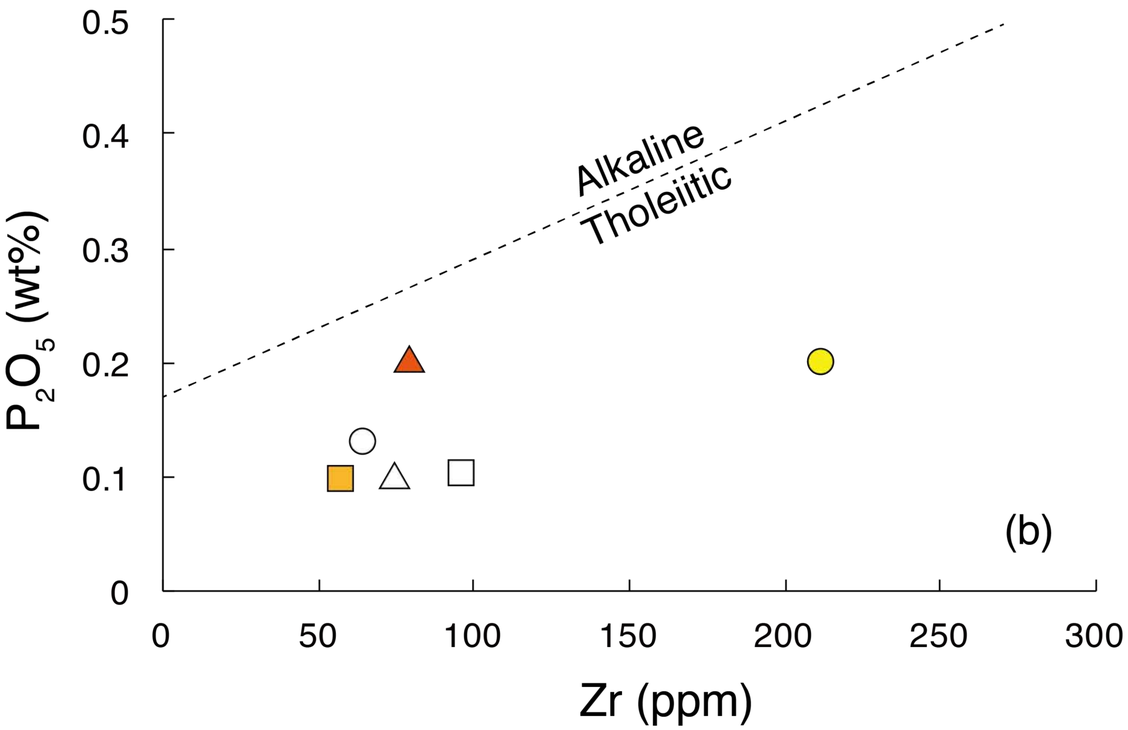
0.5
0.4
0.3
0.2
0.1
0
P_2O_5 (wt%)
Alkaline
Tholeiitic
0
50
100
150
200
250
300
Zr (ppm)
(b)

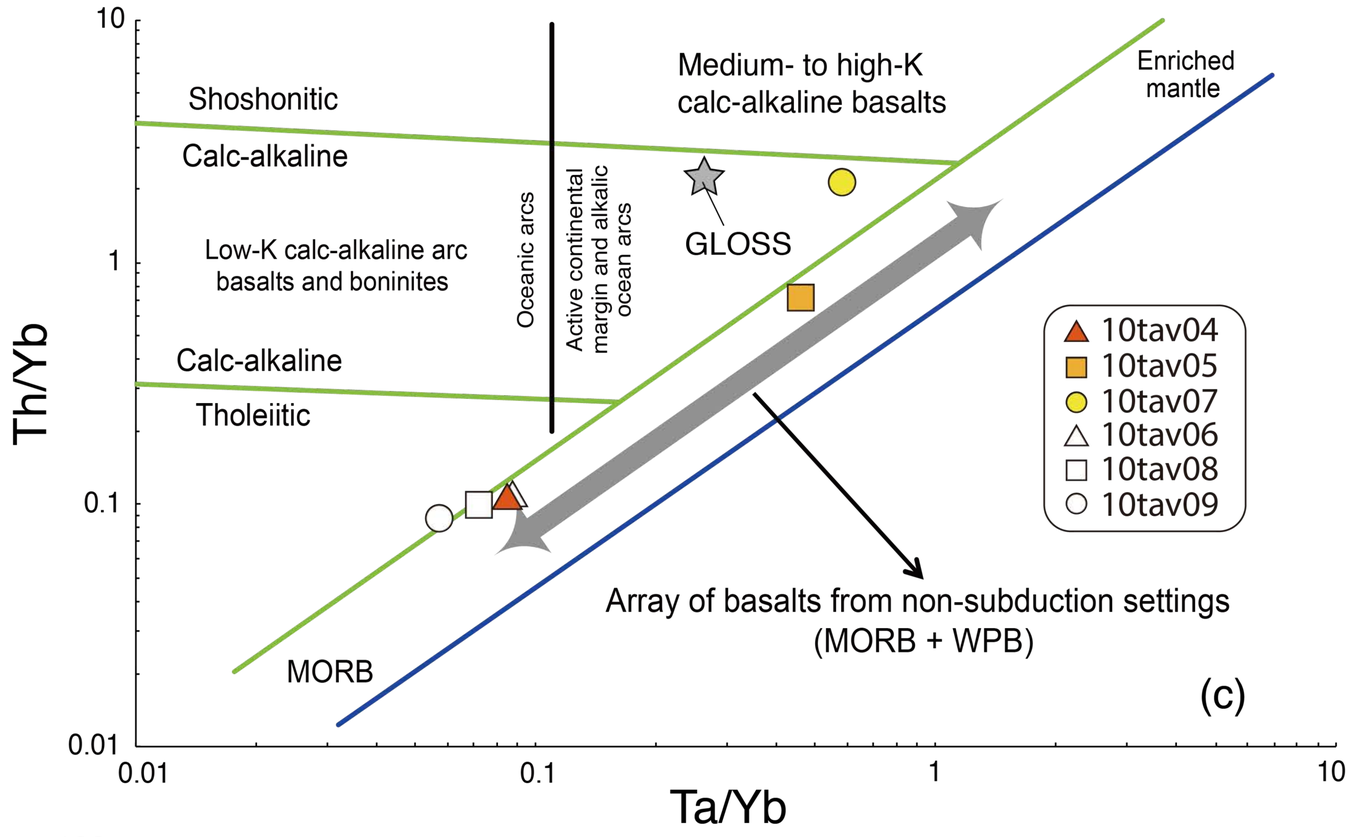
10
1
0.1
0.01
Th/Yb
Shoshonitic
Calc-alkaline
Low-K calc-alkaline arc basalts and boninites
Calc-alkaline
Tholeiitic
Oceanic arcs
Active continental margin and alkalic ocean arcs
Medium- to high-K calc-alkaline basalts
Enriched mantle
GLOSS
MORB
Array of basalts from non-subduction settings (MORB + WPB)
10tav04
10tav05
10tav07
10tav06
10tav08
10tav09
(c)
0.01
0.1
1
10
Ta/Yb

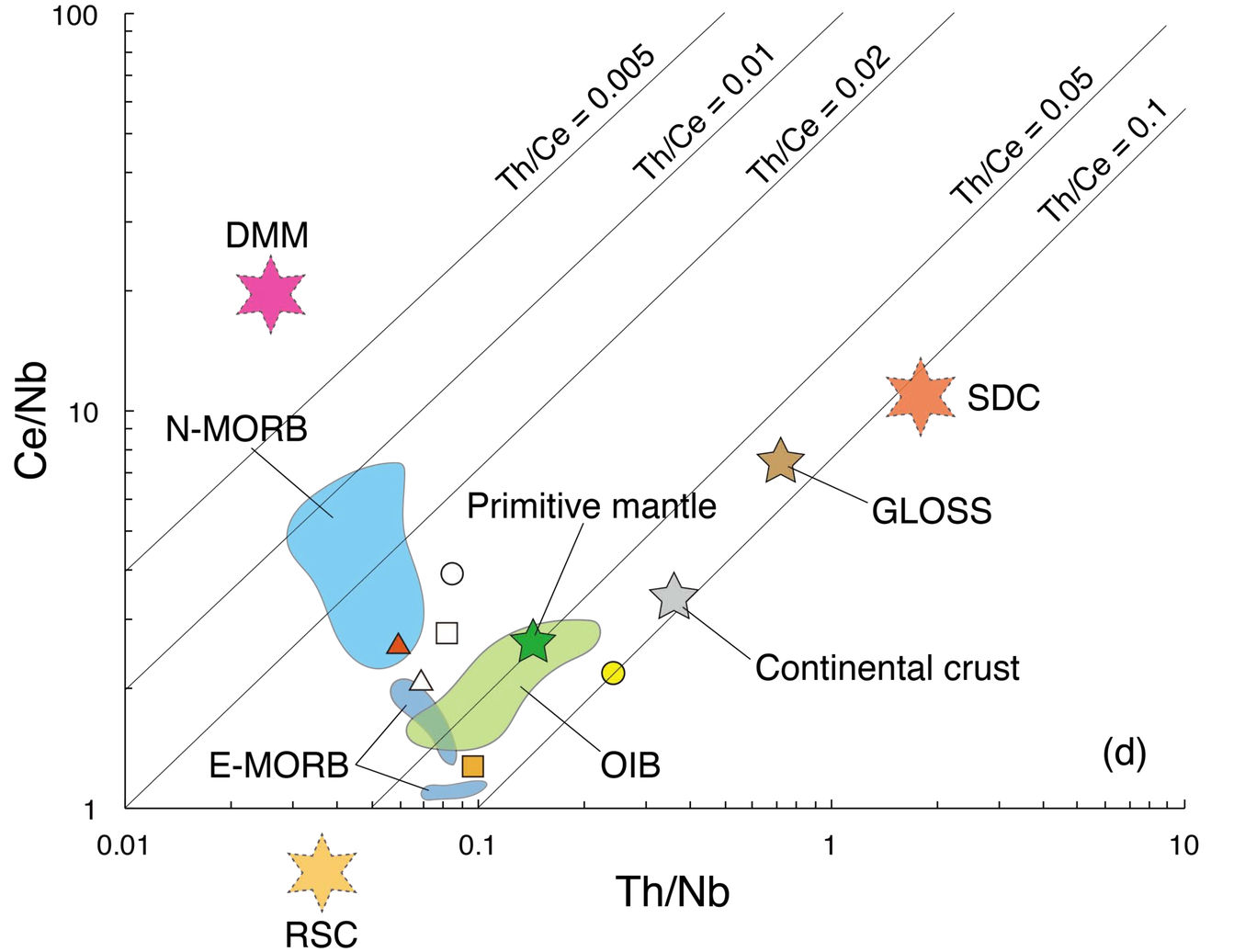
100
10
1
Ce/Nb
Th/Ce = 0.005
Th/Ce = 0.01
Th/Ce = 0.02
Th/Ce = 0.05
Th/Ce = 0.1
DMM
N-MORB
Primitive mantle
SDC
GLOSS
Continental crust
E-MORB
OIB
RSC
(d)
0.01
0.1
1
10
Th/Nb

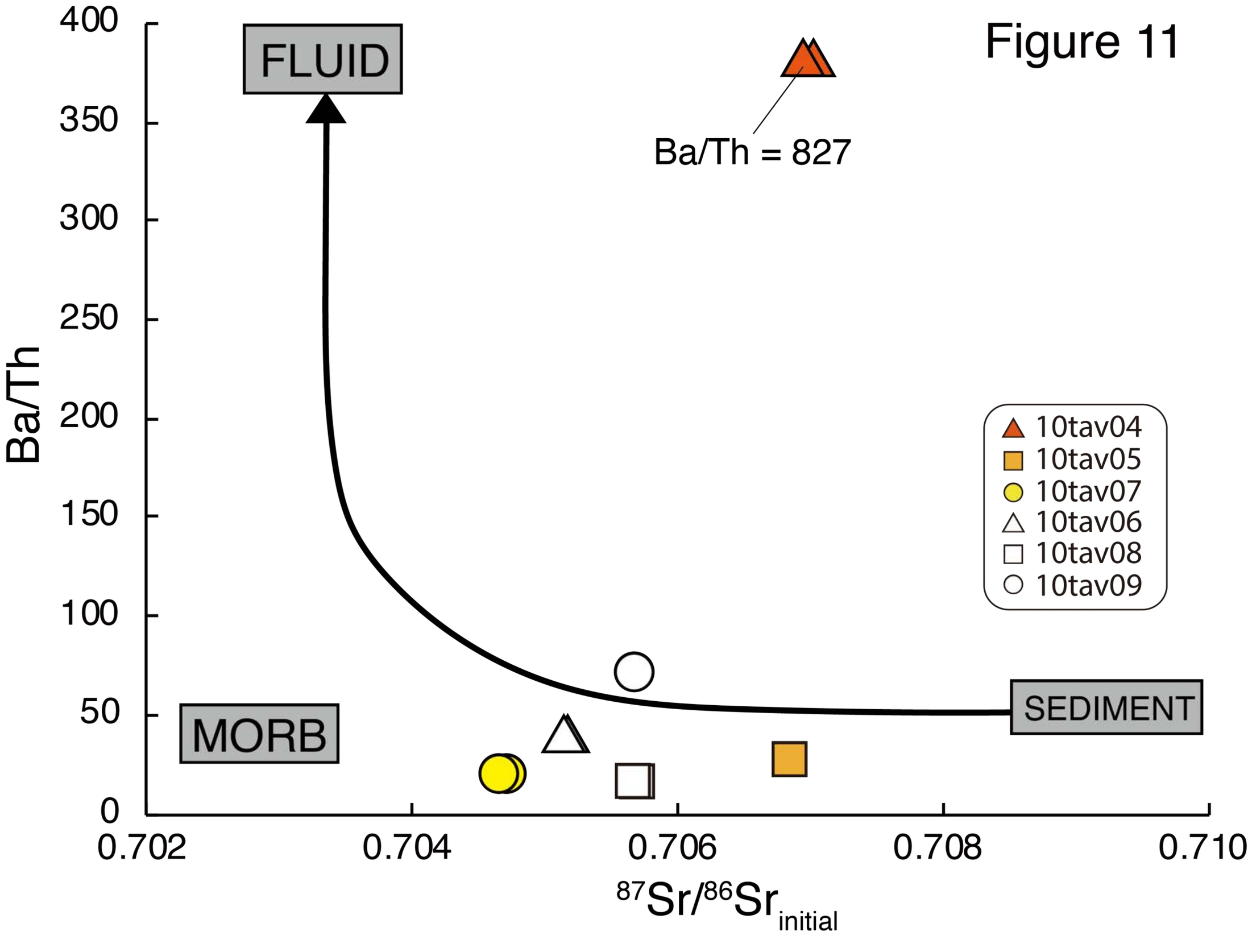
Figure 11
FLUID
Ba/Th = 827
MORB
SEDIMENT
10tav04
10tav05
10tav07
10tav06
10tav08
10tav09
Ba/Th
400
350
300
250
200
150
100
50
0
0.702
0.704
0.706
0.708
0.710
87Sr/86Sr initial

Figure 12

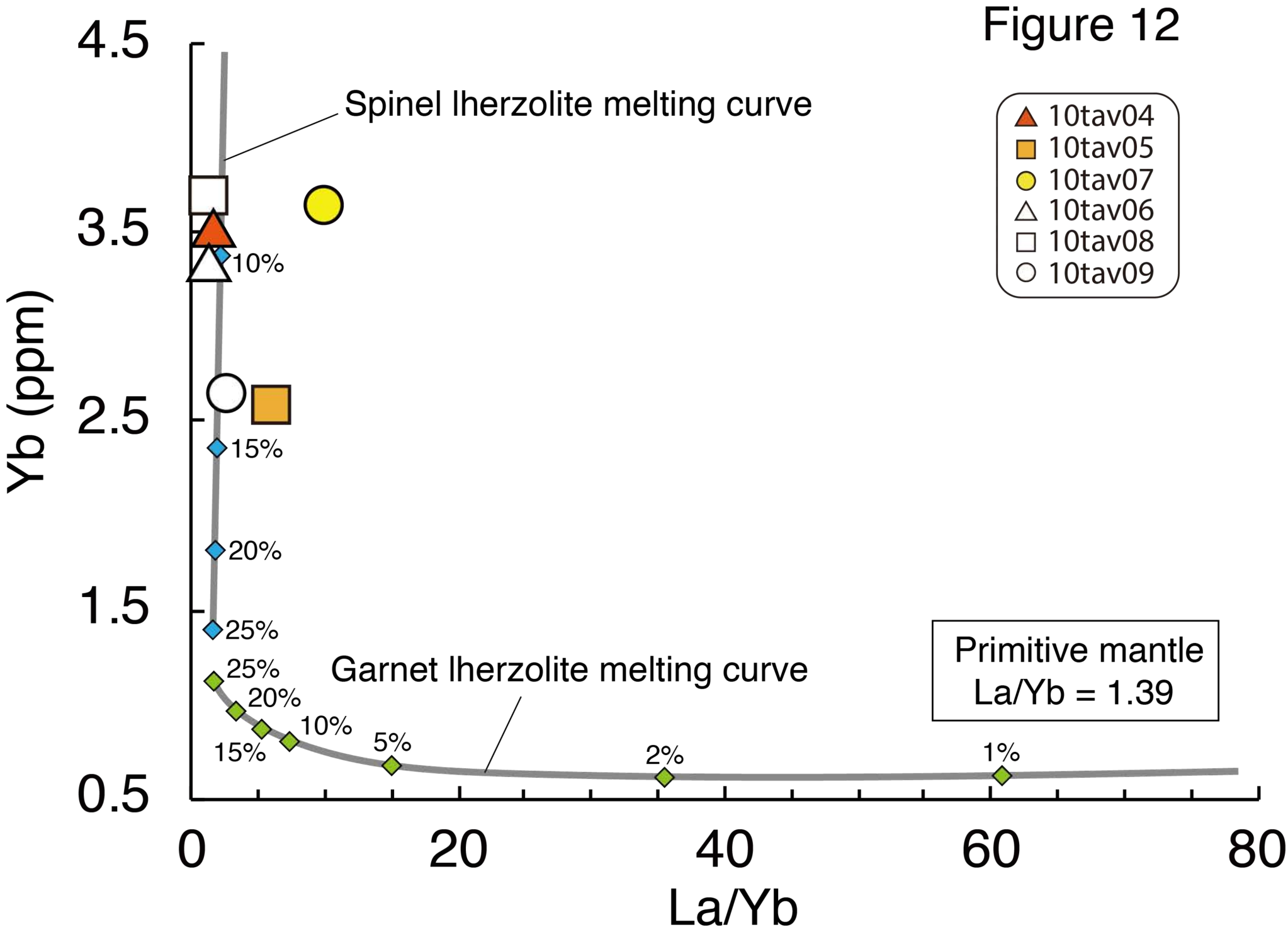
4.5
3.5
2.5
1.5
0.5
Yb (ppm)
0
20
40
60
80
La/Yb
Spinel lherzolite melting curve
Garnet lherzolite melting curve
10%
15%
20%
25%
25%
20%
15%
10%
5%
2%
1%
10tav04
10tav05
10tav07
10tav06
10tav08
10tav09
Primitive mantle
La/Yb = 1.39

Figure 13

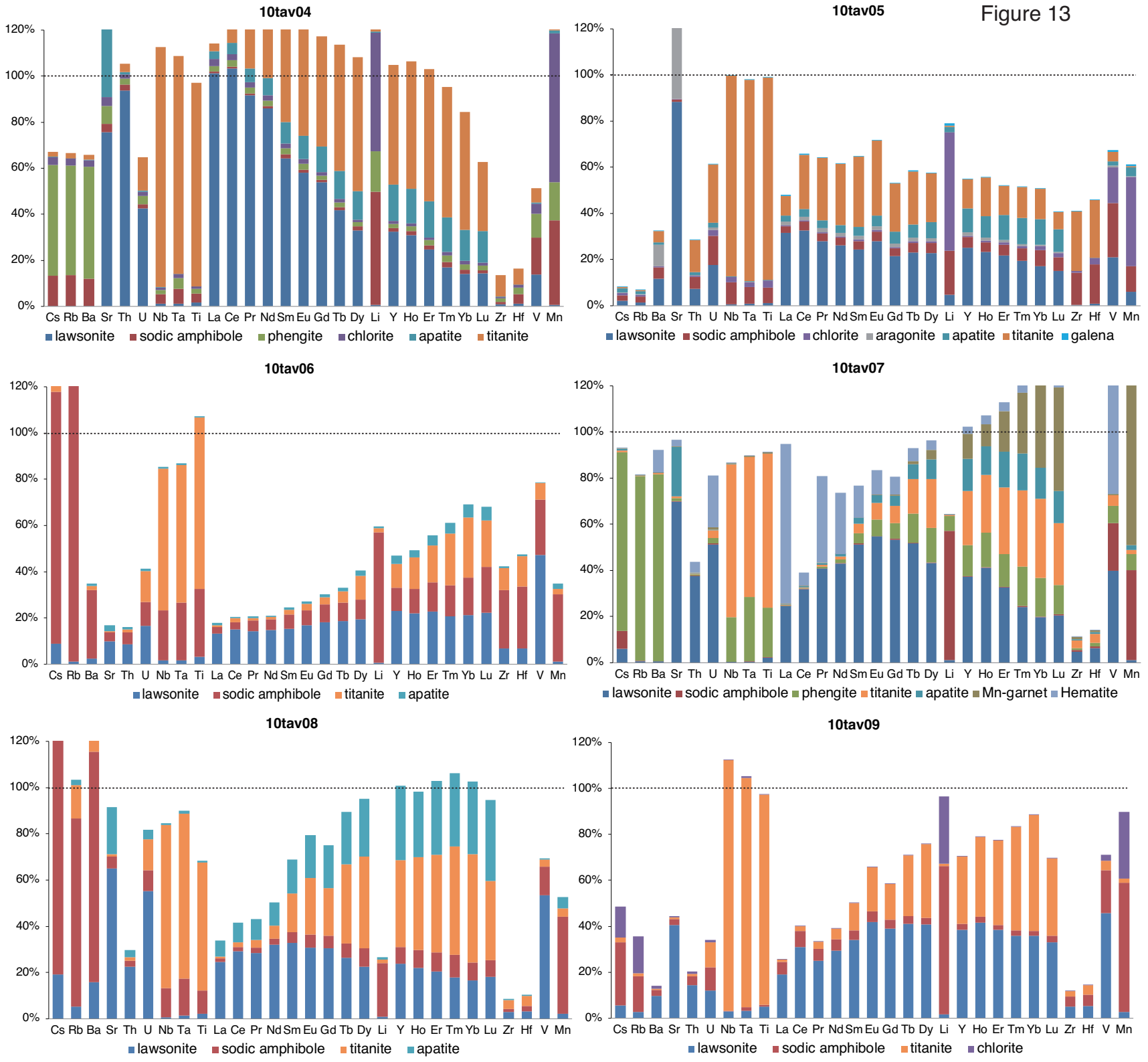
10tav04
120%
100%
80%
60%
40%
20%
0%
Cs Rb Ba Sr Th U Nb Ta Ti La Ce Pr Nd Sm Eu Gd Tb Dy Li Y Ho Er Tm Yb Lu Zr Hf V Mn
lawsonite
sodic amphibole
phengite
chlorite
apatite
titanite
10tav05
120%
100%
80%
60%
40%
20%
0%
Cs Rb Ba Sr Th U Nb Ta Ti La Ce Pr Nd Sm Eu Gd Tb Dy Li Y Ho Er Tm Yb Lu Zr Hf V Mn
lawsonite
sodic amphibole
chlorite
aragonite
apatite
titanite
galena
10tav06
120%
100%
80%
60%
40%
20%
0%
Cs Rb Ba Sr Th U Nb Ta Ti La Ce Pr Nd Sm Eu Gd Tb Dy Li Y Ho Er Tm Yb Lu Zr Hf V Mn
lawsonite
sodic amphibole
titanite
apatite
10tav07
120%
100%
80%
60%
40%
20%
0%
Cs Rb Ba Sr Th U Nb Ta Ti La Ce Pr Nd Sm Eu Gd Tb Dy Li Y Ho Er Tm Yb Lu Zr Hf V Mn
lawsonite
sodic amphibole
phengite
titanite
apatite
Mn-garnet
Hematite
10tav08
120%
100%
80%
60%
40%
20%
0%
Cs Rb Ba Sr Th U Nb Ta Ti La Ce Pr Nd Sm Eu Gd Tb Dy Li Y Ho Er Tm Yb Lu Zr Hf V Mn
lawsonite
sodic amphibole
titanite
apatite
10tav09
120%
100%
80%
60%
40%
20%
0%
Cs Rb Ba Sr Th U Nb Ta Ti La Ce Pr Nd Sm Eu Gd Tb Dy Li Y Ho Er Tm Yb Lu Zr Hf V Mn
lawsonite
sodic amphibole
titanite
chlorite

Figure 14

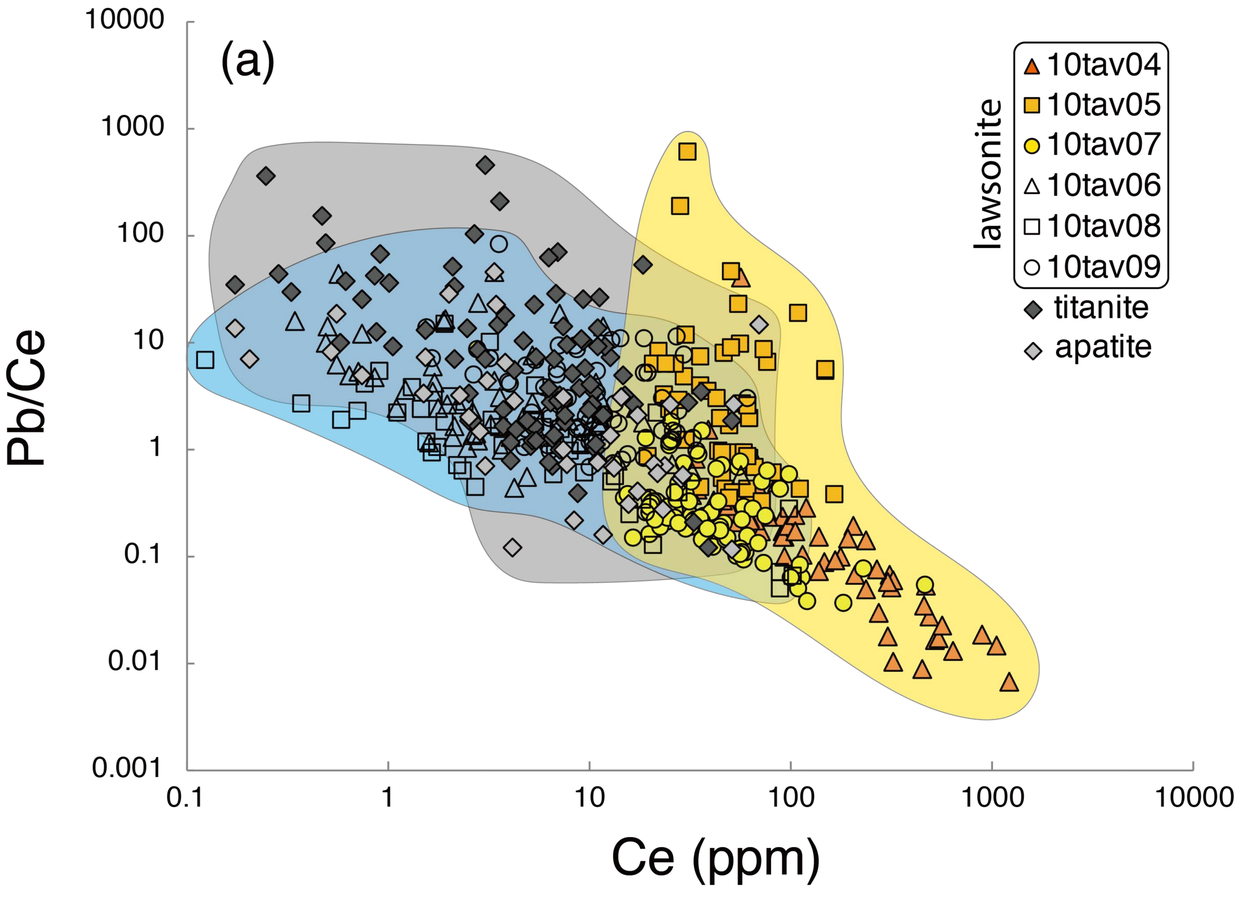
(a)
Pb/Ce
Ce (ppm)
10000
1000
100
10
1
0.1
0.01
0.001
0.1
1
10
100
1000
10000
lawsonite
10tav04
10tav05
10tav07
10tav06
10tav08
10tav09
titanite
apatite

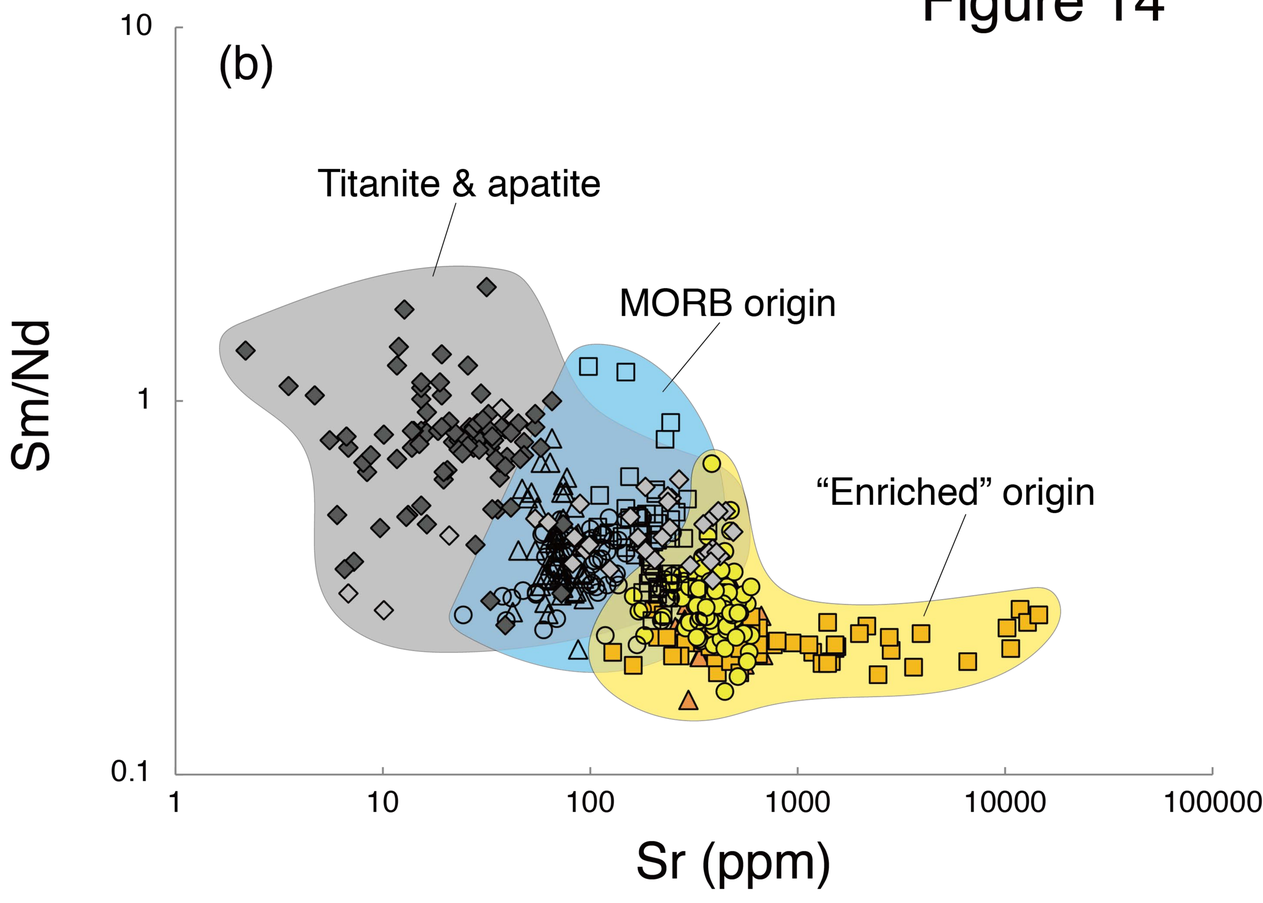
(b)
Sm/Nd
Sr (ppm)
10
1
0.1
1
10
100
1000
10000
100000
Titanite & apatite
MORB origin
“Enriched” origin

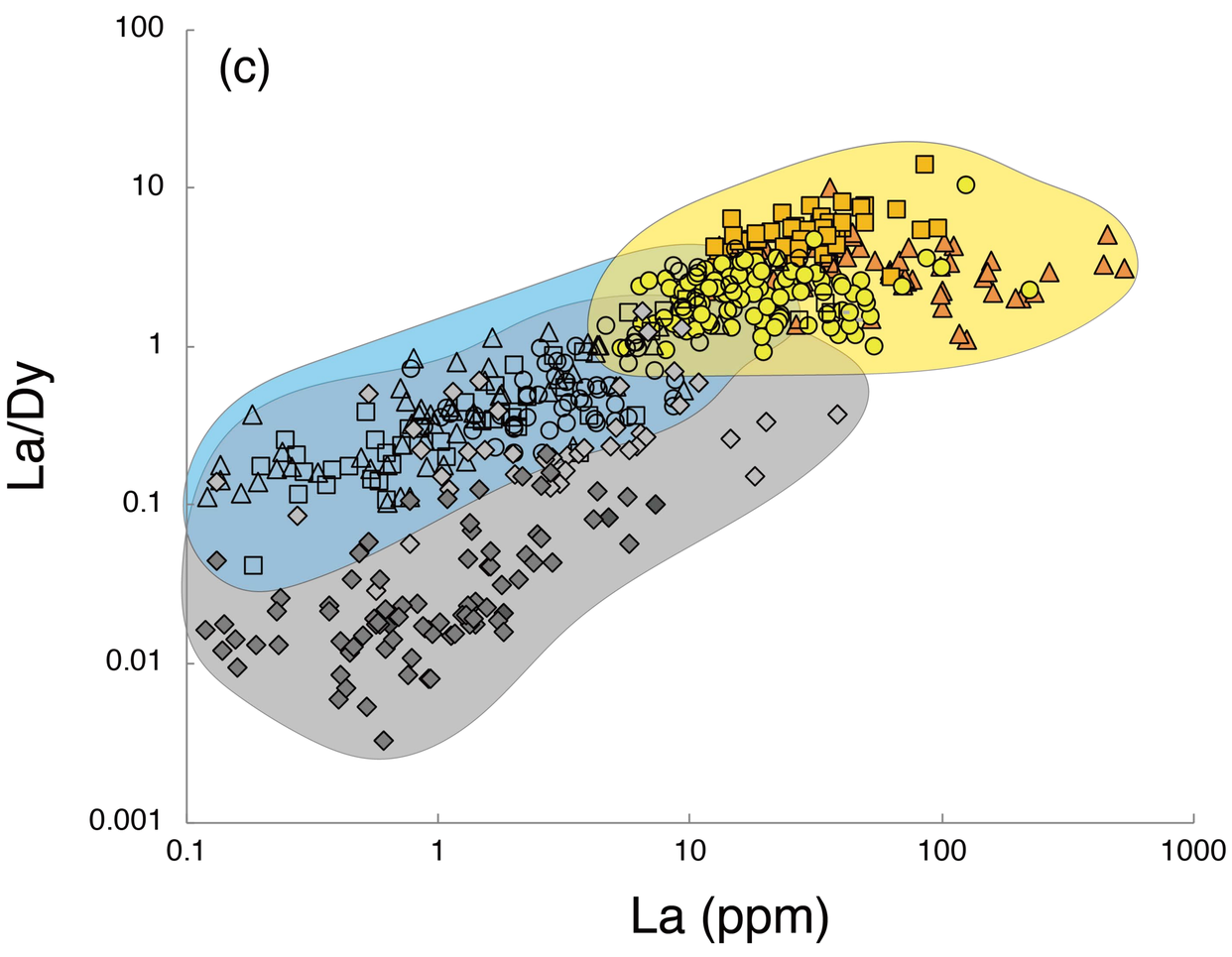
(c)
La/Dy
La (ppm)
100
10
1
0.1
0.01
0.001
0.1
1
10
100
1000

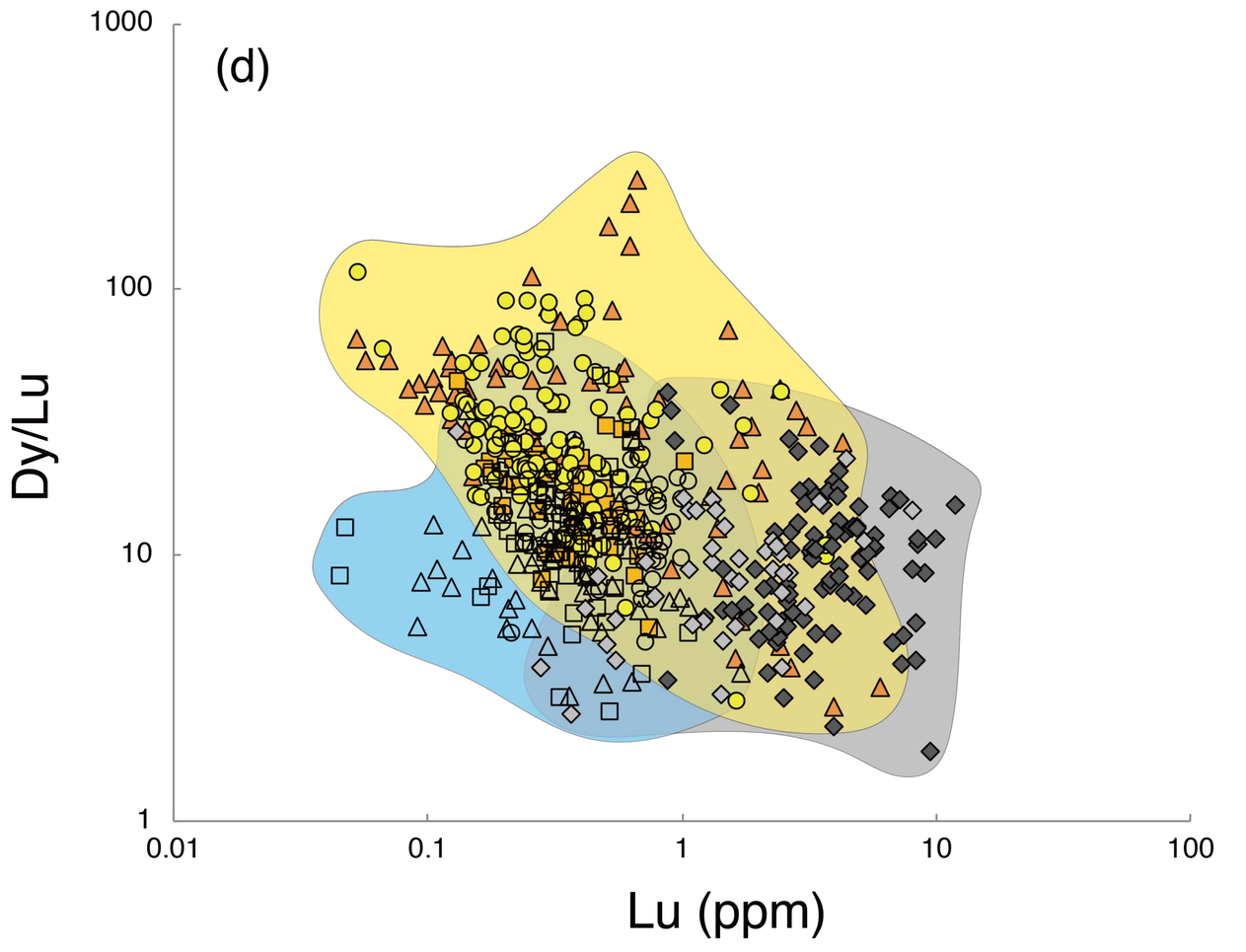
(d)
Dy/Lu
Lu (ppm)
1000
100
10
1
0.01
0.1
1
10
100

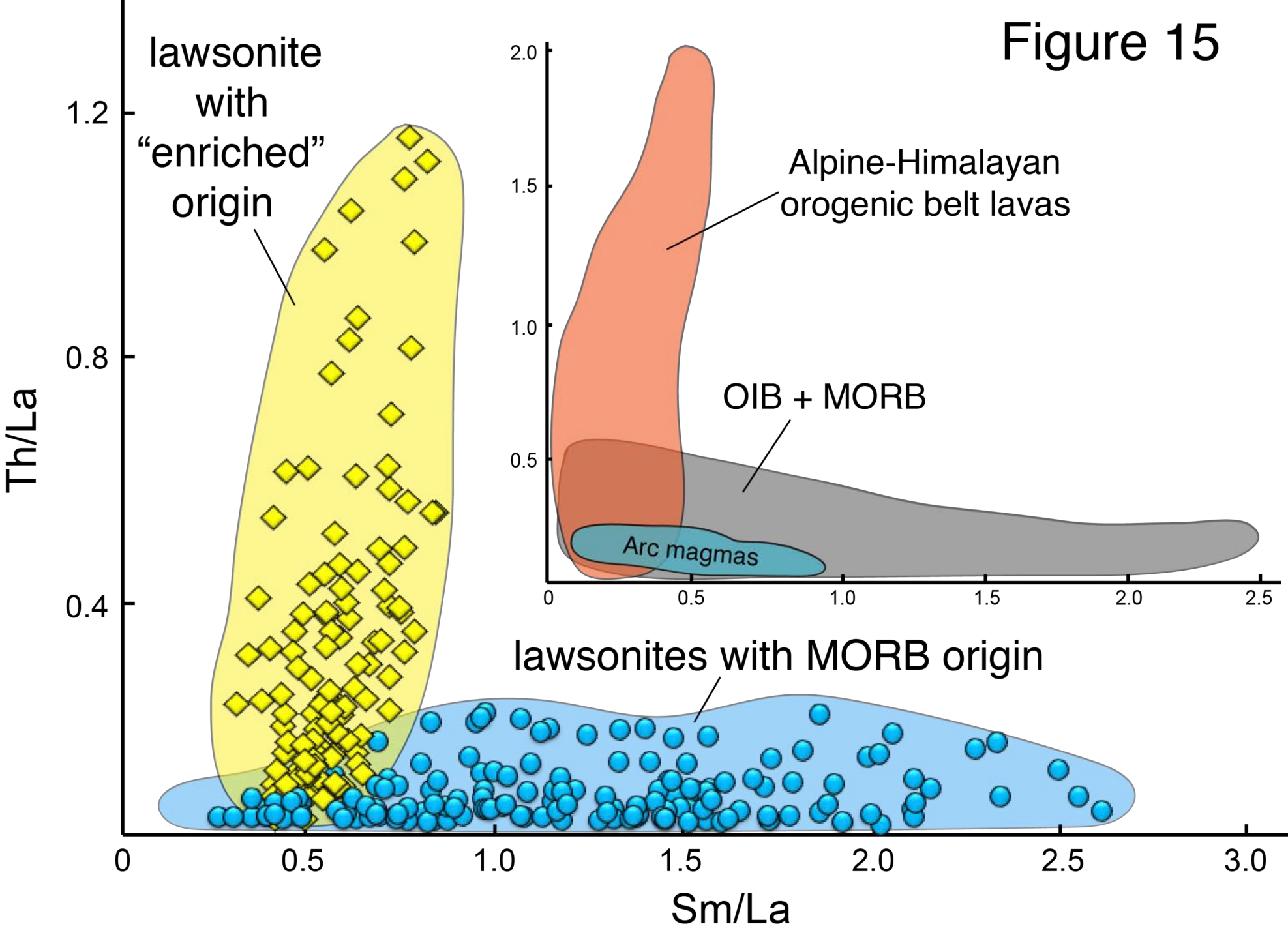
Figure 15
lawsonite with "enriched" origin
Alpine-Himalayan orogenic belt lavas
OIB + MORB
Arc magmas
lawsonites with MORB origin
Th/La
Sm/La
0
0.4
0.8
1.2
0.5
1.0
1.5
2.0
2.5
3.0

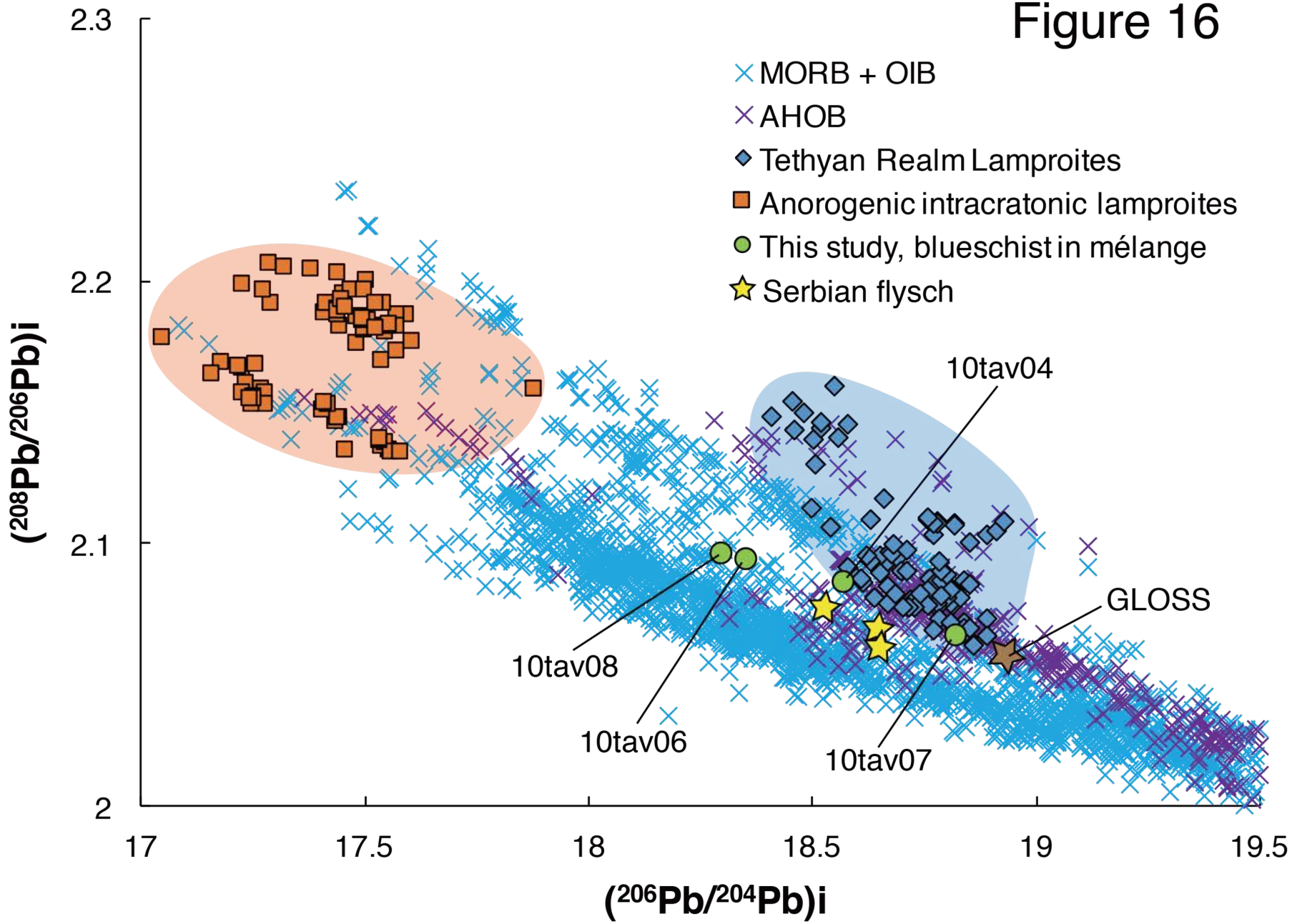
Figure 16
MORB + OIB
AHOB
Tethyan Realm Lamproites
Anorogenic intracratonic lamproites
This study, blueschist in mélange
Serbian flysch
10tav04
GLOSS
10tav08
10tav06
10tav07
2.3
2.2
2.1
2
17
17.5
18
18.5
19
19.5
(208Pb/206Pb)i
(206Pb/204Pb)i